

Utah State University

DigitalCommons@USU

All Graduate Theses and Dissertations

Graduate Studies

5-2009

Novel Growth of InGaAs/GaAs Nanostructures by Molecular Beam Epitaxy

Dong Jun Kim
Utah State University

Follow this and additional works at: <https://digitalcommons.usu.edu/etd>



Part of the [Physics Commons](#)

Recommended Citation

Kim, Dong Jun, "Novel Growth of InGaAs/GaAs Nanostructures by Molecular Beam Epitaxy" (2009). *All Graduate Theses and Dissertations*. 258.
<https://digitalcommons.usu.edu/etd/258>

This Dissertation is brought to you for free and open access by the Graduate Studies at DigitalCommons@USU. It has been accepted for inclusion in All Graduate Theses and Dissertations by an authorized administrator of DigitalCommons@USU. For more information, please contact digitalcommons@usu.edu.



NOVEL GROWTH OF INGAAS/GAAS NANOSTRUCTURES BY MOLECULAR BEAM
EPITAXY

by

Dong Jun Kim

A dissertation submitted in partial fulfillment
of the requirements for the degree

of

DOCTOR OF PHILOSOPHY

in

Physics

Approved:

Dr. Haeyeon Yang
Major Professor

Dr. J. R. Dennison
Committee Member

Dr. Mark Riffe
Committee Member

Dr. T. C. Shen
Committee Member

Dr. Anhong Zhou
Committee Member

Dr. Byron Burnham
Dean of Graduate Studies

UTAH STATE UNIVERSITY
Logan, Utah

2009

Copyright © Dong Jun Kim 2009

All Rights Reserved

ABSTRACT

Novel Growth of InGaAs/GaAs Nanostructures by Molecular Beam Epitaxy

by

Dong Jun Kim, Doctor of Philosophy

Utah State University, 2009

Major Professor: Haeyeon Yang
Department: Physics

This dissertation presents an extensive study of the epitaxial growth mechanism by a novel growth method. This novel growth method was developed at Utah State University and is a modification of the Stranski-Krastanov (S-K) growth mode. Our new growth method consists of a two-step process, low temperature growth and high temperature annealing. During low temperature growth, diffusion is minimized, resulting in the deposition of a pseudomorphic epilayer. During high temperature annealing, diffusion is induced from the pseudomorphic epilayer, resulting in the transformation of the epilayer into nanostructures. Benefits of this novel growth method are a significantly smaller segregation and suppressed intermixing due to the barrier wetting layer during sample growth. InGaAs nanostructures on GaAs(001) surfaces are examples of this new growth method. They were grown by molecular beam epitaxy (MBE) and analyzed using real-time reflection high energy electron diffraction (RHEED) and *in situ* scanning tunneling microscopy (STM). Our novel approach resulted in quantum dot chains and quantum dashes formed by annealing pseudomorphic layers of two different thicknesses of InGaAs on GaAs(001). These nanostructure shapes are different from those features formed by the conventional Stranski-Krastanov growth mode. The results indicate the potential to better understand nanostructures for future optoelectronic device applications.

(114 pages)

ACKNOWLEDGMENTS

My first thanks go to my thesis advisor, Professor Haeyeon Yang, for giving me the opportunity to work in a very interesting area, and for his support and guidance throughout my graduate studies. Also, many people have played important roles in helping me to accomplish the task of my graduate study and this dissertation writing. Especially, I am deeply grateful to the members of my committee, Dr. J. R. Dennison, Dr. Mark Riffe, Dr. T.C. Shen, and Dr. Anhong Zhou, for their advice, guidance, encouragement, patience, and revision of the dissertation draft. I would like to thank my lab colleague, E. Addison Everett, for his kind and valuable help in my research. We had a memorable time on the research and outside the research as well. I would also like to thank the Physics Department office staff, Mrs. Karalee Ransom and Mrs. Shelley Isaacson, for their high quality service on helping the graduates.

Finally, I would express my deep gratitude to my wife, Eun Kyoeng Lee, daughter Minyoung, son Minwoo, and my mother, Young Hee Kwon, for their never-ending support and love regarding everything during my study. Lastly, I would like to thank my father, Chan Ho Kim, for his unwavering faith in my mind.

Dong Jun Kim

CONTENTS

	Page
ABSTRACT	iii
ACKNOWLEDGMENT	iv
LIST OF FIGURES	vii
CHAPTER	
1 INTRODUCTION.....	1
1.1 Overview.....	1
1.2 Fundamentals	
1.2.1 Molecular Beam Epitaxy.....	4
1.2.2 Reflection High Energy Electron Diffraction.....	5
1.2.3 Scanning Tunneling Microscope.....	10
1.2.3.1 STM Tip Etching.....	13
1.2.3.2 Nanostructuring.....	14
1.2.4 Epitaxial Growth.....	15
1.2.5 Epitaxial Growth Modes	15
1.2.6 Growth Procedures.....	17
1.2.6.1 Sample Preparation and Mounting.....	17
1.2.6.2 Temperature Calibration and Oxide Desorption.....	18
1.2.6.3 GaAs Buffer Layer Growth.....	19
1.2.6.4 In _{0.4} Ga _{0.6} As QD Growth Using the Conventional Stranski-Krastanow Growth.....	21
1.3 Employed Approaches	
1.3.1 In _{0.4} Ga _{0.6} As QD Growth by Low Temperature Deposition and Annealing Method.....	26
1.3.2 Quantum Volume Measurements.....	27
2 ENABLING IN SITU ATOMIC SCALE SURFACE IMAGING FOR VERTICAL MOLECULAR BEAM EPITAXY MACHINES.....	32
2.1 Introduction.....	32
2.2 Molecular Beam Epitaxy System Description.....	32
2.3 Scanning Tunneling Microscope System Attachment.....	33
2.4 Cassette and Transfer Line Modifications.....	35
2.5 Summary.....	38
3 ANNEALING INDUCED TRANSITION OF FLAT STRAINED INGAAAS EPILAYERS INTO THREE-DIMENSIONAL ISLANDS.....	41

3.1	Introduction.....	41
3.2	Experimental Procedure.....	42
3.3	Strained Pseudomorphic $\text{In}_{0.4}\text{Ga}_{0.6}\text{As}/\text{GaAs}(001)$	43
3.4	Annealing Temperature Effect.....	46
3.5	$\text{In}_{0.4}\text{Ga}_{0.6}\text{As}$ QD Chain Formation.....	46
3.6	Summary.....	49
4	EFFECT OF ARSENIC OVERPRESSURE ON GROWTH OF PSEUDOMORPHIC INGAAS.....	51
4.1	Introduction.....	51
4.2	Experimental Procedure.....	52
4.3	RHEED Oscillation Behavior with Different Arsenic Flux.....	53
4.4	STM Study of Arsenic Overpressure Effect.....	56
4.5	Summary.....	61
5	SHAPE CONTROL OF INGAAS NANOSTRUCTURES ON NOMINAL GAAS(001):DASHES AND DOTS.....	63
5.1	Introduction.....	63
5.2	Experimental Procedure.....	65
5.3	Quantum Dash Formation.....	66
5.4	Indium Segregation Effect.....	67
5.5	STM Study of Quantum Dashes.....	69
5.6	Summary.....	71
6	SUPPRESSED SEGREGATION AND INTERMIXING OF INGAAS/GAAS QUANTUM DOTS BY A NOVEL GROWTH METHOD.....	74
6.1	Introduction.....	74
6.2	Experimental Details.....	75
6.3	Results and Discussion.....	77
6.4	Summary.....	82
7	CONCLUSIONS AND FUTURE WORK.....	84
7.1	Thesis Conclusion	84
7.2	Future Work.....	85
	APPENDICES.....	87
A	GROWTH OF NANODOTS ON A STRAINED GAAS EPILAYER USING SCANNING TUNNELING MICROSCOPE.....	88
B	Permission Letters.....	99
	CIRICULUM VITAE.....	103

LIST OF FIGURES

Figure	Page
1.1 Schematic top view of the MBE system with the newly installed STM chamber	6
1.2 Photograph of the MBE-STIM system at Utah State University.....	7
1.3 Layout of the RHEED system.	8
1.4 Observed $\beta(2\times 4)$ RHEED patterns for GaAs growth on a GaAs(001) oriented surface at 580 °C: (a) 0° off (110) azimuth; (b) ~ 4° off (110) azimuth.....	9
1.5 Modes of electron diffraction. Transmission and reflection provide different spot shapes and locations.....	9
1.6 Ball and stick models of the GaAs(001)-c(4×4)(a) and $\beta(2\times 4)$ reconstruction surface. Each model shows top view and side view.....	11
1.7 Illustration of the STM with a constant current mode.....	12
1.8 Photograph of STM tip etching facility and circuit configuration.....	13
1.9 The STM image of oval domed shaped nanodots and nanostructuring parameters.....	14
1.10 Schematic views of epitaxial growth.	16
1.11 Schematic of three growth modes, (a) island or Volmer-Weber growth mode, (b) layer by layer or Frank-van der Merwe growth mode, (c) layer plus island or Stranski-Krastanov growth mode	17
1.12 Observed RHEED patterns of the initial surface at 480 °C (a), (b) partial oxide desorption $T_s=570$ °C, time=5 min, (c) complete oxide desorption $T_s=580$ °C, time = 7 min, (d) $T_s=590$ °C,time = 5 min. T_s is substrate temperature.....	19
1.13 Surface reconstruction phase diagram of the GaAs(001) surface and corresponding RHEED periodicities.	20
1.14 Typical RHEED specular intensity for GaAs(001)- $\beta(2\times 4)$ reconstruction surface growth. [1-10] azimuth.	21
1.15 STM images of GaAs(001) - 2×4 reconstructed surface.....	22

1.16	Intensity oscillations of the specular beam in the RHEED pattern for InGaAs growth on GaAs(001).	23
1.17	Schematic plot of $\text{In}_{0.4}\text{Ga}_{0.6}\text{As}$ QD growth procedure with a cross-sectional schematic of QDs. (b) STM image of $\text{In}_{0.4}\text{Ga}_{0.6}\text{As}$ QD layer grown on GaAs(001) substrate using the conventional S-K growth. RHEED patterns during the deposit (c) 2D deposition of GaAs buffer layer, (d) the 3D deposition of InGaAs epilayer.....	24
1.18	Evolution of structure and composition of epilayer and substrate due to the Indium segregation and Intermixing, for typical InGaAs growth on GaAs substrate in the S-K growth mode.	26
1.19	Novel growth mode of $\text{In}_{0.4}\text{Ga}_{0.6}\text{As}$ QD growth with a cross-sectional schematic of QDs..	28
1.20	STM image of InGaAs/GaAs QD chain obtained by annealing at 460°C. The image size is 500 nm × 500 nm.	28
1.21	Proposed volume calculation models.	29
2.1	Schematic side view of the preparation chamber and STM chamber	34
2.2	Schematic diagrams of (a) a home-made tantalum STM sample plate, (b) a home-made 4 in. diameter moly-block to grow a STM sample in the MBE chamber (a STM moly block), and (c) a modified cassette with a STM block attached in the middle and a pin on the top.....	36
2.3	STM images of InGaAs QDs as-grown on a GaAs(001) surface.	39
3.1	STM images of the 10.24ML thick InGaAs epilayer grown at 360°C.....	44
3.2	STM images of an InGaAs SAQDs. (a) A large 500nm x 500nm image shows SAQDs by annealing the 8.85ML InGaAs flat epilayers at 460°C for two minutes. Image (b) is for 9.07ML InGaAs SAQDs by a continuous S-K growth at 450°C.	45
3.3	Annealing temperature effect on morphology; 500nm × 500nm STM images for the InGaAs QDs formed through roughening transformation during the annealing period of two minutes but at different annealing temperatures.....	47
4.1	RHEED oscillations for the same growth period (25 seconds) during epitaxial growths at different arsenic overpressures.....	55

4.2	Filled state STM images of from the pseudomorphic $\text{In}_{0.4}\text{Ga}_{0.6}\text{As}$ epilayers at different resolutions. The sizes of the images are; $500\text{nm} \times 500\text{nm}$ for (a) and (b), $100\text{nm} \times 100\text{nm}$ for (c) and (d).....	57
4.3	Filled state STM images of from the pseudomorphic $\text{In}_{0.4}\text{Ga}_{0.6}\text{As}$ epilayers at different resolutions. The sizes of the images are; $40\text{nm} \times 40\text{nm}$ for (a) and (b), $7\text{nm} \times 7\text{nm}$ for (c) and (d).....	58
4.4	Filled state STM images of from the pseudomorphic $\text{In}_{0.4}\text{Ga}_{0.6}\text{As}$ epilayers at different resolutions. The size of contour plots (a) and (b) is $7\text{nm} \times 4\text{nm}$	60
5.1	STM images; from the surface prepared by annealing the pseudomorphic $\text{In}_{0.4}\text{Ga}_{0.6}\text{As}$ layers with thicknesses of 6.56 ML (a); 8.85ML (b); and by continuous growth of 6.7ML (c).....	68
6.1	Schematic diagram of two different growth methods: modified growth with a constant coverage(sample A) and conventional growth mode with a constant temperature(sample B) during the InGaAs growth.	76
6.2	STM images of InGaAs QDs formed after a 10.2ML deposition and 9.8ML deposition...78	
6.3	Scattering plots of the aspect ratio and dot length in $[1-10]$ directiona and $[110]$ direction.	79
6.4	Volume distributions of InGaAs quantum dots grown at 460°C with InGaAs coverage of 10.2ML (a) and 9.8ML ML (b), respectively.	81
6.5	Average dot volume and dot density as a function of nominal wetting layer thickness.....	82
6.6	Cross section views of the strain distribution in wetting layer for two different growth mechanism. (a) represents sample A, and (b) represents sample B.	83
A.1	All STM images were obtained using 3V (filled state) with a constant current mode at 0.1nA.....	91
A.2	Size dependence on applied bias voltage. The STM tips stayed on each spot for 100 ms at 7nA of the tunneling current.	94
A.3	Size dependence on tunneling current and bias voltage. The structuring time is 100 ms for all nanodots.	95

A.4 Growth of oval-shaped nanodots over structuring time. The growth is anisotropic as the aspect ratio, length over width, increases over time.....	96
--	----

CHAPTER 1

INTRODUCTION

1.1 Overview

The self-assembled growth method is an epitaxial growth technique used in the formation of high quality nanostructures in a semiconductor system. By deposition of epitaxial layers with specific properties, particular structures can be realized on the surface without any fabrication devices.¹ Nanostructures by the self-assembled growth are characterized for optoelectronic device applications due to their special electronic properties.² But, there is a limited ability to control structures to fulfill requirements for design applications using the self-assembled growth method due to uncertainty in growth mechanisms, such as diffusion.³ Thus, an understanding of the self-assembled growth mechanisms is important in order to improve the quality of nanoscale fabrication. The key concepts in understanding the growth mechanisms are segregation and intermixing between the epilayer and substrate. These result in uncertain shapes and distributions in nanostructure formation, because deformation of nanostructures can occur due to a compositional drop through segregation and intermixing.^{4,5}

In order to better understand the self-assembled growth mechanisms, I investigated a novel self-assembled growth mode. Nanostructures by a novel growth mode are formed through the transition of two-dimensional strained layers into three dimensional structures. In this study, I compared this new self-assembled growth method with the conventional Stranski-Krastanov (S-K) growth mode. The S-K growth mode was chosen because it is the most common and most researched growth mode of the self-assembled growth method.² In S-K growth mode, a planar wetting layer is formed first by a pseudomorphic two-dimensional layer, followed by the nucleation and growth of three-dimensional islands above a critical thickness of the wetting layer.⁵ During the growth, surface segregation and intermixing between the epilayer and

substrate creates randomness in the shape and distributions of the islands.⁶ Also, self-assembled quantum dots are formed during deposition without growth interruption through the S-K growth mode.

Our novel type growth mode consists of a low temperature deposition and post-growth annealing. To further study the growth mechanism, all growth was performed at low temperature to avoid significant diffusion, and the subsequent annealing was performed at high temperature to promote nucleation. The new method depresses diffusion on the strain-induced surface and suppresses the intermixing between the epilayer and substrate for smaller compositional variations. This may lead to a better understanding of conventional growth mechanisms which may involve relevant processes such as adsorption, desorption, diffusion and surface reactions.⁷

We fabricated aligned InGaAs quantum (QD) structures, including QD chains and quantum dashes (QDhs), on a GaAs(001) surface using MBE, a technique which is being widely used to grow high quality epitaxial layers. Using *in situ* STM images, we inspected the variation of typical shape and size distributions of QD chains and QDhs with various parameters in the growing and annealing processes. This inspection provides an opportunity to understand the mechanisms of self-assembled growth of QDs.

In another novel approach, we fabricated nanoscale dots on a strained GaAs surface using an STM at room temperature. We conducted a morphological analysis of surface diffusion under an electric field on the nanoscale. Also, we tried to understand a detailed structural analysis of two dimensional InGaAs pseudomorphic layers by controlling the indium segregation.

The contents of this dissertation are organized as follows:

Chapter 1 presents some background of self-assembled growth as well as general experimental procedures used for calibrations and sample growth and analysis. It is useful in understanding the subsequent chapters of this thesis.

Chapter 2 describes the STM-MBE ultra high vacuum (UHV) system used in our experiment. A commercial MBE and STM system are connected together via a third custom-built UHV chamber. Notably, a newly developed sample transfer system is presented, which allows us to acquire *in situ* atomic scale surface images of epitaxial layers. This chapter also describes successful *in situ* STM images of MBE grown nanostructures as a result of the system modification.⁸

Chapter 3 presents the results of the STM study of the annealing induced QDs from flat strained $\text{In}_{0.4}\text{Ga}_{0.6}\text{As}$ epilayers. The employed growth method is different from the conventional growth mode. It consists of low temperature pseudomorphic layer growth and subsequent annealing at a higher temperature. Low temperature growth leads to a different strain effect due to the small intermixing between different layers and insignificant segregation on the surface. The annealing process promotes anisotropic diffusion leading to the formation of $\text{In}_{0.4}\text{Ga}_{0.6}\text{As}$ quantum dot-chains. This chapter also discusses the temperature effect during the sample annealing process.⁹

Chapter 4 presents a morphological study on pseudomorphic $\text{In}_{0.4}\text{Ga}_{0.6}\text{As}$ grown on top of GaAs(001) surfaces. Indium segregation on $\text{In}_{0.4}\text{Ga}_{0.6}\text{As}$ surfaces is investigated during epilayer growth by RHEED.

Chapter 5 presents a method to fabricate $\text{In}_{0.4}\text{Ga}_{0.6}\text{As}$ QDhs and QDs on nominal GaAs(001) using the modified S-K growth mode. *In situ* STM images are used to illustrate the shape control of InGaAs QDhs or QDs. This chapter also explains the difference in growth conditions between QDhs and QD chains.¹⁰

Chapter 6 describes the formation of InGaAs/GaAs(001) QDs by two competing growth mechanisms as investigated by STM and RHEED. We fabricated two QD samples with different growth mechanisms, varying deposition thickness with a constant growth temperature and

varying growth temperature with a constant deposition thickness. Our investigation suggests a significant difference in surface segregation and intermixing during dot formation from two different growth mechanisms. The STM study confirmed significant changes in QD shape and deduced chemical composition changes of the wetting layer from the two competing growth mechanisms.

In chapter 7, a conclusion is presented with suggestions for future research.

Appendix A describes nanodot fabrication on strained surfaces by STM. The strained surface is a GaAs capping layer on top of InGaAs/GaAs QD layers grown by MBE. Using the nanostructuring function in our Omicron STM, we investigated electric field-induced diffusion. High-bias voltages with various feedback currents were applied to the GaAs capping layer. We investigated the morphological changes on the surface. Then, we proposed new aspects of diffusion under an electric field on the nanoscale structures.¹¹

1.2 Fundamentals

In this section, basic concepts of epitaxial growth used in this research are presented. Also the experimental apparatus and procedures used for MBE sample growth and STM analysis are presented. Starting with MBE, the principles of MBE growth are discussed with the preview of the experimental results of InGaAs QD growth. *In situ* analysis techniques used in this research, STM and RHEED, are discussed. STM is used to determine grown-sample surface morphology and surface nanostructuring. RHEED is used for *in situ* monitoring of surface structure changes on substrates. Our MBE-STM multi-chamber system and its applications are also described.

1.2.1 Molecular Beam Epitaxy

MBE is a technique for producing high quality epitaxial structures by a process involving the reaction of one or more thermal molecular beams under ultra high vacuum (UHV) conditions.¹² By depositing epitaxial layers with particular properties, specialized nano-device

structures can be realized. To prevent the beam nature of mass flow toward the substrate and to maintain a low contamination condition on sample surfaces, a growth chamber should always maintain UHV conditions in the range of 10^{-11} torr. To investigate atomic scale morphologies of MBE grown samples under low contamination conditions, the MBE growth chamber has been connected to an STM chamber as a multi-chamber UHV system. Figure 1.1 shows a schematic diagram of our MBE-STM UHV chamber system. It consists of an MBE growth chamber, an STM chamber, a load lock chamber, and a preparation chamber between them. The sample can be transported from the growth chamber to the STM chamber via a transport system that is enclosed in the preparation chamber. Details of the MBE-STM system and sample transport system are described in Chapter 2. A photograph of our MBE-STM system is shown in Fig. 1.2.

1.2.2 Reflection High Energy Electron Diffraction

RHEED is an important *in situ* real time tool used to monitor the surface quality during growth.¹³ We used it to measure the growth rate of the GaAs buffer layer and the InGaAs layer in our research. It is also a very useful tool to characterize structure information, deoxidization of the surface, stage temperature calibration, and growth thickness control. Figure 1.3 shows the key features of a RHEED system. The RHEED gun emits high energy electrons (10 keV for our system), which strike the surface at a small angle (typically $1\sim 4^\circ$). The high energy electrons result in high penetration depth into the surface. But, a few atomic layers are probed by the incident glancing angle. Thus, RHEED is highly sensitive to the sample surface. Electrons reflect from the surface and strike a phosphor RHEED screen forming a pattern consisting of a specular reflection and a diffraction pattern. The phosphor RHEED screen is located on the opposite side of the chamber from the RHEED electron gun (see Fig. 1.2., a photograph of the MBE-STM system). The pattern on the RHEED screen is collected by a charge-coupled device (CCD)

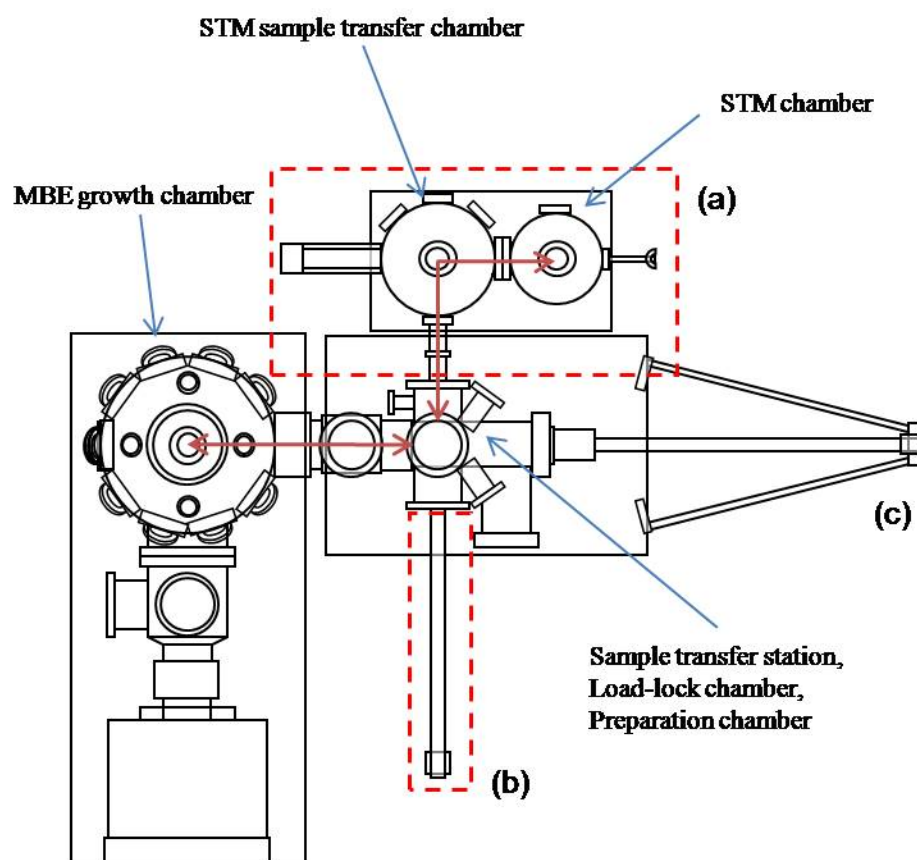
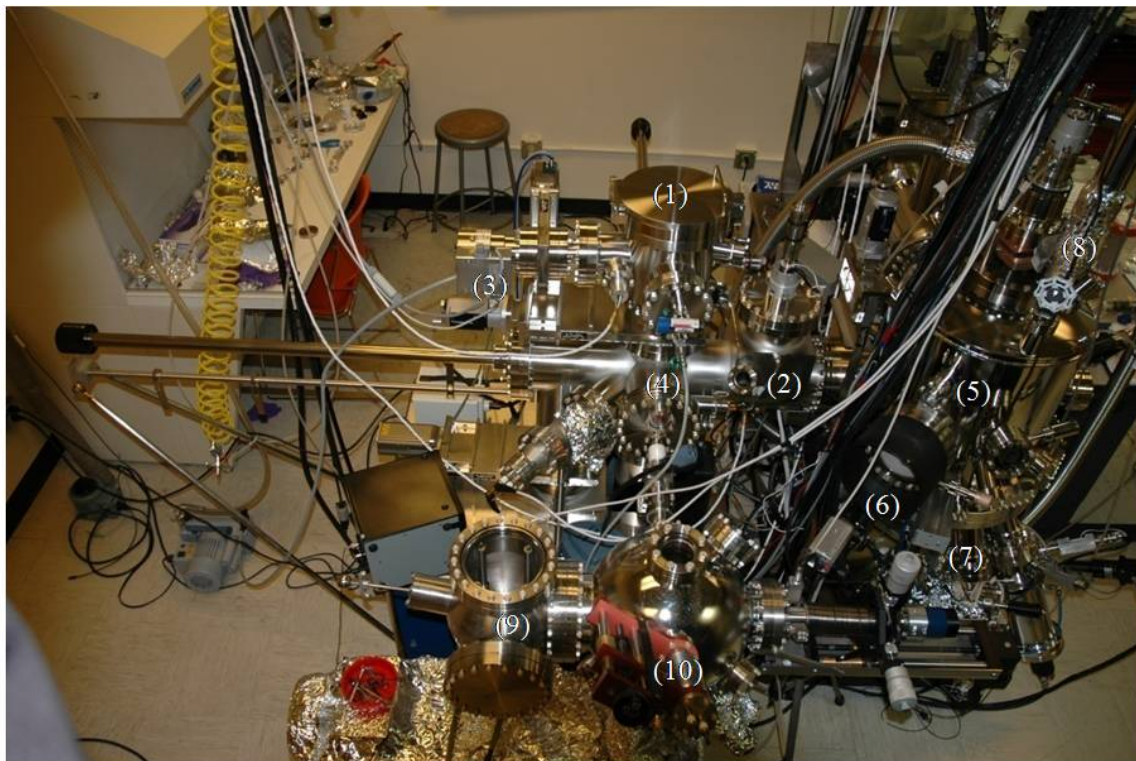


FIG. 1.1. Schematic top view of the MBE system with the newly installed STM chamber (a), newly installed magnetic rod (b), and the factory supplied magnetic rod (c). Solid (brown) lines indicate the sample transfer line from/to the growth chamber to/from preparation chamber and from/to the STM chamber to/from the preparation chamber.



- | | |
|-----------------------------------|---------------------------------|
| (1) Load-lock(L/L) chamber | (6) RHEED screen and CCD camera |
| (2) Degas stage | (7) Effusion cells |
| (3) L/L Turbo Molecular Pump(TMP) | (8) LN2 input pipe |
| (4) Preparation chamber | (9) STM stage |
| (5) MBE growth chamber | (10) E-beam gun |

FIG. 1.2. Photograph of the MBE-STIM system at Utah State University.

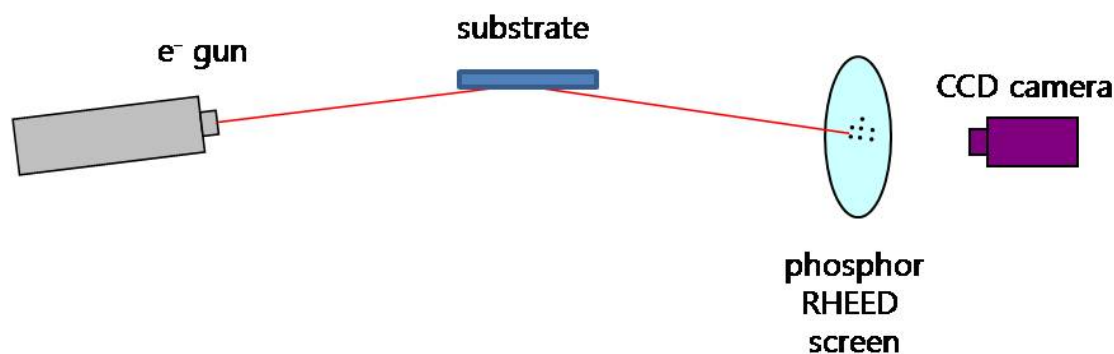


FIG. 1.3. Layout of the RHEED system. The diffraction pattern on the phosphor screen is collected and captured with a CCD camera.

camera, which is connected to a LabView VI image interface card in our computer. We use commercial software to acquire and process these RHEED patterns. With this software we analyze the beam intensity changes in the diffraction pattern to obtain growth rates and other surface information. Figure 1.4 shows typical 4×4 RHEED patterns from a reconstructed GaAs buffer layer growth. The 4×4 RHEED pattern consists of a specular spot, fourfold spots ($1/4$, $2/4$, $3/4$), and integer order spots. A specular spot and integer order spot are indicated by (1) and (2) in Fig. 1.4(a). Fourfold spots are indicated by corresponding numbers.¹⁴ The specular spot is the beam spot from the RHEED beam with equal incident and reflected beam angles. In Fig. 1.4(a), the RHEED beam is oriented along the (110) direction, (see Fig. 1.6, GaAs phase diagram). Figure 1.4(b) shows a RHEED pattern obtained after a sample rotation of 4 degrees. The specular spot is still observed in the center, but the other diffraction spots have rotated down and are weaker relative to the specular spot. The specular spot intensity is dependent upon growth rate, and deposition coverage. Features of the RHEED patterns also provide surface morphology information. If the surface is rough, RHEED diffraction appears spotty due to the transmission through the particles on the surface, as shown in Fig. 1.5(a). If the surface is relatively flat, then the RHEED patterns appear as elongated streaks due to transmission and reflection diffraction of the beam, as shown in Fig. 1.5(b).¹⁵

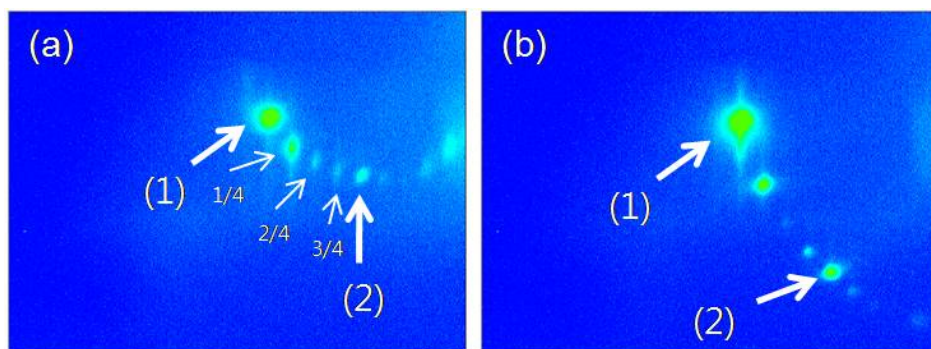


FIG. 1.4. Observed $\beta 2(2 \times 4)$ RHEED patterns for GaAs growth on a GaAs(001) oriented surface at 580 °C: (a) 0° off (110) azimuth; (b) $\sim 4^\circ$ off (110) azimuth. The electron energy is 10 keV. (1) indicates a specular spot in a RHEED pattern, (2) indicates integer order spot, and other spots are sub-order peak.

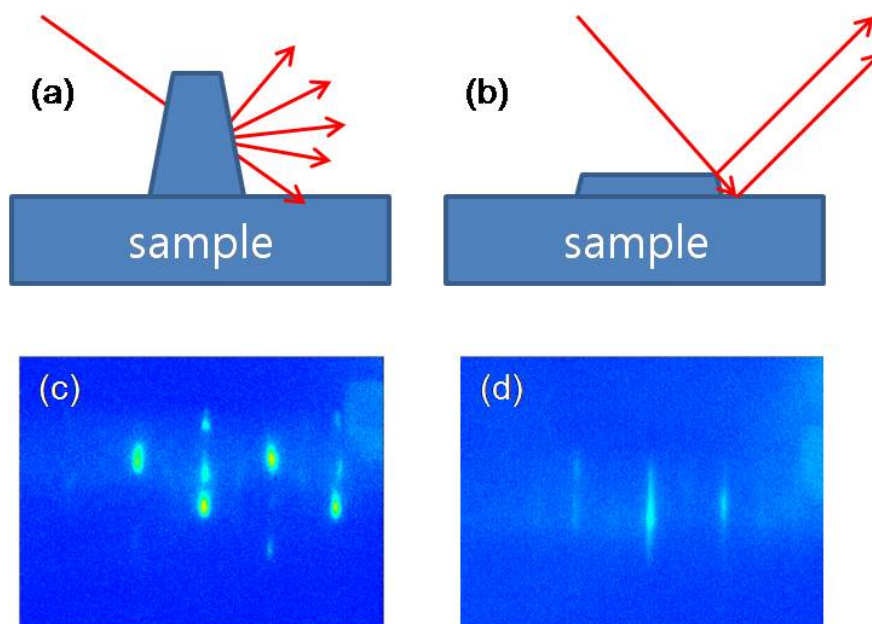


FIG. 1.5. Modes of electron diffraction. Transmission and reflection provide different spot shapes and locations. (a) and (c) indicate a transmission reflection diffraction, resulting in spotty features; (b) and (d) indicate reflection diffraction, resulting in elongated streaks.

The GaAs(001) oriented surface is one of the most studied semiconductor samples in our research. In the buffer layer growth, three different GaAs reconstructions are observed.¹⁶ At low temperature growth, the GaAs surface is in the arsenic-rich $c(4 \times 4)$ phase. During the temperature increase with a constant arsenic flux, the GaAs surface changes from $c(4 \times 4)$ to a (2×4) phase, and can be detected using RHEED. This phase transition is controlled by the growth temperature and arsenic beam equivalent pressure (BEP) as shown in Fig. 1.13. The GaAs(001)- $c(4 \times 4)$ surface is obtained by cooling a (2×4) surface. The arsenic rich (2×4) phase is the most important structure because it is used as a substrate in QD growth in MBE. As shown in Fig. 1.6 (b) and (c), top layer of the arsenic rich (2×4) phase is arsenic along the dimer row direction. In our observation, there are two different models of the arsenic rich (2×4) phases. One is the three As-dimer model, $\beta(2 \times 4)$, as shown in Fig. 1.6 (b). Another is the two As-dimer model, $\beta 2(2 \times 4)$, as shown in Fig. 1.6 (c).¹⁷ The $\beta 2(2 \times 4)$ phase consists of two arsenic dimers and a trench, and a $\beta(2 \times 4)$ phase with three arsenic dimers in a row with one missing arsenic dimer.¹⁸ STM has been used for the study of the unit cell GaAs structure, which consists of two As-dimers and a trench, as shown in Fig. 1.6 and Fig. 1.15(d).

1.2.3 Scanning Tunneling Microscopy

STM is a very suitable technique to investigate atomic scale semiconductor nanostructures.^{19, 20} It is based on a technique controlling the tunnel current between a tip and the sample surface. An electrically biased metallic tip (typically tungsten) is scanned across a surface of the MBE grown sample at a few angstroms distance. The constant current flow between the tip and the sample (due to the tunneling effect) strongly depends on the tip-surface distance and can measure distance changes with great accuracy (see Fig. 1.7(a)). The changing distance signal is collected by computer and generates a surface topographical image signal of the surface. This

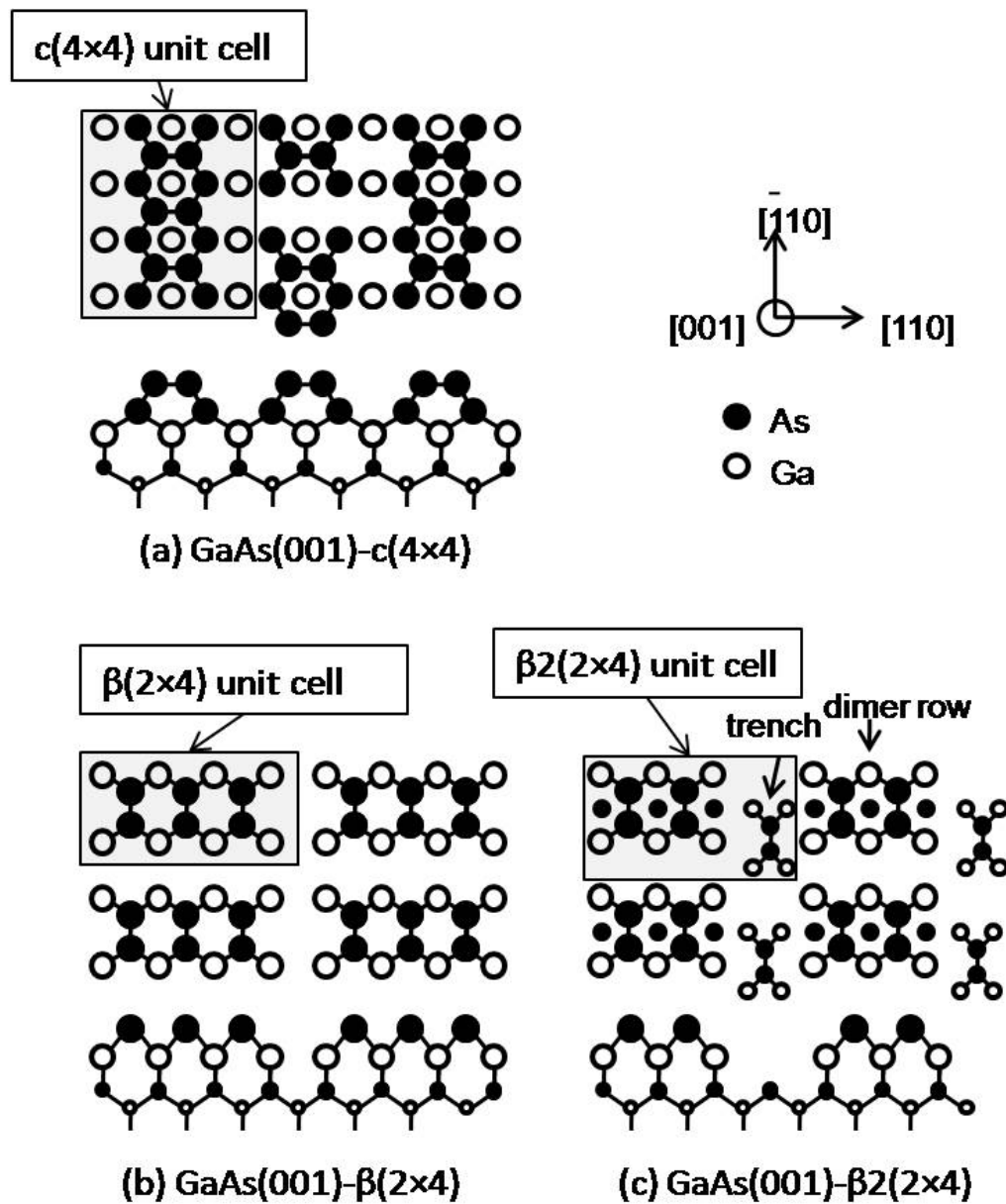


FIG. 1.6. Ball to stick models of the GaAs(001)-c(4 × 4) (a) and β(2 × 4) reconstruction surface. Each model shows a top view (above) and a side view (below). Filled and empty circles represent arsenic and gallium respectively. The small circuit in the model represents the 2nd layer (lower figures).

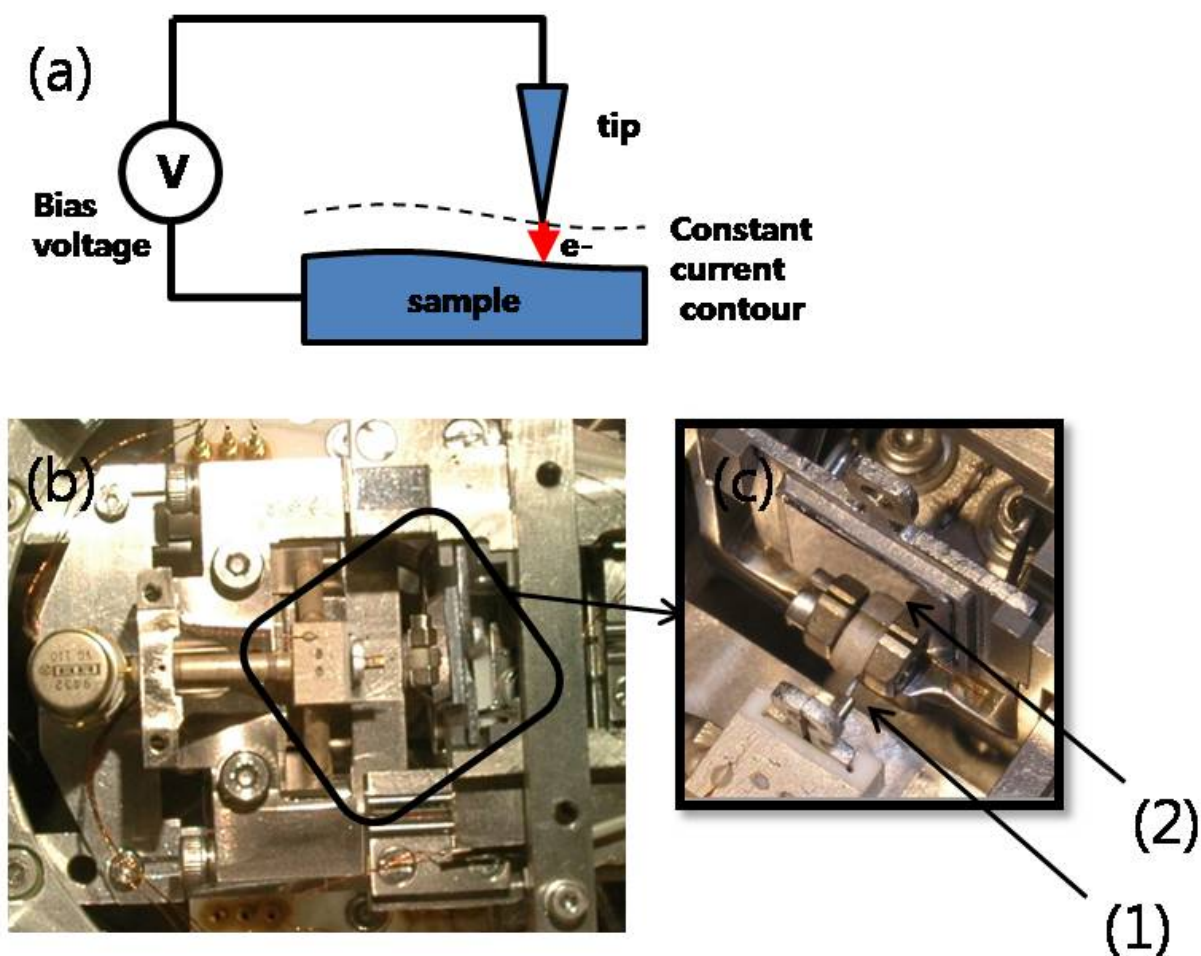


FIG. 1.7 (a) Illustration of an STM with a constant current mode: a feedback loop maintains a constant tunnel current between the tip and the surface, while the STM is scanned over the sample. Photograph of STM stage (b) and STM tip and sample (c), (1) indicates STM tip and (2) indicates sample.

method only works with conducting samples, e.g. metal, graphite, and semiconductors. Figure 1.7 (b) and (c) shows photographs of the Omicron STM stage in our MBE-STM system.

1.2.3.1 STM Tip Etching

Tip etching technique plays very important role in the STM measurement process, because the resolution of an STM image is decided by the size, shape and contamination of the tip end.²¹ If the tip has multiple ends or is contaminated by another material, the tunneling junction is unstable, and can cause noise in the STM imaging. The STM tip is prepared by electro-chemically etching polycrystalline tungsten wires. A circuit diagram of our tip etching facility is shown in Fig. 1.8(b), and a photograph of the facility is shown in Fig. 1.8(a). We begin the tip etching process with a small piece of tungsten wire with a diameter of 0.008 inches. The top part of the tungsten wire is pushed into the center of the tungsten loop. Then, a drop of 1.0 M NaOH solution is placed on the loop and moves the loop so the tungsten wire passes through the loop. The 1.0 M solution is made with 5 g of NaOH and 100 mL of distilled water. The tip etching is done by sweeping the tungsten loop over the wire. If the tip end is sharp enough, the applied

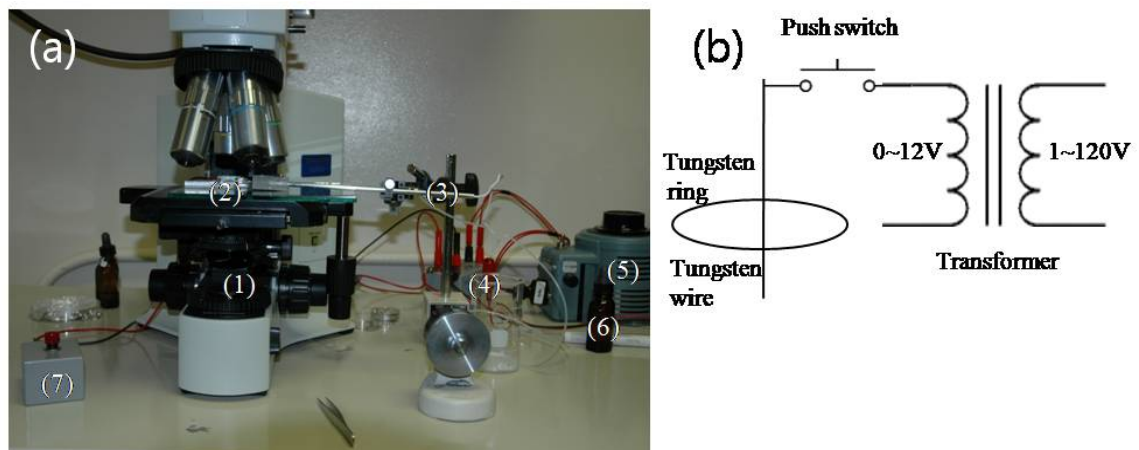


FIG. 1.8. (a) A Photograph of the USU STM tip etching facility, consisting of a microscope(1), etching stage(2), micro stage(3), transformer(4), variac(5), NaOH chemical bottle(6), and push-button switch(7) . (b) The experimental tip-etching circuit configuration of the tip etching facility. Tungsten wire is used as a ring and tip material.

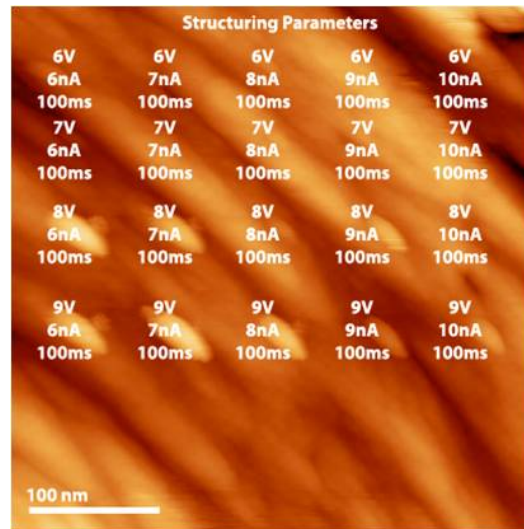


FIG. 1.9. STM image of oval-domed shaped nanodots, with nanostructuring parameters.

voltage to the tip etching stage is decreased. After the tip etching, the tip is removed from the stage in the microscope and is rinsed using distilled water to remove any chemicals.

1.2.3.2 Nanostructuring

The STM is not only used as a powerful instrument for nanostructure imaging, it is also used as a device for the modification of atomic scale surfaces.²² The nanostructuring is done with an Omicron STM and is used to modify nanodot structures. The nanostructuring is performed by applying voltage pulses over the regular STM tunneling voltage.²³ Using Omicron STM software, the surface is selected and the STM is programmed to create a 5×5 grid of structuring events.²³ Figure 1.9 shows nanostructured QDs on a GaAs capping layer. Each event on the capping layer is programmed with three parameters. The first two parameters are the bias voltage and tunneling current. Both are changed while the feedback loop is still active. The third parameter is the amount of time each event is active. That is, the amount of time the bias voltage and tunneling current are changed from the values used for imaging to the values used for creating nanostructures. Appendix A includes detailed experimental procedures of the nanostructuring process for QDs.

1.2.4 Epitaxial Growth

Epitaxial growth of the heterostructure fabricated using the MBE such as InGaAs on GaAs substrate is the main subject of our research. Heteroepitaxy is a kind of epitaxy fabricated by lattice mismatched materials, which means the lattice constant difference between the substrate and epitaxial layer. The relative lattice mismatch²⁴ is defined as:

$$f = \frac{(a_e - a_s)}{a_s} \quad (\text{Eq.1})$$

where a_s and a_e are the bulk lattice constants of the substrate and the epitaxial layer. The lattice constant of GaAs at 300 K is 5.65 Å, and the lattice constant of In_{0.4}Ga_{0.6}As at 300 K is 5.80 Å. Thus the lattice mismatch between the GaAs substrate and In_{0.4}Ga_{0.6}As is 2.6%. Here, the lattice constant of In_{0.4}Ga_{0.6}As is known to obey Vegard's law²⁵ with an alloy composition of 40% indium and 60% gallium. Vegard's law has been used to determine the lattice constant of In_{0.4}Ga_{0.6}As, which has a linear relation between the lattice constant of 40% indium and 60% gallium. Vegard's equation is

$$a_{\text{InGaAs}} = xa_{\text{InAs}} + (1-x)a_{\text{GaAs}} \quad (\text{Eq.2})$$

where the lattice constant of InAs, a_{InAs} , is 6.05 Å and the lattice constant of GaAs, a_{GaAs} , is 5.65 Å.

1.2.5 Epitaxial Growth Modes

There are three main growth modes for heteroepitaxial growth. Depending on surface energy of substrate γ_s , surface energy of island γ_i , and interface energy between island and substrate $\gamma_{i/s}$, three fundamental growth modes can be realized in heteroepitaxy. Figure 1.10 shows schematics of two epitaxial growth modes neglecting strain.⁷ Figure 1.10(a) represents non wetting layer growth, in which an epitaxial layer that forms a 3D island on the surface of the substrate. Figure 1.10(b) represents wetting, in which an epitaxial layer uniformly covers the

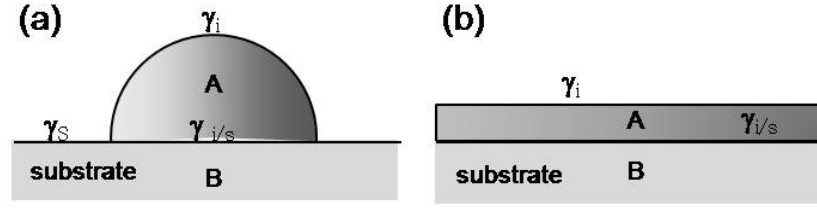


FIG. 1.10. Schematic views of 3D island growth (a) and 2D layer growth (b). γ_i :surface energy of island, γ_s :surface energy of substrate , $\gamma_{i/s}$:interface energy of island-substrate.

surface of substrate.

As schematically shown in Fig. 1.10(a) and Fig. 1.10(a), when γ_s is smaller than the sum of γ_i and $\gamma_{i/s}$, three-dimensional (3D) islands nucleate on the substrate. In this case, the substrate and epilayer have a big lattice mismatch and adatoms are more attracted each other than to the surface due to high surface energy. This is called the Volmer-Weber growth mode. Small clusters are nucleated directly on the substrate surface and then grow into islands to minimize interface energy and surface energy, as shown in Fig. 1.10(a).^{13, 26}

The Frank-van der Merwe growth mode shows an opposite nature as compared with the Volmer-Weber growth mode. This growth mode consists of layer-by-layer growth, in which the lattice mismatch between the materials is very small and adatoms are more attracted to the surface of substrate due to low surface energy, as shown in Fig. 1.10(b) and 1.11(b). In this growth mode, the surface energy of the substrate γ_s is much bigger than the sum of surface energy of island γ_i and the surface energy of interface between substrate and island $\gamma_{i/s}$.^{13, 26}

The S-K growth mode (Fig. 1.11(c)) is the intermediate case, where there is a moderate lattice mismatch between the materials. This growth mode consists of a layer by layer growth which forms a two dimensional (2D) wetting layer of material up to a certain critical thickness, followed by a transition to 3D island growth, QDs, due to the large lattice mismatch between the epilayer and substrate.⁵ The lattice mismatch causes an accumulation of strain energy with

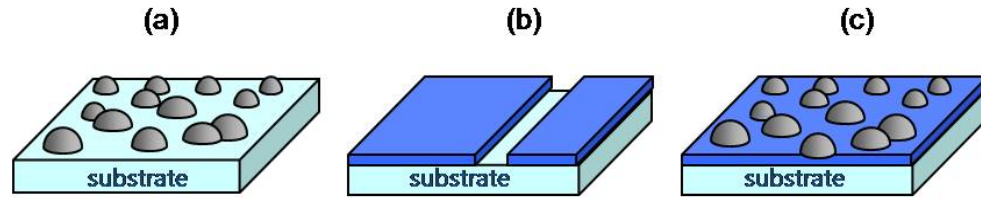


FIG. 1.11. Schematic of three growth modes. (a) island, non-wetting, or Volmer-Weber growth mode, (b) layer by layer, wetting, or Frank-van der Merwe growth mode, (c) layer plus island, incomplete wetting, or Stranski-Krastanov growth mode .

increasing epilayer thickness. To minimize the strain energy on the surface, the strain is relaxed through the formation of QDs out of a strained epilayer.⁶ Strain relaxation is a key process in S-K growth.^{1,5,6} Density and size distribution of the QD are controlled by variation of growth conditions and the choice of material.

The S-K growth mode is the most common growth mode of the self-assembled QD growth modes. The S-K growth involves deposition of one chemical composition on the substrate of another composition with a mismatched lattice ranging from 2% to 10%.^{5,27} If the lattice mismatch is larger than 10%, direct 3D growth, called Volmer-Weber growth, occurs. If the lattice mismatch is smaller than 2%, a 2D layer by layer growth, called Frank Van-der-Merwe growth, occurs on the surface of the substrate.⁶ Usually, a relatively small sized QD appears from a large lattice mismatch, while a small mismatch leads to a larger QD.

1.2.6 Growth Procedures

All epitaxial growth in this research were grown using a solid source MBE (SVTA, model BLT-N35). In this section, I described the general procedures for sample growth and corresponding concepts for each step.

1.2.6.1 Sample Preparation and Mounting

Commercial *n*-type GaAs(001) wafers are usually shipped in a state ready to use. Thus,

there is no need for any chemical cleaning process. The sample is measured and cut to a size of 12 mm^2 from a GaAs(001) epi-ready wafer, sized to engage in to a home-made tantalum STM sample plate. Melted indium is used to solder to the 1-mm wide ledge surrounding the square opening of the sample plate and then introduced into the center of a 4-inch molybdenum block. The sample plate is designed to allow it to transfer into the Omicron STM stage for *in situ* STM scanning.

The 4-inch molybdenum block is designed to be transferred into the MBE growth stage from the cassette. This moly-block is first loaded into the cassette. The cassette is then loaded into the load-lock chamber and transferred into the preparation chamber. Prior to moving into the growth chamber, the moly-block temperature is increased to $300 \text{ }^\circ\text{C}$ for 30 min at the degas stage in the preparation chamber. By heating the substrate and moly-block, contaminants, including water, are evaporated from the surface.

1.2.6.2. Temperature Calibration and Oxide Desorption

There are small differences between the real temperature and measured temperature in the growth stage. This occurs because a thermocouple is located in the heating zone of stage, but is not in direct contact with the substrate.²⁸ Thus, temperature calibration is needed to more accurately measure the growth conditions of GaAs samples. Temperature calibration for the stage is based on the desorption temperature of the native oxide layer on GaAs(001) substrates and the transition temperature between (2×4) and $c(4 \times 4)$ reconstructions on GaAs substrates, as observed by RHEED. The surface of the substrate is initially contaminated with oxygen. In the MBE growth chamber, the oxide layer of the samples can be thermally desorbed by heating the substrate to $580 \text{ }^\circ\text{C} \sim 600 \text{ }^\circ\text{C}$ under As_4 flux. A (2×4) reconstructed GaAs(001) surface appears, which is a ready state for buffer layer growth. Figure 1.12 shows the evolution of RHEED patterns with time and temperature changes for oxide desorption on GaAs(001). Initially no

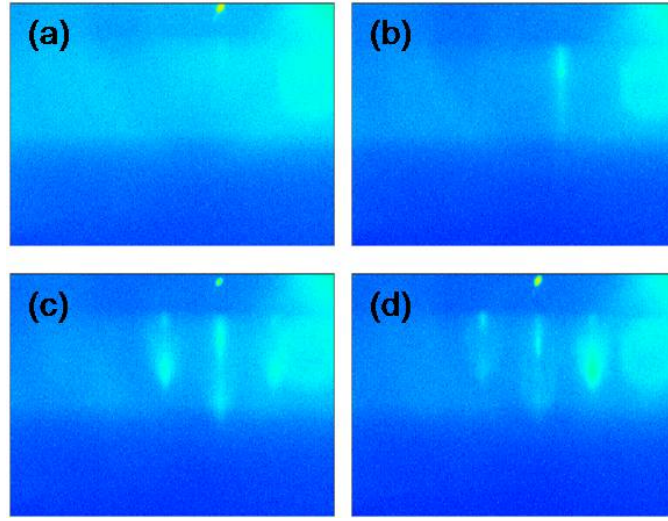


FIG. 1.12. Observed RHEED patterns (10 KeV, incident beam azimuth $[110]$) of the (a) initial surface at 480 °C, (b) partial oxide desorption $T_s = 570^\circ\text{C}$, time = 5 min, (c) complete oxide desorption $T_s = 580^\circ\text{C}$, time = 7 min, and (d) $T_s = 590^\circ\text{C}$, time = 5 min. T_s is the substrate temperature.

significant RHEED patterns can be seen due to the oxide layer, while some streaked patterns and spotty patterns are observed during the oxide desorption process. The background intensity slowly disappears with higher temperature.

The first observation of the transition temperature for a (2×4) GaAs(001) surface reconstruction is at 500 °C under an As_4 flux 6×10^{-6} torr.²⁹ Figure 1.13 shows RHEED patterns of surface reconstruction from (2×4) to $c(4 \times 4)$ under the same growth temperature with increasing As_4 flux. The $2/4^{\text{th}}$ fractional order spot intensity increases until it is equivalent with the $1/4^{\text{th}}$ and $3/4^{\text{th}}$ intensities (see Fig. 1.4). These reconstructed GaAs surface changes are caused by the chemical potential due to changes in the substrate temperature and As_4 flux.^{17, 30}

1.2.6.3 GaAs Buffer Layer Growth

The substrate as well as the buffer layer plays an important role in the formation of thin epitaxial layers. A successful accommodation of lattice mismatch and a smooth surface for high-quality GaAs growth are expected from the buffer layer growth.^{16, 31} Once the oxide is

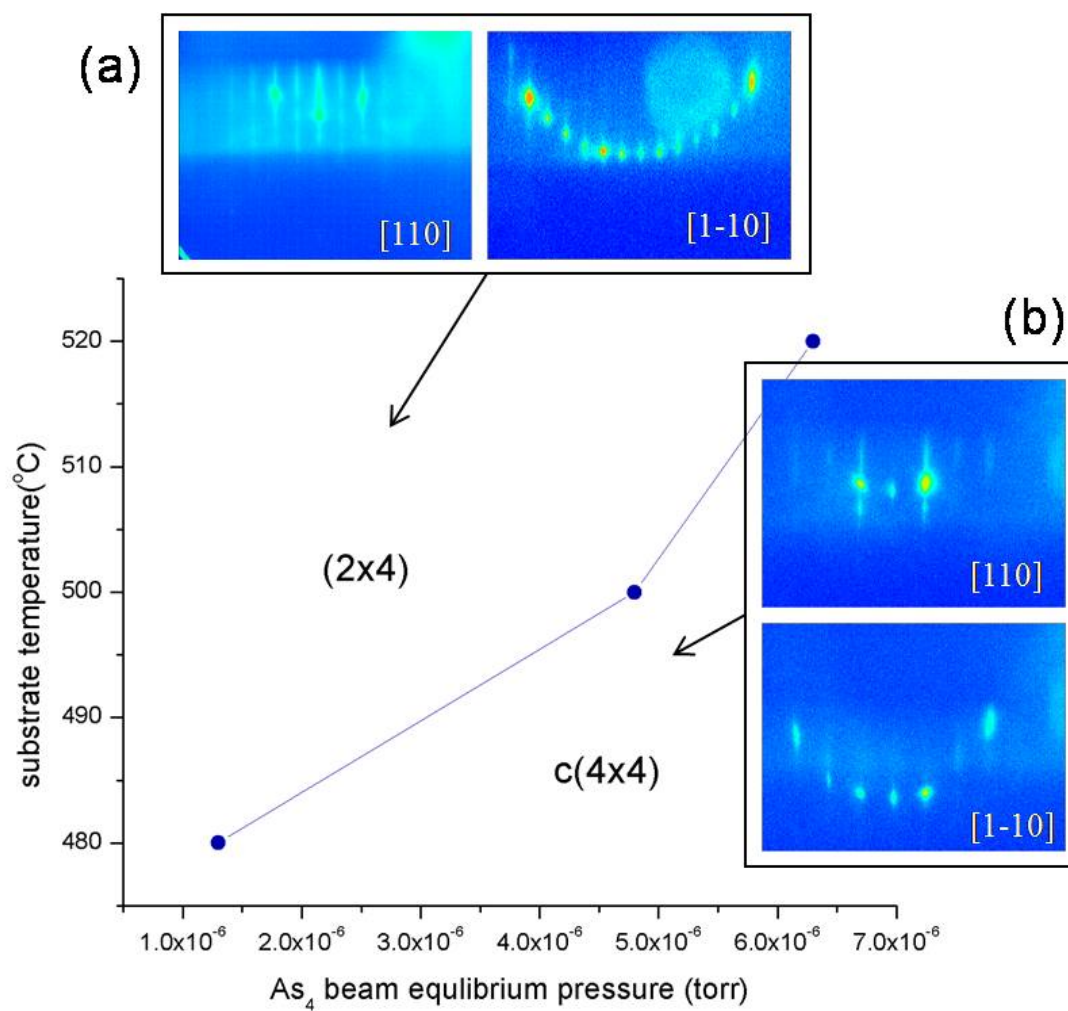


FIG. 1.13. Surface reconstruction phase diagram of the GaAs(001) surface and corresponding RHEED periodicities. RHEED patterns (a) indicate a $\beta 2(2 \times 4)$ -GaAs(001) reconstructed surface and (b) indicates a $c(4 \times 4)$ -GaAs(001) reconstructed surface.

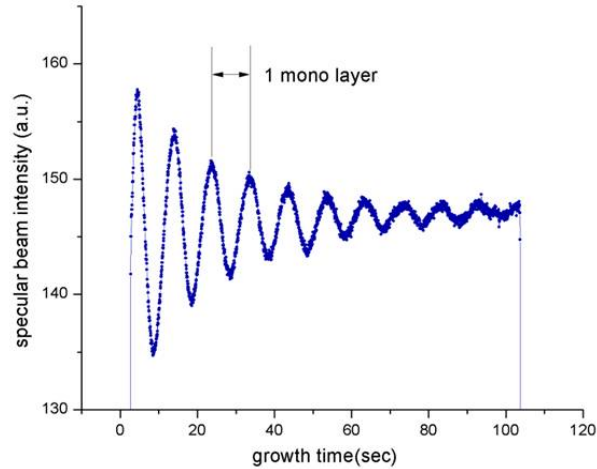


FIG. 1.14. Typical RHEED specular intensity for GaAs(001)- $\beta(2 \times 4)$ reconstruction surface growth. Substrate temperature = 500 °C, As₄ beam equilibrium pressure (B.E.P.) = 6.0×10^{-6} torr.

desorbed from GaAs substrate, a buffer layer of thickness $\sim 1 \mu\text{m}$ can be grown on GaAs(001) substrates under the following conditions: a growth temperature of 580 °C, an As₄/Ga flux ratio of ~ 30 , and a growth rate of $1.0 \mu\text{m}/\text{hour}$. Such conditions have resulted in a smooth reconstructed GaAs surface. Figure 1.15 shows atomic scale As-rich GaAs(001)- (2×4) reconstructed surfaces. These images were taken using an STM with an applied bias voltage of -3.0 V and a tunneling current of 0.1 nA as scanning parameters. Figure 1.13(a) shows RHEED patterns after a GaAs buffer layer growth. RHEED diffraction patterns of the $[110]$ and $[1-10]$ azimuth indicate the reconstructed GaAs(001)- (2×4) surface. The fourfold periodicity is evident from the appearance of fractional-order streaks between the integral-order streaks. RHEED intensity oscillations from the specular beam are used to follow the growth of GaAs buffer layers as shown in Fig. 1.14. One period of the oscillations represents a single atomic layer. The damping of the oscillations is related to the step density reaching a steady state of layers.³²

1.2.6.4 In_{0.4}Ga_{0.6}As QD Growth Using the Conventional S-K Growth Mode

The heteroepitaxy of InGaAs on GaAs follows the conventional Stranski-Krastanov

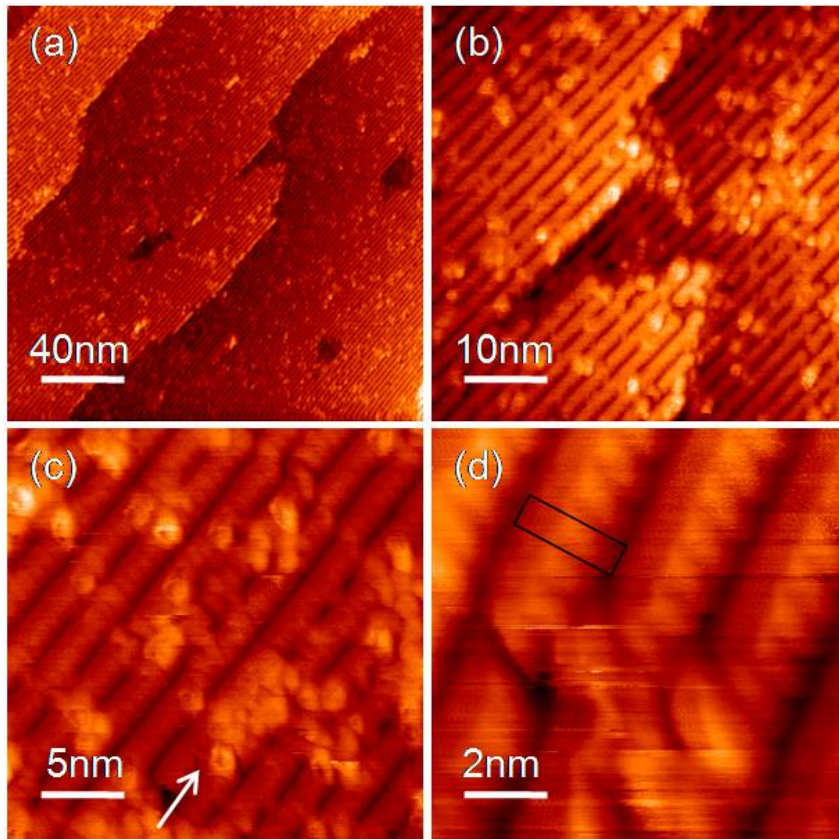


FIG. 1.15. STM images of a GaAs(001) – (2×4) reconstructed surface. Image dimensions are: (a) $200 \text{ nm} \times 200 \text{ nm}$; (b) $50 \text{ nm} \times 50 \text{ nm}$; (c) $25 \text{ nm} \times 25 \text{ nm}$; (d) $10 \text{ nm} \times 10 \text{ nm}$. The arrow in (c) indicates the $[1-10]$ azimuthal direction. The rectangular box in (d) indicates a unit cell of GaAs(001)- $\beta 2(2 \times 4)$.

growth mode, which has been explained previously. Our observations indicate that the critical thickness with 40% indium and 60% gallium is around 6 ML with an As_4 B.E.P. of 6.0×10^{-6} torr. Usually, the critical thickness of the InGaAs epilayer increases with a decrease in the misfit of the GaAs substrate. $\text{In}_{0.4}\text{Ga}_{0.6}\text{As}$ single layers are grown on GaAs(001) at different growth temperatures and different As fluxes. The growth rate of the $\text{In}_{0.4}\text{Ga}_{0.6}\text{As}$ layers is 0.16 ML/sec respectively, monitored by real time RHEED. Figure 1.16 shows the RHEED intensity oscillations measured at the specular peak giving the growth rate of 0.16 ML/sec and total deposition thickness of 6.54 ML. Figure 1.17(c) and (d) compare RHEED pattern changes from GaAs buffer layer to InGaAs deposition. At the transformation of initial 2D surface into the 3D islands, the RHEED pattern changes from the streaky pattern to the spotty pattern and chevron pattern. This chevron shape after depositing the $\text{In}_{0.4}\text{Ga}_{0.6}\text{As}$ layer, indicates the formation of QDs by strain relaxation based on the Stranski-Krastanov growth mode. As soon as the deposition

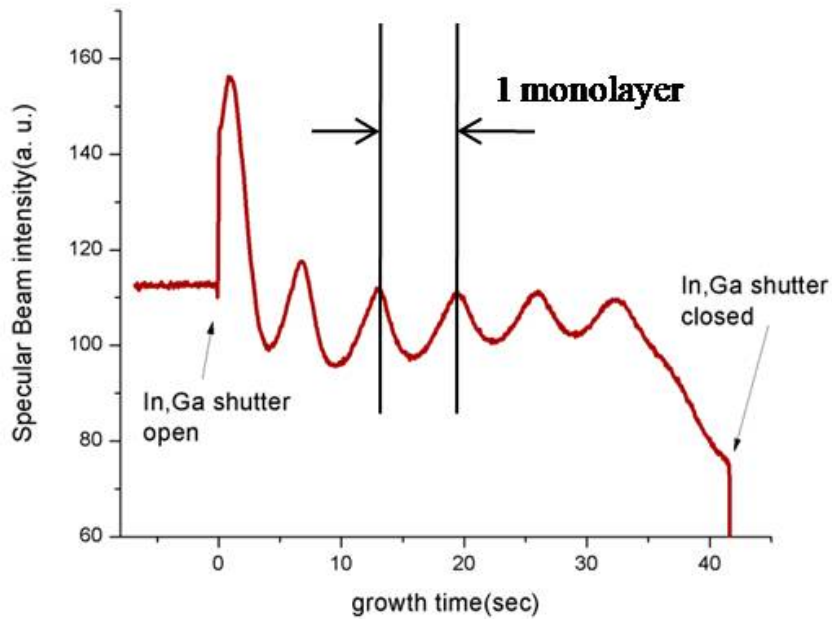


FIG. 1.16. Intensity oscillations of the specular beam in the RHEED pattern for InGaAs growth on GaAs(001). This observation was made in the [1-10] azimuth at the specular spot.

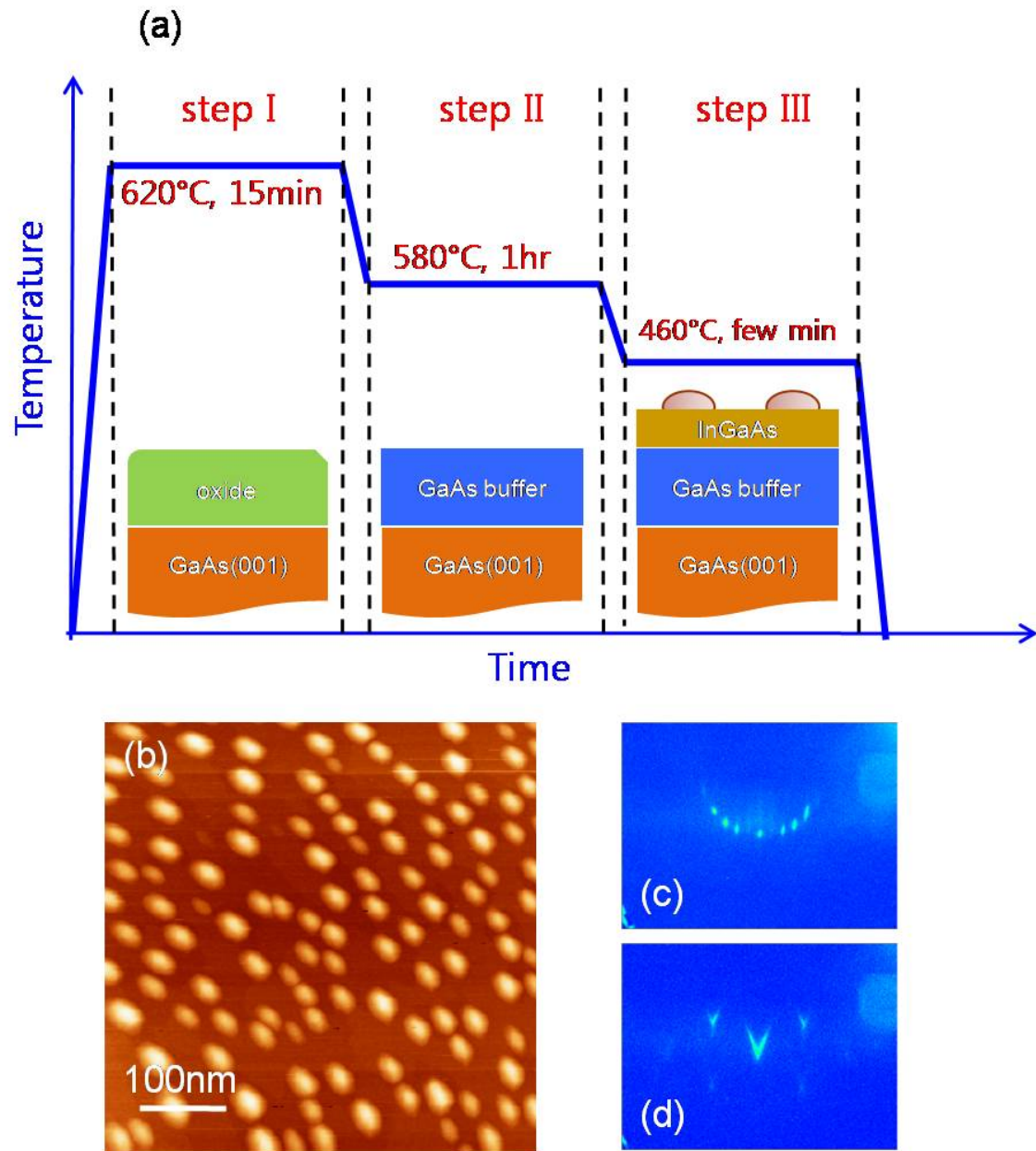


FIG. 1.17. Schematic plot of $\text{In}_{0.4}\text{Ga}_{0.6}\text{As}$ QD growth procedure with a cross-sectional schematic of QDs. The STM image of $\text{In}_{0.4}\text{Ga}_{0.6}\text{As}$ QD layer grown on GaAs(001) substrate using the conventional S-K growth is shown in (b). The size is $500\text{nm} \times 500\text{nm}$. RHEED patterns during 2D deposition of GaAs buffer layer are shown in (c), and (d) shows the 3D deposition of the InGaAs epilayer.

was terminated, the sample is quickly cooled by cutting the heating power off, and the sample is transferred to the STM chamber for *in situ* morphological measurements. Figure 1.17(a) shows the growth procedure of $\text{In}_{0.4}\text{Ga}_{0.6}\text{As}$. Step I represents oxide desorption, Step II represents GaAs buffer layer growth step, and Step III represents InGaAs growth process. Desorption of the native oxide on the GaAs wafer can be removed at 620 °C heating for 15 min. For the growth of InGaAs, GaAs buffer layer growth was performed for 1 hour at the growth temperature of 580°C. Then it was cooled down to the InGaAs growth temperature, $T = 460^\circ\text{C}$. The $\text{In}_{0.4}\text{Ga}_{0.6}\text{As}$ strained layer was grown at a growth rate of 0.16ML/sec and a typical As/Ga flux ratio of 30.

Figure 1.17(b) shows an STM image of 6.5 ML thick $\text{In}_{0.4}\text{Ga}_{0.6}\text{As}$ single layer QDs using the conventional S-K growth mode. The STM measurements were performed *in situ* in constant current mode in vacuum. The bias voltage was -5V , and a tunneling current was 0.065 nA. In the S-K growth mode, surface segregation of indium is one of the serious problems of the InGaAs growth on GaAs since indium molecules move to the top layer of InGaAs layers. The surface composition of indium is different from the bulk composition of indium.³³ Indium segregation to the top layers makes non-uniform strain distribution during the island transformation period as shown in Fig. 1.18. This strain gradient greatly influences the shape of self-assembled QDs because of uneven strain relaxation from the interlayer of the wetting layer. Intermixing of the QDs between the substrate and InGaAs epilayer also a very important process to control the size and composition. The effect of intermixing is to reduce the strain from the interface of substrate and epilayer, thus providing a random compositional distribution to form QDs. Intermixing is a temperature-dependent process. According to the paper from Joyce et al., intermixing can be suppressed at the growth temperature of 420°C or lower.³⁴

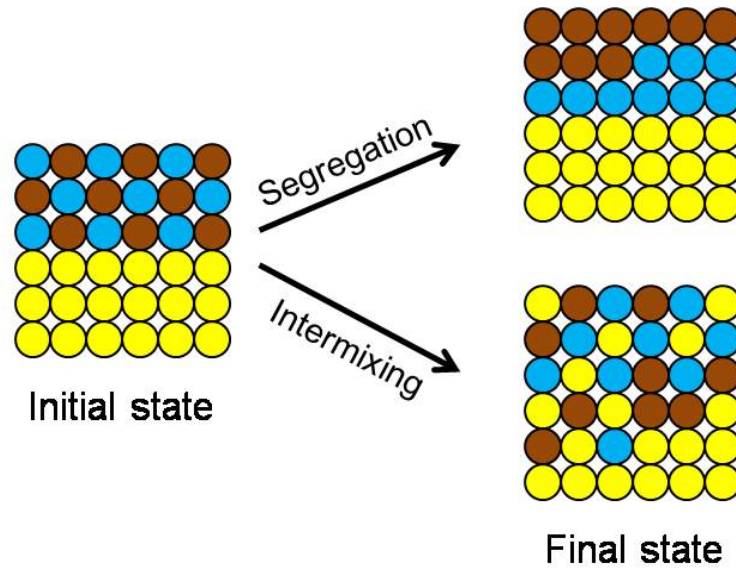


FIG. 1.18. Evolution of structure and composition of epilayer and substrate due to the indium segregation and intermixing, for typical InGaAs growth on a GaAs substrate in the S-K growth mode.

1.3 Employed Approaches

We employed a different growth method, which is a type of S-K growth. This method consists of a low temperature growth and high temperature annealing process. In the conventional S-K growth, randomness of dot shape, and positioning due to the surface segregation and intermixing between the substrate and epilayer were main issues to solve. Therefore, we proposed a modified growth method and studied the growth mechanism by morphology analysis using *in situ* scanning STM and RHEED. Our investigation of this growth method suggests significant small segregation by diffusion and suppressed intermixing due to the barrier layer during the sample growth sequences. In this section, I described detailed experimental procedures for this modified growth method.

1.3.1 $\text{In}_{0.4}\text{Ga}_{0.6}\text{As}$ QD Growth by Low Temperature Deposition and Annealing Method

Strained-but-flat InGaAs epilayer on GaAs (001) substrates are grown at a growth

temperature of 380 °C as shown in Fig. 1.19. A strained-but flat surface is then confirmed by RHEED. At this low temperature growth, segregation and intermixing are expected to be suppressed due to low kinetic energy resulting in short diffusion lengths.³⁵ Following the InGaAs deposition at low temperature growth, a period of post-growth annealing is performed with arsenic pressure. In our experiment, the sample is heated above 460 °C with an As₄ beam equilibrium pressure of 5.9×10^{-6} torr for the annealing period ranging from 10 sec to 2 min. *In situ* RHEED is used to monitor QD formation, as shown in Fig. 1.17.

After annealing, the sample temperature is rapidly cooled down by turning off the heating power. Subsequently, the samples are transferred into the STM chamber, with a base pressure of 2×10^{-10} torr, via an ultra high vacuum transport mechanism developed by our group.³⁶ Room temperature STM images are obtained with a bias voltage of -3 V and a tunneling current in the range of 0.05 nA. Figure 1.20 shows successful STM images of the QD chain surface after 10.7 ML InGaAs deposition on the GaAs(001) substrate.

1.3.2 QD Volume Measurement

In the study of self-assembled growth, previous quantitative measurements about the size distribution of the 3D islands have been done using a simple assumption, i.e., the QD is a simple shape such as a dome or truncated oval shape.^{37, 38} However, real QD shapes are more like a oblate ellipsoid shape, or even more complicate shapes. Hence, the QD volume analysis approach presented here yields more precise estimations for the various sizes and shapes of nanostructures fabricated by the proposed growth method. It starts with a volume calculation of one slice of a QD. Figure 1.21 shows the top view (a) and 3D view (b) of a QD. The surface area and volume of the QD is calculated from the summation of those slices. Thinner slices can be used for more accurate calculation. The average thickness of a slice in our calculation is 2 nm. To calculate the

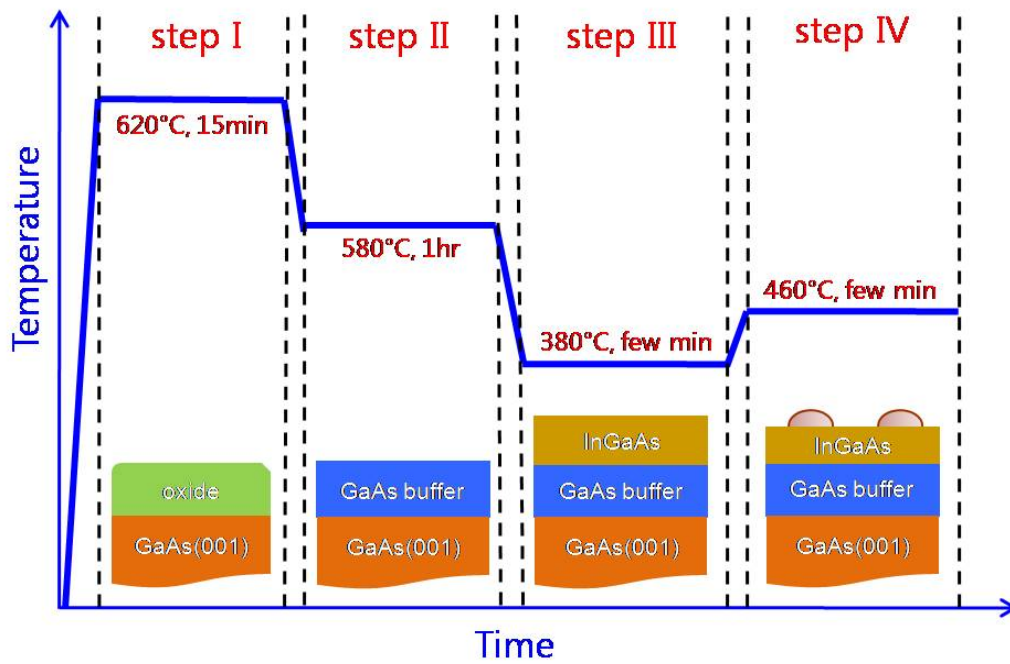


FIG. 1.19. Novel growth mode of $\text{In}_{0.4}\text{Ga}_{0.6}\text{As}$ QD growth with a cross-sectional schematic of QDs.

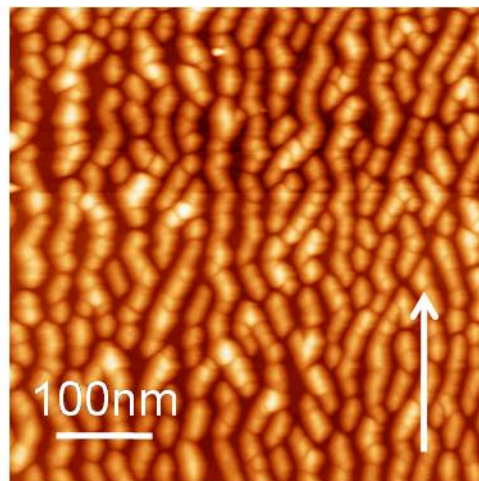


FIG. 1.20. STM image of InGaAs/GaAs QD chain obtained by annealing at 460°C . The image size is $500\text{ nm} \times 500\text{ nm}$. The bias voltage was -3.0 V and the tip current was 0.08 nA . The arrow indicates the $[1-10]$ dimer row direction.

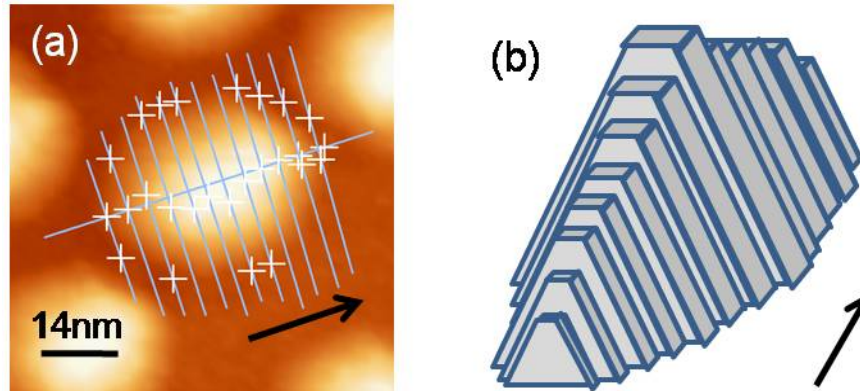


FIG. 1.21. Proposed volume calculation models with (a) as a top view of an STM image of InGaAs QD to measure the width, height, and thickness of a slice. The arrow indicates the $[1-10]$ dimer row direction. Size is $70 \text{ nm} \times 70 \text{ nm}$, and (b) is the schematic for a summation of all slices needed to calculate the total QD volume. The arrow in (b) indicates the same direction with the arrow in (a).

total volume of QDs, height-volume or surface area-base area correlation factors are used. These correlation factors are collected from different shapes of QDs under different growth parameters. Then, all QDs in a certain area are classified by this factor to estimate the total QD volume.

References

- [1] John A. Venables, *Introduction to Surface and Thin Film Processes* (Cambridge University press, Cambridge, 2000).
- [2] J. A. Venables, G. D. T. Spiller, and M. Hanbuecken, *Rep. Prog. Phys.* **47**, 399 (1984).
- [3] G. Biasiol et al., *Appl. Phys. Lett.* **87**, 223106 (2005).
- [4] T. R. Ramachandran, R. Heitz, P. Chen, and A. Madhukar, *Appl. Phys. Lett.* **70**, 640 (1997).
- [5] D. Bimberg, M. Grundmann, and N. N. Ledentsov, *Quantum Dot Heterostructures* (John Wiley & Son, New York, 1988).
- [6] Werner Seifert, N. Carlsson, M. Miller, M-E. Pistol, L. Samuelson, and L.R. Wallenberg, *Prog. Crystal Growth and Charat.* **33**, 423(1996).
- [7] A. Zangwill, *Epitaxy: Physics at Surfaces* (Cambridge University Press, New York, 1988).

- [8] D. J. Kim, D. Cha, G. J. Salamo, and H. Yang, *J. Vac. Sci. and Technol. B* **24**, 2776 (2006).
- [9] D. J. Kim, E. A. Everett, and H. Yang, *J. Appl. Physics* **101**, 106106 (2007).
- [10] D. J. Kim and H. Yang, *Nanotechnology* **19**, 475601 (2008).
- [11] J. Abel, D. J. Kim, E. A. Everett, and H. Yang, *J. Crystal Growth* **310**, 2244 (2008).
- [12] A.Y. Cho and J. R. Arthur, *Prog. Solid-State Chem.* **10**, 157 (1975).
- [13] M. A. Herman, *Molecular Beam Epitaxy* (Springer-Verlag, New York, 1989).
- [14] H. H. Farrell and C. J. Palmstrøm, *J. Vac. Sci. Technol. B* **8**, 903 (1990).
- [15] V. P. Labella et al., *Surf. Sci. Rep.* **60**, 1 (2005).
- [16] D. K. Biegelsen, R. D. Bringans, J. E. Northrup, and L. E. Swartz, *Phys. Rev. B* **41**, 5701 (1990).
- [17] V.P. LaBella, H. Yang, D.W. Bullock, P.M. Thibado, P. Kratzer, and M. Scheffler, *Phys. Rev. Lett.* **83**, 2989 (1999).
- [18] W. G. Schmidt, S. Mirbt, and F. Bechstedt, *Phys. Rev. B* **62**, 8087 (2000).
- [19] G. Binning, H. Rohrer, C. Gerber, and E. Weibel, *Phys. Rev. Lett.* **50**, 120 (1983).
- [20] G. Binning, H. Rohrer, C. Gerber, and W. Weibel, *Phys. Rev. Lett.* **49**, 57 (1982).
- [21] A. J. Melmed, *J. Vac. Sci. Technol. B* **9**, 601 (1991).
- [22] L. J. Whiman, J. A. Strosio, R. A. Dragoset, and R. J. Celota, *Science* **251**, 1206 (1991).
- [23] The SPM SO V2.2 Software Manual, Omicron Nanotechnology (1993).
- [24] H. Gao and W. D. Nix, *Annu. Rev. Mater. Sci.* **29**, 173 (1999).
- [25] L. Vegard, *Z. Phys.* **5**, 17 (1921); *Z. Kristallogr.* **67**, 239 (1928).
- [26] A. Pimpinelli and J. Villain, *Physics of Crystal Growth* (Cambridge University Press, New York, 1988).
- [27] P. Bhattacharya et al., *Annu. Rev. Mater. Res.* **34**, 1 (2004).
- [28] *MBE Stage Part Manual*, MI, SVTA Company (2005).

- [29] V. P. LaBella, D. W. Bullock, C. Emery, Z. Ding, and P. M. Thibado, Appl. Phys. Lett. **79**, 3065 (2001).
- [30] V. P. Labella, M. R. Krause, Z. Ding, and P. M. Thibado, Surface Science Reports **60**, 1 (2005).
- [31] T. Hashizume, Q. Xue, J. Zhou, A. Ichimiya, and T. Sakurai, Phys. Rev. Lett. **73**, 2208 (1994).
- [32] W. Braun, *Applied RHEED: Reflection High-Energy Electron Diffraction During Crystal Growth* (Springer, New York, 1999).
- [33] Y. Tu and J. Tersoff, Phys. Rev. Lett. **93**, 216101 (2004).
- [34] P. B. Joyce et al. Phys. Rev. B **58**, R15981 (1998).
- [35] N. Liu, J. Tersoff, O. Baklenov, A. L. Holmes, Jr., and C. K. Shih, Phys. Rev. Lett. **84**, 334 (2000).
- [36] D. J. Kim, E. A. Everett, and H. Yang, J. Appl. Phys. **101**, 106106 (2007).
- [37] G. Biasiol, S. Heun, et al., Appl. Phys. Lett. **87**, 223106 (2005).
- [38] D. K. Biegelsen, R. D. Bringans, J. E. Northrup, and L. E. Swarts, Phys. Rev. B **41**, 5701 (1990).

CHAPTER 2

ENABLING *IN SITU* ATOMIC SCALE SURFACE IMAGES FOR VERTICAL MOLECULAR BEAM EPITAXY MACHINE*

2.1 Introduction

Optical properties of nanostructures such as quantum dots (QDs) and quantum wires (QWRs) are directly dependent on their size and shape. To optimize growths of novel nanostructures, information on morphology is fundamental. Also, the atomic scale study requires the ability to examine *as-grown* surfaces of novel nanostructures. To investigate contamination-free atomic scale surface morphologies, a quick and reliable sample transfer mechanism is needed to move samples from a molecular beam epitaxy (MBE) growth chamber to a scanning tunneling microscopy (STM) chamber, without exposing the samples to air.

We describe a STM sample transfer design and its integration into a *vertical* MBE system instead of *horizontal* growth chambers^{1,2,3} with which successful *in situ* surface images of QDs and QWRs were reported.^{4,5} This system enables us to transfer STM tips, STM samples for UHV cleaving, and STM sample plates between a MBE and a STM machine.

2.2 MBE System Description

The MBE system (SVTA, model BLT-N35) consists of three functional modules; load lock, preparation, and growth chambers. The growth chamber has a vertical configuration with the source cells pointing vertically upward. The growth front is on a horizontal plane, i.e., the wafers are always horizontal, facing down during the loading, transferring, and growth processes.

Samples are introduced into the preparation chamber through a quick access hatch located on top of the cylindrical load-lock chamber. The unmodified, factory supplied, cassette can accommodate up to ten 4 in. wafers. The load-lock chamber sits on top of the preparation chamber, which is attached to the growth chamber at right angle. A rack and pinion linear

*Dong Jun Kim, Deokjoon Cha, Gregory J. Salamo and Haeyeon Yang.

transporter or “elevator” in the preparation chamber moves the cassette vertically from/to the load-lock chamber to/from the preparation chamber. A magnetic linear motion drive in the preparation chamber is used to transfer samples horizontally from/to the MBE growth chamber. To unload a sample from the cassette, a factory-provided sample-handling fork at the end of the magnetic drive goes between the stacks of the cassette, “lifts” one moly platen when the cassette moves down, and moves out of cassette horizontally. Then the magnetic drive loads the sample into a sample heater in the prep chamber and/or into the growth chamber.

2.3 STM System Attachment

A commercial STM (Omicron RT-STM) system was attached to the preparation chamber for analysis of epitaxially grown samples. A custom-made, 13 in. diameter spherical vacuum chamber connects the STM imaging station chamber and the MBE preparation chamber. This chamber has a total of 16 ports with two 8 in., one 6 in., three 4.5 in. and ten 2.75 in. metal seal flanges. These ports can accept various viewports, vacuum pumps, manipulators, e-beam guns, and vacuum measurement gauges. The STM system is mounted on a rubber vibration isolator to reduce vibrational noise from the floor.

Two blank 8 in. UHV Conflat (CF) metal seal flanges are modified to hold 2.75 in. CF flanges with 1.5 in. inner diameter opening along the centerline (see Fig. 2.1). The 2.75 in. CF flanges allow mounting a 12 in. long rotatable wobble stick (Thermonics, FWS-44R-275-2) and a 48 ft long magnetic liner-transfer drive (VG Scienta) on a flange opposite to the STM chamber. The 2.75 in. out-diameter glass viewport flange and an UHV electrical break are mounted on the modified 8 in. flange on the STM side. A bellows for vibration isolation is mounted on the spherical chamber and a UHV 2.75-in. out-diameter gate valve is attached to the electrical break

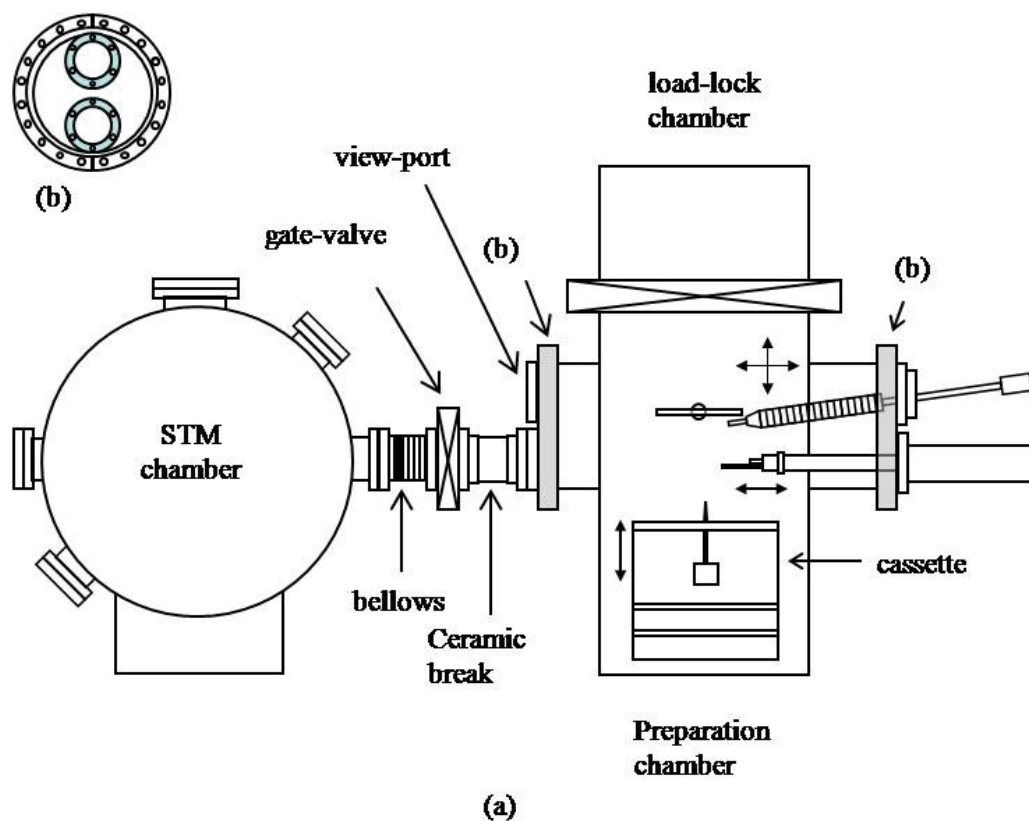


FIG. 2.1. (a) Schematic side view of the preparation chamber and STM chamber (not to scale). The STM chamber is connected to the preparation chamber by a ceramic break and bellows. The inside arrows indicate directions of each motion. (b) Schematic front view of the 8-inch diameter flange with two holes for 2.75-inch flanges. These flanges have replaced the existing 8-inch blank flanges in the preparation chamber.

in series. A two-pronged transfer head (Omicron) is attached at the end of the new transfer rod. This combination enables the transfer of STM sample plates from the MBE preparation chamber to the STM chamber.

2.4 Cassette and Transfer Line Modifications

A cassette is the main component of the sample loading/ unloading system. We modified the cassette to hold STM sample plates and transfer them from the preparation chamber to the spherical chamber for *in situ* imaging. Also, STM sample plates for cross-sectional imaging can be loaded into the modified cassette. After imaging, the samples can be moved back to the cassette for unloading.

To bring a STM sample plate into the MBE growth chamber, a molybdenum sheet with 0.100 in. thickness was machined to a 4 in. diameter circular platen to fit on the rack of the cassette [see Fig. 2.2(b)]. This moly platen has a square opening area which conforms to the shape of the STM plates, allowing the source flux to condense on a substrate surface. The opening area has a recessed step [gray area in Fig. 2.2(a)] about 0.040 in. thick to expose the sample surface below the horizontal plane of the moly platen (see Fig. 2. 2). This allows a clear path from the electron gun, to the sample, and then to the phosphorous screen so that real time surface analysis through reflection high energy diffraction is possible during MBE growths.

During the MBE growth as well as the transfer from the preparation chamber to the growth chamber, sample wafers including STM sample plates are held by gravity only on the step edge of the opening without any fastener.

To remove the STM sample plate from the modified moly platen, a 0.7 in. long pin is mounted vertically on the top center of the cassette. Using the magnetic transfer rod, the STM

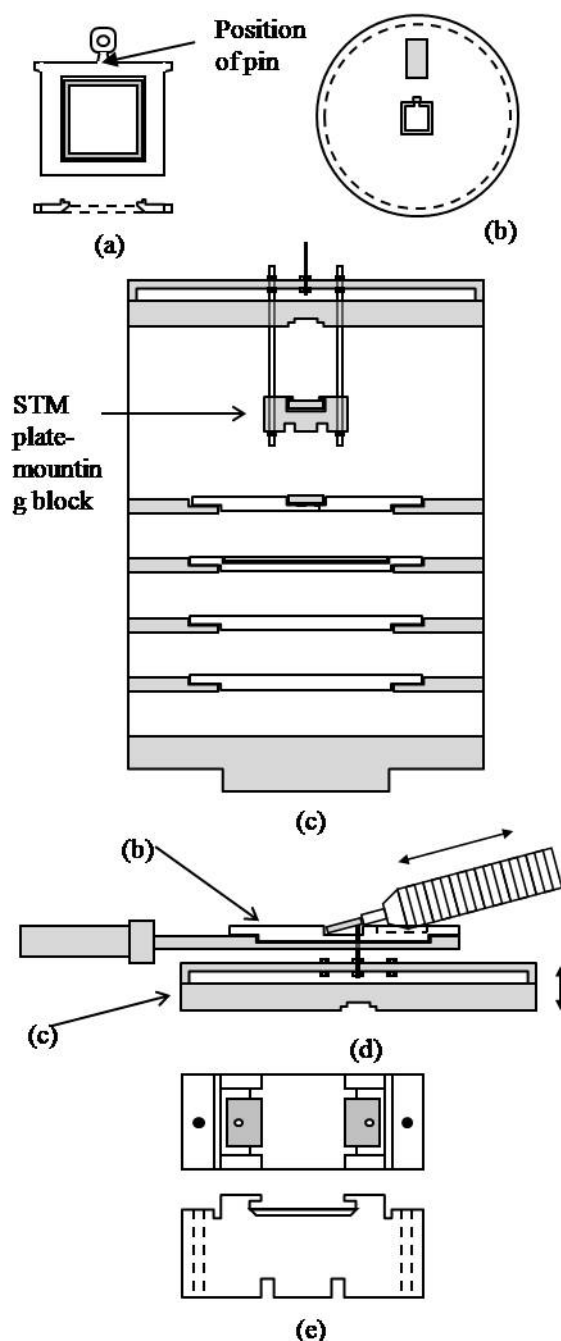


FIG. 2.2. Schematic diagrams of (a) a home-made tantalum STM sample plate, (b) a home-made 4 in. diameter moly-block to grow a STM sample in the MBE chamber (a STM moly block), and (c) a modified cassette with a STM block attached in the middle and a pin on the top. A transfer process using a wobble stick (on the right) and a magnetic drive (on the left) is shown in (d). The 4 in. STM moly block stays on the fork of the magnetic drive during removal of the sample plate. The elevator moves the modified cassette up, pushing the neck of the STM sample plate up at an angle. The plate is then picked up by a wobble stick with a pincer, shown at the right top of (d). (e) is a diagram of the STM plate mounting block, top view (upper drawing) and side view (lower drawing).

sample plate in the moly platen is positioned above the cassette in such a way that the pin can be aligned with the “neck” of the sample plate [see Fig. 2.2(a)]. When the cassette moves up, the pin pushes the neck up so that the STM sample plate is raised out of the custom-made moly platen at an angle. The head of the STM plate is raised up about 0.2 in. from the horizontal plane [see Fig. 2.2(d)]. The head of the STM sample plate is at a right angle with the magnetic drive, pointing toward the wobble stick. The wobble stick then approaches the sample plate following a recessed track [gray rectangular area in Fig. 2.2(b)] on the moly platen and picks up the sample plate by grabbing the head with the end jaws [Fig. 2.2(d)]. It is attached at the upper port on the custom-made 8 in. flange, opposite to the STM chamber [see Fig. 2.1]. So far, the sample surface has been face down. To have the sample surface face up, the wobble stick makes 180° rotation. With the wobble stick being held against the flange, the magnetic drive retracts to clear space for the cassette to move upward to about the same height as the wobble stick. The wobble stick then inserts the plate into the slot of a home-made stainless block in the cassette [see Fig. 2.2(c)]. The plate is now positioned with the sample face up, held by a pair of brackets, and ready to be transferred into the STM chamber.

The stainless steel block was attached at the bottom of the top handle of the cassette. The block is to hold STM sample plates or STM tip carrier plates. The block is designed to engage an Omicron sample-handling head with two prongs. The head can load/unload Omicron STM sample plates from/to the slot when it is attached at the end of a magnetic drive with 360° rotation. A “new” drive transfers STM sample plates, sample plates for UHV cleaving, and STMtip carrier plates to/from the 13 in. spherical chamber from/to the MBE preparation chamber. This 48 ft magnetic drive is attached to the lower port of the modified 8 in. flange in the preparation chamber (Fig. 2.1, below the wobble stick). An Omicron provided commercial

sample-handling head (push-pull transfer head) is attached to the end of the magnetic rod. This head removes the plate from the slot and loads the plate into the manipulator in the chamber. A slot with brackets is attached at the end of the manipulator [similar to Fig. 2.2(e)]. The manipulator moves the STM sample plate or the STM tip carrier plate close to the imaging station, where an Omicron provided wobble stick removes the plate from the manipulator and places it into either the imaging stage or the carousel.

2.5 Summary

The modifications enabled us to get successful STM images from *as-grown* surfaces. The reconstruction structure of a MBE grown GaAs(001) surface was confirmed by the *in situ* STM by transferring the sample using the modifications made. Figure 2.3(a) shows an example of InGaAs quantum dots formed on a GaAs(001) surface via the Stranski-Krastanow growth mechanism.⁶ All the STM images in Fig. 2.3 were taken with a sample bias of -3 V (filled electronic state) at the constant current mode with a feedback set current of 0.1 nA. The modification also allowed us to load substrates for cleaving a cross-section STM. The UHV cleaving of (001) oriented substrates exposes (110) surfaces similar to GaAs(110) surfaces.⁷ Figure 2.3(b) shows STM images of an InP(110) surface with step height of ~ 0.2 nm, produced by UHV cleaving of InP(001) surfaces. The rectangle in the inset of Fig. 2.3(b) represents the unit surface area of (110) surface of an InP substrate.

References

- [1] L. J. Whitman *et al.*, J. Vac. Sci. Technol. B **14**, 1870 (1996).
- [2] J. B. Smathers *et al.*, J. Vac. Sci. Technol. B **16**, 3112 (1998).
- [3] M. Krause *et al.*, J. Vac. Sci. Technol. B **23**, 1684 (2005).

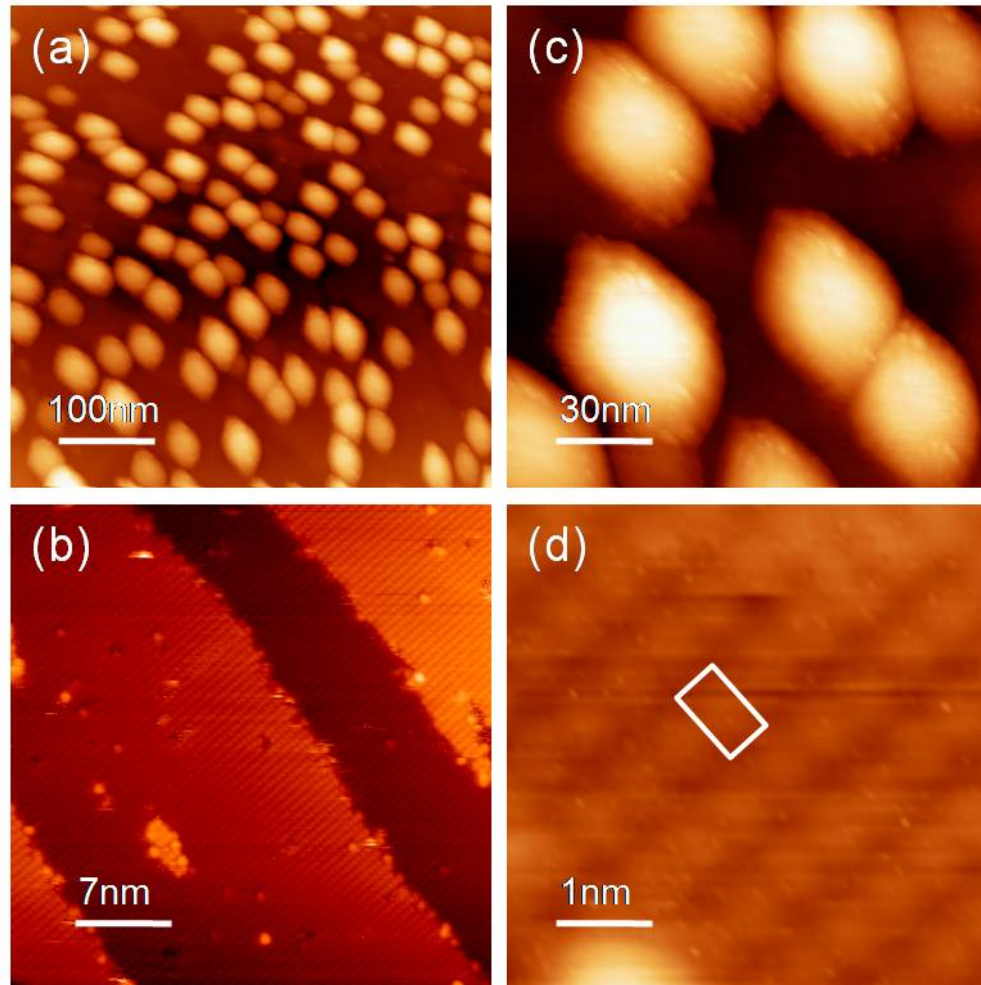


FIG. 2.3. STM images of (a) and (c) are InGaAs QDs as-grown on a GaAs(001) surface. The scan area is $500 \times 500 \text{ nm}^2$ for (a), $150 \times 150 \text{ nm}^2$ for (c). STM images of (b) and (d) are a cleaved InP(110) surface. The scan area is $35 \times 35 \text{ nm}^2$ for (b), $5 \times 5 \text{ nm}^2$ for (d), The rectangle in the (d) is the size of the surface unit cell of an InP(110) surface.

- [4] Haeyeon Yang, P. Ballet, and G. J. Salamo, J. Appl. Phys. **89**, 7871 (2001).
- [5] Haeyeon Yang *et al.*, J. Appl. Phys. **91**, 3925 (2001).
- [6] D. Bimberg, M. Grundmann, N. N. Ledentsov, *Quantum Dot Heterostructures* (John Wiley & Son, New York, 1988).
- [7] C. K. Shih *et al.*, Phys. Rev. B **40**, 10044 (1989).

CHAPTER 3

ANNEALING INDUCED TRANSITION OF FLAT STRAINED INGAAS EPILAYERS INTO THREE-DIMENSIONAL ISLANDS*

Abstract

We report a novel array of self-assembled quantum dots through roughening transformation of strained but atomically flat layers into three-dimensional (3D) islands. *Atomically flat* two-dimensional InGaAs epilayers were grown on GaAs(001) substrates below 360°C. When heated higher than 420°C, they were observed to undergo roughening transitions. The morphology, height and width, of the resultant 3D features were found to be a strong function of the annealing time and temperature. Furthermore, at a certain set of parameters, dot-chains were observed. The strain field of the flat layer seemed uniform in the roughening stage, but induces anisotropic diffusion at the subsequent growth stage.

3.1 Introduction

Self-assembled quantum dots (SAQDs) show promises for future optoelectronic devices as an alternative approach to traditional top-down techniques because SAQDs can have small enough defective surface states commonly found in a top-down process,¹ as evidenced in commercially available lasers based on SAQDs.² The potential of SAQDs for the optoelectronic devices is due to the fact that the electronic structures can be controlled by controlling the size and shape. Tremendous research effort has been focused^{3, 4} to find ways to control the shape and size of SAQDs, including the recent report on QD chains.⁵

Traditionally, SAQDs were reported to form during a deposition period either with or without growth interruption through the Stranski-Krastanov (SK) growth mode. Nucleation and growth of SAQDs depend on the substrate temperature and strain amount. For example, strained but smooth In_{0.5}Ga_{0.5}As epilayers were reported on GaAs(001) at 320 °C, mismatch of 3.5%

*Dong Jun Kim, Deokjoon Cha, Gregory J. Salamo and Haeyeon Yang.

while a mismatch of 7.2% resulted in SAQDs at the same substrate temperature.^{6,7} In this study, we grew *strained-but-flat* InGaAs with an indium composition of 37% on GaAs(001) substrates layer by layer at low temperatures, instead of layer-then-island fashion.⁸ Subsequent annealing at a higher temperature enabled us to focus on the effect of strain and strain-induced diffusion on nucleation and growth.

3.2 Experimental Procedure

The growth studies were done using a commercial molecular beam epitaxy (MBE) machine, SVTA model BLT-35N, and a commercial ultrahigh vacuum (UHV) scanning tunneling microscope (STM) attached to the MBE machine through a UHV port for *as-grown* surface images.⁹ An n-type GaAs substrate with a nominal (001) orientation was loaded into the load-lock chamber, then into a preparation chamber of mid- 10^{-10} torr of vacuum. The wafer was outgassed in the preparation chamber at 300 °C for 30 min before it was loaded into the growth chamber. After the oxide layer was removed at 580 °C under arsenic pressure, confirmed by reflection high energy electron diffraction (RHEED), a 1- μ m thick GaAs buffer was grown on the substrate at 580 °C at a growth rate of 0.5 m/h.

The substrate was then cooled down below 400 °C, where about 8~10 ML (monolayer) InGaAs was deposited on the buffer layer. The InGaAs growth rate was 0.17 ML/ s, measured from RHEED oscillations in real time, with an arsenic flux of 2×10^{-6} torr.¹⁰ The oscillations were persistent to the end of the growth, confirming layer-by-layer growth, quite similar to those of a GaAs buffer grown on a GaAs(001) substrate. The indium composition, ~37%, was estimated by subtracting the GaAs growth rate from that of the InGaAs, both grown at the same temperature. Next, the substrate with two-dimensional (2D) InGaAs epilayers was moved to the UHV-STM

chamber through a UHV port.⁹ After STM examinations, the same samples were moved back to the MBE growth chamber, then heated up to 440, 460, and 480 °C at a rate of 20 °C/min under arsenic fluxes of 1.4×10^{-6} , 5.9×10^{-6} , and 5.9×10^{-6} torr, respectively, and annealed for 2 min. After annealing, the substrates were rapidly cooled by turning power off to the substrate heater. The substrate temperature decreased at a rate of 100 °C/min down to 300 then 50 °C/min down to 200 °C when the substrates were removed from the growth chamber.

The weak fractional order peaks of the RHEED patterns taken before, during, and after the InGaAs depositions show streaks, which suggests that the growth front had a mixture of 2×4 and $c(4 \times 4)$ surface reconstructions. The RHEED patterns showed no chevrons during the InGaAs deposition and cool down processes, although chevrons, similar to those from InAs QDs on GaAs(001) substrates, were observed from samples grown at higher temperatures with the same thickness.¹¹

3.3 Strained Pseudomorphic $\text{In}_{0.4}\text{Ga}_{0.6}\text{As}/\text{GaAs}(001)$

The surface morphology of the InGaAs epilayer was imaged at room temperature for the filled surface state which confirmed that the strained layers were atomically smooth across the whole sample surface. Figure 3.1(a) is a STM image taken from the strained 2D surface. All STM images were obtained using bias voltage -3.0 V (filled state) at constant current mode with 0.1 nA. The speckles on the large (500 nm) scale image are 1 ML high islands, as confirmed by high resolution images [see Fig. 3.1(b)]. The center of the inset shows one such island with the image size of 10 nm. The high resolution STM images also confirmed that the surface had a mixture of the surface reconstructions.

During the heating up process after the STM imaging, the InGaAs epilayers showed no chevrons in the RHEED pattern up to 370 °C. Chevrons began to show up at 380 °C and

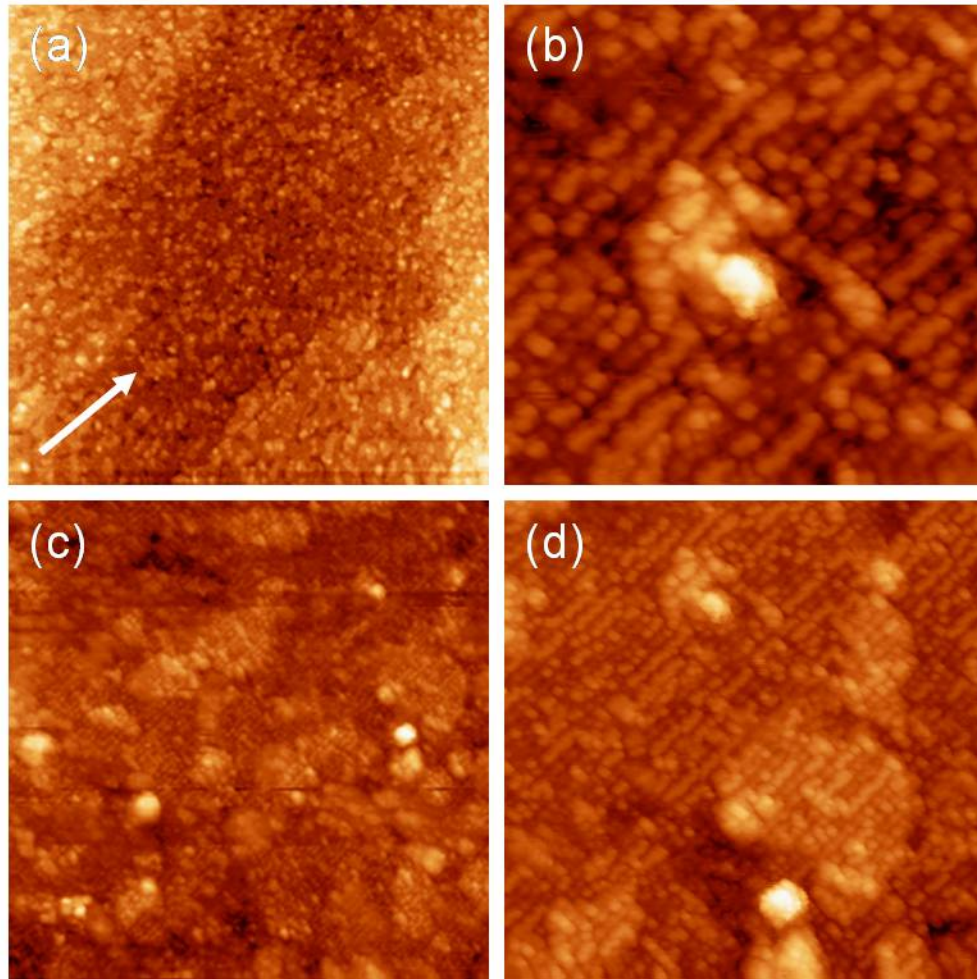


FIG. 3.1. All STM images were obtained using -3V (filled state) with constant current mode at 0.1nA ; (a) is a $500\text{nm} \times 500\text{nm}$ STM image of the 10.24ML thick InGaAs epilayer grown at 360°C . The speckles in (a) are one monolayer high islands, which is confirmed by a high resolution picture of $50\text{nm} \times 50\text{nm}$, (b). (c) is $100\text{nm} \times 100\text{nm}$. In image (b), two 1ML high islands are noted. (d) is $14\text{nm} \times 14\text{nm}$ for the island in (b) (near top center). The arrows in the images indicate the $[1-10]$ azimuthal direction.

increased in brightness as the temperature was increased. Eventually diffraction peaks from the formation of three dimensional (3D) features dominated around 410 °C, at which temperature the fractional order peaks all disappeared. During the annealing period, however, the brightness of the chevron peaks stayed almost the same.

After the annealing, the substrates were moved back to the STM chamber for imaging the surface morphology. The STM images confirmed transformation of the 2D strained epilayers into 3D islands. Figure 3.2(a) shows a STM image from the sample annealed at 460 °C for 2 min. For comparison, STM images from a sample grown continuously at 450 °C are shown in Fig. 3.2 (b). The separation between dots formed by annealing was more uniform and had a narrower distribution than those formed by continuous growth, as shown in Fig. 3.2(b). Large flat void areas are visible, similar to other published images.^{12,13} The void areas were not noticeable in the STM images of the annealed samples.

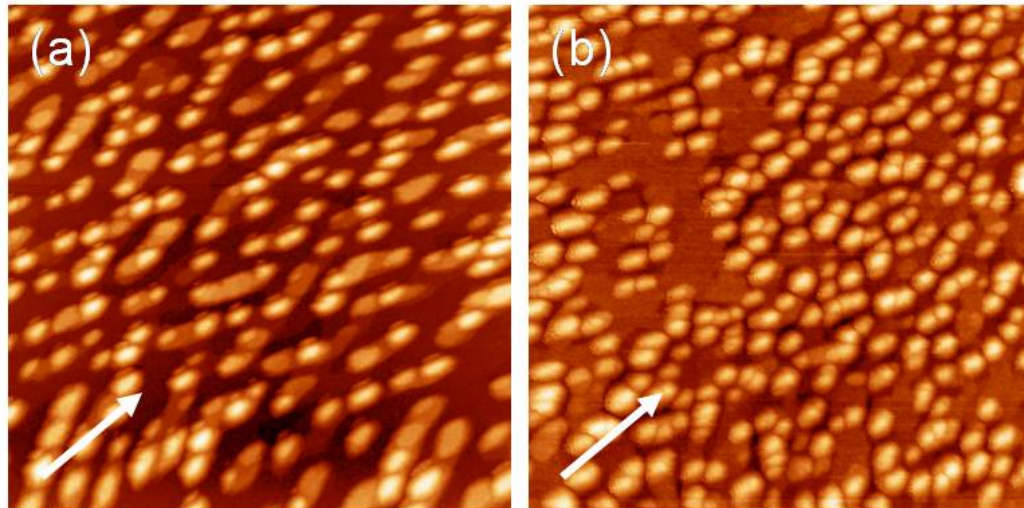


FIG. 3.2. STM images of an InGaAs SAQDs. (a) A large 500nm \times 500nm image shows SAQDs by annealing the 8.85ML InGaAs flat epilayers at 460°C for two minutes. Image (b) is for 9.07ML InGaAs SAQDs by a continuous S-K growth at 450°C. The arrows in the images indicated the [1-10] direction. The arrows in the images indicate the [1-10] azimuthal direction.

3.4 Annealing Temperature Effect

The morphology of the annealed dots depends on the annealing temperature. Figure 3.3 shows STM images of samples annealed at 440, 460, and 480 °C for (a) 10.13 ML, (b) 10.24 ML, and (c) 9.75 ML, respectively. The dots annealed at higher temperatures have larger base areas (width and length) but reduced heights and lower density than those annealed at lower temperatures. Clearly, the strained InGaAs epilayers were transformed into dots with shorter heights and larger widths by annealing at a high temperature, where the bases of the dots connected to each other. The measured mean values of dot height (width) are 10.4 ± 1.3 (26.4 ± 3.6), 8.3 ± 1.4 (29.6 ± 3.8), and 6.7 ± 1.5 nm (36.1 ± 7.2 nm) for annealing temperatures of 440, 460, and 480 °C, respectively. The morphology of a SAQD can be, therefore, controlled by the parameters of the annealing such as annealing period and temperature.

3.5 $\text{In}_{0.4}\text{Ga}_{0.6}\text{As}$ QD Chain Formation

Striking features were observed on the sample annealed at 460 °C, where the dots had a smaller width and longer length than those annealed at 440 °C. The dots were aligned along straight lines, forming dot chains. The alignment had rather abrupt kinks with obtuse angles of about 120°. The turning points were well defined and clearly visible in Fig. 3.3(b) while they were not as noticeable in images from samples annealed at higher [Fig. 3.3(c)] and lower [Fig. 3.3(a)] temperatures. The dot chains are mostly off the [1-10] direction, as shown in Fig. 3.1(b). The majority of the dot chains are aligned along the azimuthal directions of [5-10], [5-20], and [1-50]. Less than 5% of the total length of the dot chains is along the [1-10] direction. This is significantly different from other elongation examples of dot chains, as published by Wang et al.⁵ using stacked strained layers of InGaAs/GaAs; those by Leon et al.¹⁴ and Jeppesen et al.¹⁵ where dot chains were observed along the step edge direction. The reported dot chains are mostly

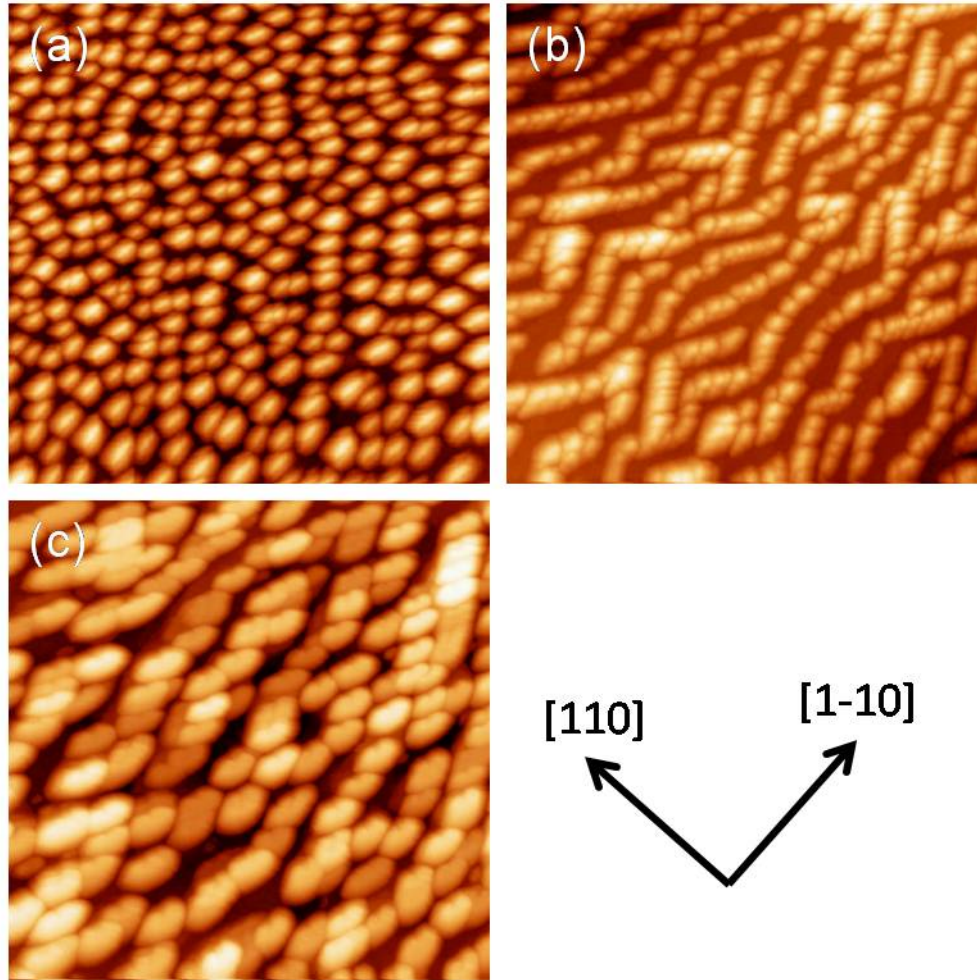


FIG. 3.3. Annealing temperature effect on morphology; $500\text{nm} \times 500\text{nm}$ STM images for the InGaAs QDs formed through roughening transformation during the annealing period of two minutes but at different annealing temperatures, (a) at 440°C , (b) 460°C and (c) 480°C . The InGaAs strained layers were grown at 360°C and the thickness were 10.13ML for (a), 10.24ML for (b), and 9.75ML for (c), respectively.

aligned along the dimer row direction, $[1-10]$ direction, of GaAs (001) substrates. Formation of dot chains was also observed by direct deposition of InGaAs on GaAs in our recent results (unpublished). These dot chains were aligned along the $[1-10]$ direction.

At first glance, the dots in the dot chains seemed elongated along the chaining directions. However, preliminary analysis¹⁶ of the STM images of the dot chains showed that the individual dots have similar morphologies to other InGaAs dots that were elongated along the $[1-10]$ direction, although the dot chains were aligned in several different directions. The InGaAs dots in the dot chain were taller than those of the recent STM study¹⁷ on InAs dots on GaAs(001). The facet planes of the dots in the dot chains were identified as $\{135\}B$ at the base while $\{137\}A$ at the top for those dots in the dot chain elongated along the $[1-50]$ direction. Also, the facet plane depends on the size of the dot in the dotchain. This confirms the similar RHEED observations for the dot chains and those of InAs/GaAs SAQDs.¹¹

The alignment of dots was not apparent in lower temperature annealing. Higher temperature annealing, however, resulted in flattened but elongated dots. The elongation is along the dimer row, the $[1-10]$ azimuthal direction. It was reported that adatom diffusion along the $[1-10]$ direction was faster than that along the $[110]$ direction for Ga adatom diffusion on GaAs(001),¹⁸ and an even faster track for In adatoms on strained surfaces.¹⁹ It is obvious that the role of diffusion becomes significant for the morphology of 3D features during the annealing processes at higher temperatures. Similar behavior was reported^{20, 21} for the growth of InAs quantum wires, which were aligned along the dimer row direction of InP001 substrates due to higher diffusion along the $[1-10]$ azimuthal direction.

Our STM images from samples annealed at different temperatures suggest that the alignment is a dynamic process, driven by diffusion. No dot chains were observed by STM

(unpublished) when the annealing period was as short as 20 s instead of 120 s. The strain field influenced the detachment process for uniform supplies of surface adatoms for the initial nucleation of precursors. In the subsequent annealing process, strain driven, anisotropic diffusion takes over for the subsequent growth of the precursors into dots and dot chains. The observation of dot alignment at 460 °C indicates the precursor nucleation was random in the beginning because no chaining is observed at the lower temperature, as seen in Fig. 3.3(a). The effect of higher temperature can be attributed to the increase in the mobility of the detached surface atoms, inducing a higher detachment rate due to increased chemical potential and longer lifetime of adatoms. The comparison reveals that the self-assembly is a subtle, but still plausible, technique to produce arrays of uniformly sized quantum dots.

3.6 Summary

In summary, we have observed that annealing induced roughening transition (nucleation) from *strained-but-flat* 2D layers to 3D islands. Our *in situ* STM results suggest that the strain field induces isotropic detachment of adatoms, which generates a more uniform density of adatoms on the surface than that of regular, continuous layer-then-island growth. Surprisingly, dot chains were observed at a specific set of annealing parameters. The growth during the annealing period is a strong function of temperature and period of annealing. The morphology of the resultant 3D features suggests that diffusion depends on the strained layer to be anisotropic.

References

- [1] P. Bhattacharya, S. Ghosh, and A. D. Stiff-Roberts, *Annu. Rev. Mater. Res.* **34**, 1 (2004).
- [2] See, for example, www.zialaser.com and www.innolume.com
- [3] M. Henini, *Nanoscale Res. Lett.* **1**, 32 (2006).

- [4] S. Kiravittaya, R. Songmuang, A. Rastelli, H. Heidemeyer, and O. G. Schmidt, *Nanoscale Res. Lett.* **1**, 1 (2006).
- [5] Z. M. Wang, K. Holmes, Y. I. Mazur, and G. J. Salamo, *Appl. Phys. Lett.* **84**, 1931 (2004).
- [6] C. W. Snyder, J. F. Mansfield, and B. G. Orr, *Phys. Rev. B* **46**, 9551 (1992).
- [7] M. V. Maximov *et al.*, *Appl. Phys. Lett.* **75**, 2347 (1999).
- [8] D. J. Srolovitz, *Acta Metall.* **37**, 621 (1989).
- [9] D. J. Kim, D. Cha, G. J. Salamo, and H. Yang, *J. Vac. Sci. Technol. B* **24**, 2776 (2006).
- [10] A. Tackeuchi, Y. Nishikawa, and O. Wada, *Appl. Phys. Lett.* **68**, 797 (1996).
- [11] H. Lee, R. Lowe-Webb, W. Yang, and P. C. Sercel, *Appl. Phys. Lett.* **72**, 812 (1998).
- [12] R. Leon and S. Fafard, *Phys. Rev. B* **58**, R1726 (1998).
- [13] F. Patella, M. Fanfoni, F. Arciprete, S. Nufri, E. Placidi, and A. Balzarotti, *Appl. Phys. Lett.* **78**, 320 (2001).
- [14] R. Leon, T. J. Senden, Y. Kim, C. Jagadish, and A. Clark, *Phys. Rev. Lett.* **78**, 4942 (1998).
- [15] S. Jeppesen, M. S. Miller, D. Hessman, B. Kowalski, I. Maximov, and L. Samuelson, *Appl. Phys. Lett.* **68**, 2228 (1996).
- [16] The images were also analyzed using the free software (available at www.nanntec.es).
- [17] M. C. Xu, Y. Temko, T. Suzuki, and K. Jacobi, *J. Appl. Phys.* **98**, 083525(2005).
- [18] H. Yang, V. P. LaBella, D. W. Bullock, Z. Ding, J. B. Smathers, and P. M. Thibado, *J. Cryst. Growth* **201/202**, 88 (1999).
- [19] E. Penev, S. Stojkovi, P. Kratzer, and M. Scheffler, *Phys. Rev. B* **69**, 115335 (2004).
- [20] H. Yang, P. Ballet, and G. J. Salamo, *J. Appl. Phys.* **89**, 7871 (2001).
- [21] H. Yang, X. Mu, I. B. Zotova, Y. J. Ding, and G. J. Salamo, *J. Appl. Phys.* **91**, 3925 (2001).

CHAPTER 4

EFFECT OF ARSENIC OVERPRESSURE ON GROWTH OF PSEUDOMORPHIC INGAAS*

Abstract

A morphological study on pseudomorphic $\text{In}_{0.4}\text{Ga}_{0.6}\text{As}$ surfaces is presented. The InGaAs layers on GaAs(001) were thinner than the critical thickness and grown by Molecular Beam Epitaxy at different arsenic overpressures. The oscillation of the specular beam of reflection high energy electron diffraction indicates that the indium segregation was suppressed significantly at a high arsenic overpressure during growth. The suppression resulted in (2×4) -like surface reconstruction, confirmed by scanning tunneling microscopy (STM). STM images indicate that the surface prepared at a lower arsenic overpressure has mixed reconstructions of 2×4 with depth variations, which suggests suppression of growth in trenches.

4.1 Introduction

Understanding the atomic arrangement on an epitaxial growth front is necessary to create high quality epitaxial layers. For example the atomic arrangement on the surface influences the diffusion kinetics of adatoms for homoepitaxy¹ as well as heteroepitaxy,^{2,3} subsequently affecting quality film growth including self-assembled quantum dots by the Stranski-Krastanov growth mode.⁴ Another important feature of the surface structural study is that the stoichiometry of a surface can be studied by examining surface structures. Reflection high energy electron diffraction (RHEED) has been employed to investigate structural variations over surface stoichiometry for epitaxial growth on GaAs surfaces.⁵ High quality device structures have been realized using the insight gained from the structural analysis on the surfaces of the growth front. For example, the flux ratio of the group V element over the group III element should be kept between 10 and 20 during growth to yield high quality GaAs films for optoelectronic device applications.⁶ As a macroscopic tool, RHEED has been very successful for two-dimensional,

*Dong Jun Kim and Haeyeon Yang (to be published)

layer by layer growths. However, a more accurate, microscopic surface characterization technique such as scanning tunneling microscopy (STM) is necessary to complement the macroscopic tool for devices based on nanostructures such as infrared photodetectors using $\text{In}_{0.4}\text{Ga}_{0.6}\text{As}$ SAQDs⁷ on GaAs(001), because RHEED does not provide enough information for the growth of nanostructures in some cases such as dot-chains⁸ and strain-induced redistribution of indium atoms⁹ in a ternary alloy on a surface.

In this letter, we report detailed structural analysis of pseudomorphic $\text{In}_{0.4}\text{Ga}_{0.6}\text{As}$ on GaAs(001) surfaces using MBE and *in situ* STM. Different V/III flux ratios were employed to control the indium segregation during growths. Local, microscopic surface images of the pseudomorphic surfaces indicate that the surfaces prepared by different growth conditions resulted in markedly different surface reconstructions. The findings indicate that the surface reconstruction of the pseudomorphic InGaAs is not as consistent with the general dependence of arsenic overpressure as that in GaAs(001) surfaces, where the surface structure changes from $\beta 2(2 \times 4)$ to mixture of $\beta(2 \times 4)$ as the stoichiometry of the surface changes toward higher arsenic coverage.⁵

4.2 Experimental procedure

The growth studies were carried out using a molecular beam epitaxy (MBE) machine (SVTA -35N) equipped with a computer controlled, valved arsenic cracker cell and a ultra high vacuum (UHV) STM (Omicron 1) attached to the MBE machine through a UHV port for *as-grown* surface images.¹⁰ An *n*-type GaAs substrate with a nominal (001) orientation was loaded into the load-lock chamber, then into a preparation chamber of mid 10^{-10} torr of vacuum. The wafer was outgassed in the preparation chamber at 300°C for 30 minutes before it was loaded into the growth chamber. The oxide layer was removed at 580°C under arsenic overpressure in the growth chamber, which was confirmed by RHEED. An electron beam voltage 9 kV was used for RHEED. Then, a one micrometer thick GaAs buffer was grown on the substrate at 580°C at a

growth rate of 0.5 μ m/hour. To calibrate the substrate temperature, the oxide-off temperature was used in conjunction with the substrate temperature monitored by RHEED pattern change at a constant arsenic flux.¹¹ The samples were then cooled down to the growth temperature (500°C) for In_{0.4}Ga_{0.6}As deposition of about 4.6 monolayers (ML), confirmed by RHEED oscillations of the specular peak. The V/III flux ratios were 25 and 34 during the pseudomorphic InGaAs growth with the deposition rate of 0.184 ML/sec. The indium composition of 40% was estimated by subtracting the GaAs growth rate from that of the InGaAs, both grown at the same temperature. The epilayer thickness was set to be smaller than the critical thickness of 6ML for the S-K growth mode, which was confirmed in separate MBE-STM experiments, where the RHEED pattern and STM surface images showed chevrons and SAQDs respectively. Upon finishing the InGaAs growth, the substrate was rapidly cooled down by turning power off to the substrate heater,⁸ while closing the arsenic valve within 60 seconds from the end of InGaAs growth. Then the substrate was moved into the STM chamber for imaging the surface morphologies. STM imaging was carried out at constant current mode of 0.1nA with the surface bias -3V relative to the tip for filled state images. STM tips were prepared by electrochemical etching of a polycrystalline tungsten wire under an optical microscope at $\times 1500$ magnification, loaded into the STM chamber, and cleaned *in situ* by electron beam heating.

4.3 RHEED Oscillation Behavior with Different Arsenic Flux

The previous MBE-STM study¹⁰ from this system suggests that the RHEED patterns after buffer growth indicate that the buffer surface was smooth and well ordered with 2×4 surface reconstructions. To quantify the amount of indium segregation during growth, RHEED oscillations during the deposition of the pseudomorphic InGaAs layers have been reported.¹² Figure 4.1 shows the RHEED oscillations during growth of In_{0.4}Ga_{0.6}As with V/III flux ratios of 25(a) and 34(b) with the arsenic fluxes of 4.8×10^{-6} and 6.4×10^{-6} torr, respectively. The segregation factor for (a) was calculated as 0.62 by fitting the oscillation data to the exponential

equations given by Martini *et al.*¹² The coefficient is significantly smaller than the reported value of 0.8 at 500 °C due to the fact that the flux ratio employed is ~4.6 times larger than that reported.¹² This suggests the high arsenic overpressure reduces the segregation of indium because the higher concentration of arsenic on the surface effectively reduces indium segregation as reported by Muraki *et al.*¹³ Although the segregation is reduced, the surface might be highly indium rich due to the “floating” indium effect, almost reaching 100% indium¹⁴ on the outermost layer after 4.6 layers of $\text{In}_{0.4}\text{Ga}_{0.6}\text{As}$ deposition even though the segregation coefficient is small. Effects of further increase of arsenic overpressure are shown in Fig. 4.1(b), which suggests that additional arsenic suppresses the segregation. The RHEED oscillations behavior is different for growth using the same indium composition but at the higher flux ratio as seen in (b). The same exponential equation did not yield a meaningful physical parameter, a negative pre-factor for the oscillation data. In our separate experiments, the similar behaviors in RHEED oscillations were observed at a slightly smaller flux ratio of 32, in which the oscillation behavior is very similar to that of homoepitaxy of GaAs on GaAs(001). This suggests that a high arsenic flux makes pseudomorphic epitaxy more like a regular homoepitaxy, due to the considerable suppression of the segregation. The oscillatory behaviors in Fig. 4.1 seem different from the previous reports by Snyder *et al.*,¹⁵ possibly due to different arsenic fluxes employed.

Comparison of RHEED patterns before and after the InGaAs growths indicates that the surface reconstructions seem similar to that of GaAs(001)-(2 × 4) structures even though the fractional order peak intensities were weaker than those from the buffer layer as seen in Fig. 4.1. The comparison of the spot positions of the first order peaks suggests that the “lateral” surface relaxation was negligible for both cases because there were no noticeable spot position changes as in the RHEED study¹⁶ on the $\text{In}_{0.5}\text{Ga}_{0.5}\text{As}$ growth on GaAs(001).

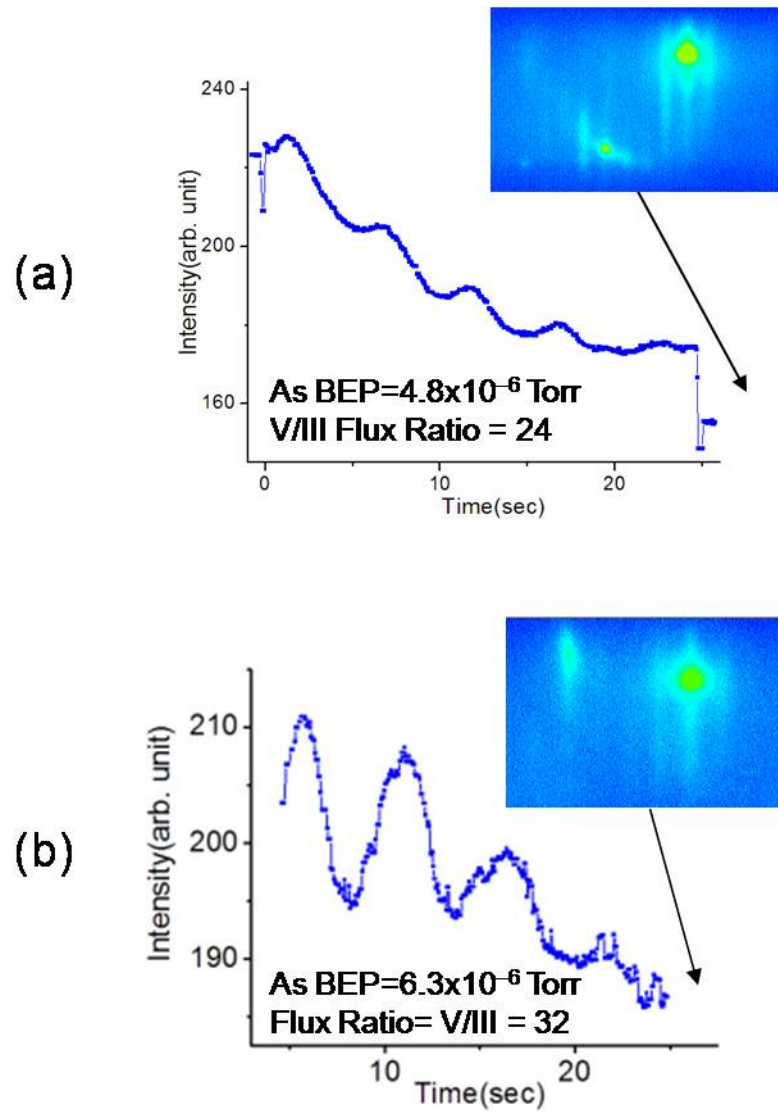


FIG. 4.1. RHEED oscillations for the same growth period (25 seconds) during epitaxial growths at different arsenic overpressures, yielding different V/III ratios of 24 for (a) and 32 for (b). The data points in the first few seconds were not recorded in (b). The corresponding RHEED patterns were taken during cooling down period, after the pseudomorphic growths, at substrate temperature around 300°C. The RHEED patterns were taken with the electron beam pointing along the [110] azimuthal direction, resulting in $4\times$ periodicity. This is similar to the RHEED pattern from the GaAs(001) buffer surface.

4.4 STM Study of Arsenic Overpressure Effect

The surface reconstruction is sensitive to the stoichiometry of a surface because the surface structure depends on bonding directions and strengths of atomic species on a surface.^{5, 11} High resolution surface images complement the macroscopic RHEED patterns to determine the surface structure and stoichiometry more accurately. *In situ* STM images were obtained from these unrelaxed surfaces, as shown in Fig. 4.2, at sizes from 500nm, (a) to Fig. 4.4, 7nm, (d). The images in the left column are from the sample grown at the flux ratio of 25 and those in the right column at 34. Large scale, inset images show no three dimensional dots, consistent with RHEED observations. They show two-dimensional (2D) islands on the surface grown at a lower arsenic overpressure, which is very similar to those¹⁷ from the InAs wetting layer on GaAs(001). These 2D islands were also found in STM images from other $\text{In}_{0.4}\text{Ga}_{0.6}\text{As}$ wetting layers grown at lower temperatures, which showed similar segregation behavior in RHEED oscillations (unpublished). The images from the surface grown under higher arsenic flux did not show these 2D islands on a terrace, which is consistent with the fact that lower arsenic overpressure induces smaller islands on the growth fronts for (001) surfaces of InAs¹⁸ as well as GaAs.¹⁹ Both images show small speckles that seem like arsenic clusters as seen in high resolution images in Fig. 4.2. The similar clusters were observed from samples grown at temperatures lower than 400 °C.⁸

Effects of the arsenic overpressure during growths on the atomic arrangements on surfaces are clearly demonstrated in the high resolution images. Figure 4.2(d) and Fig. 4.3(b) show dimer rows running zig-zag in contrast to straight lines in Fig. 4.2(c) and Fig. 4.3(b) that are from surfaces prepared with a larger arsenic flux. This difference in atomic arrangement may be due to the difference in indium segregation on the surface of Fig. 4.3(b) which has a small, nonnegligible segregation coefficient of 0.62.

Line profiles across the dimer row, [110] direction show that the trench depth in Fig. 4.3(d) is similar to that in Fig. 4.3(c). However, the measured trench depths depend on the

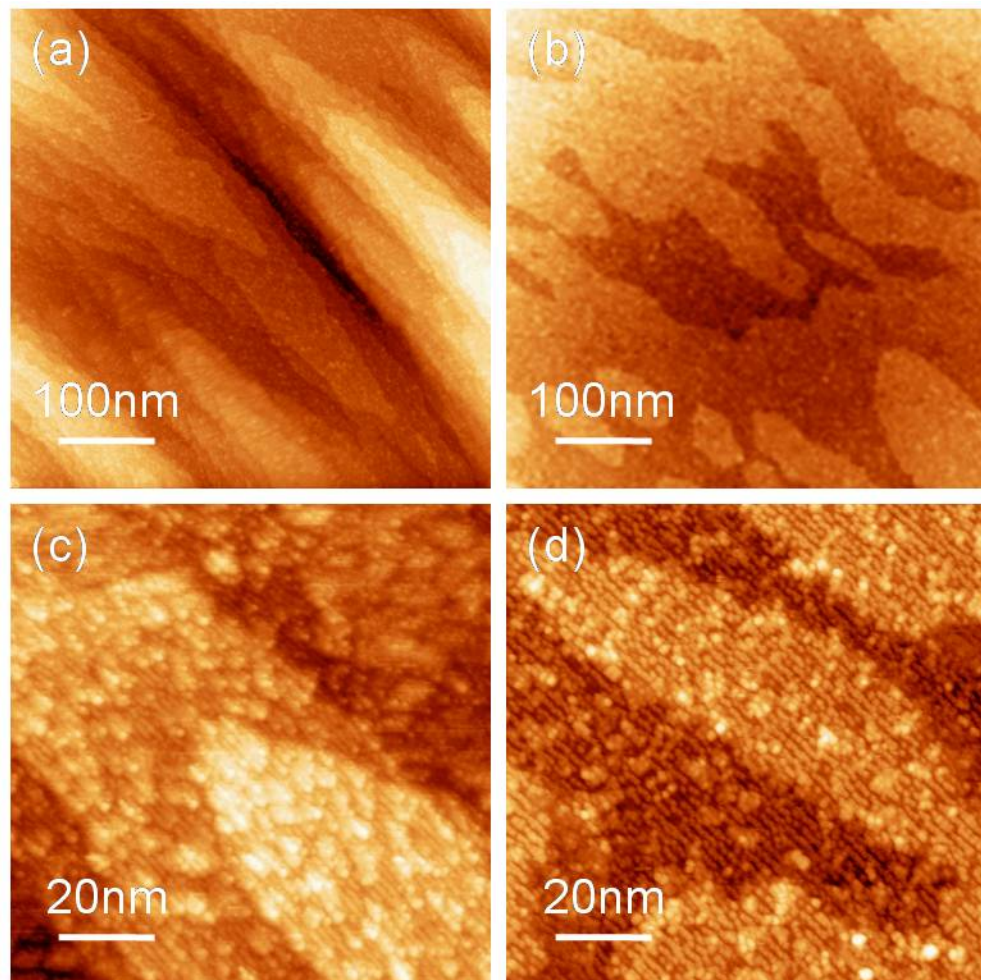


FIG. 4.2. Filled state STM images of the pseudomorphic $\text{In}_{0.4}\text{Ga}_{0.6}\text{As}$ epilayers at different resolutions. The flux ratio of 35 was used during the growth of samples in the left column and 25 for the right one. The sizes of the images are: $500\text{nm} \times 500\text{nm}$ for (a) and (b), $100\text{nm} \times 100\text{nm}$ for (c) and (d).

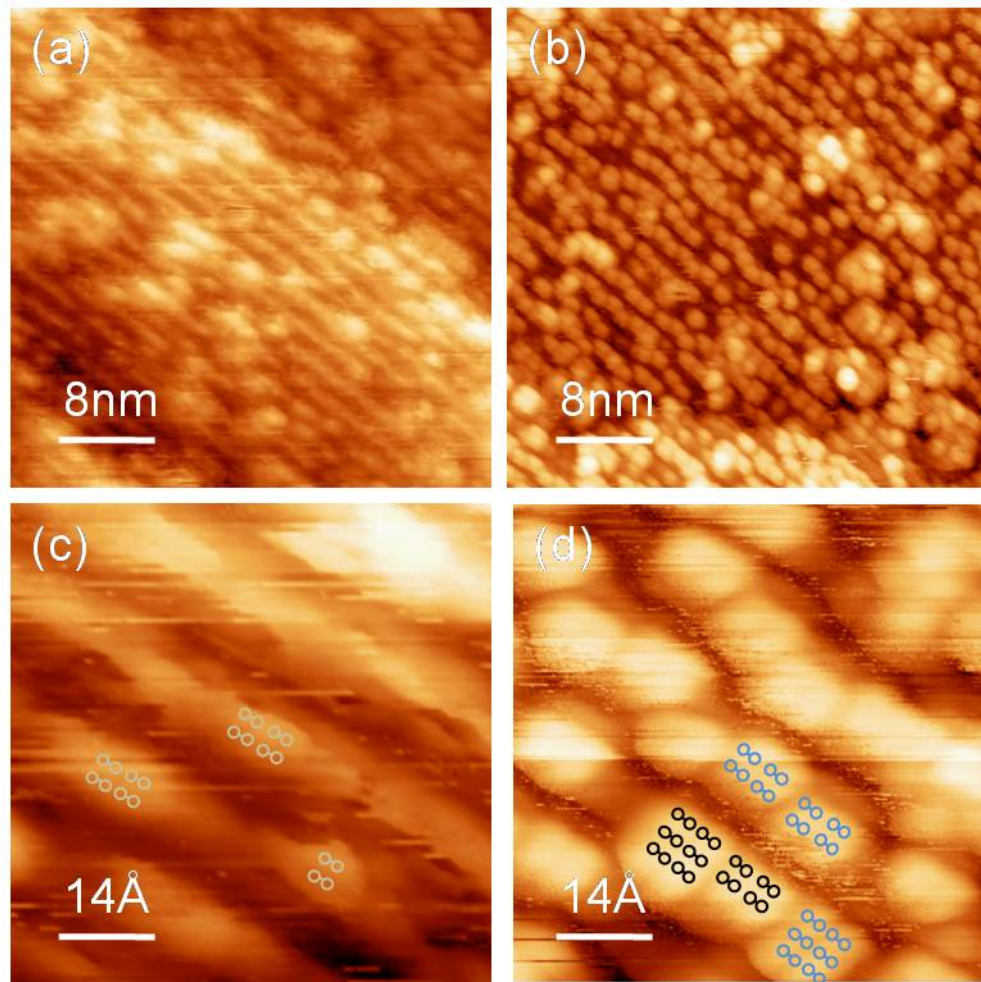


FIG. 4.3. Filled state STM images of the pseudomorphic $\text{In}_{0.4}\text{Ga}_{0.6}\text{As}$ epilayers at different resolutions. The flux ratio of 35 was used during the growth of samples in the left column and 25 for the right one. The sizes of the images are: $40\text{nm} \times 40\text{nm}$ for (a) and (b), $7\text{nm} \times 7\text{nm}$ for (c) and (d).

atomic arrangements as indicated in the contour plot as well as the line profiles, which shows that the depth near the three-dimer is estimated at $\sim 0.45\text{nm}$ while it is $\sim 0.39\text{nm}$ near the two-dimer. These depths are larger than the length of the bulk InAs bi-layer of 0.3029nm . The line profile below Fig. 4.4(a) shows the similar trench depth. In both samples, the trench depths are larger than 0.4nm , which is larger than the bulk bilayer thickness as well as the reported values of $\sim 0.3\text{nm}$ ²⁰ from the $\text{In}_{0.18}\text{Ga}_{0.82}\text{As}$ surface. This surprisingly large depth can be explained by the strain of pseudomorphic layers, which in turn affect surface reconstructions, because adatoms favor the reconstructed area over the missing dimer trench area due to the strain. The compressive strain of the epitaxial layer can make the top strained surface layers extend out due to a more abrupt composition change at a smaller epitaxial thickness in this study (4.6ML) while the same compressive strain does not favor impinging atoms staying long enough to grow in the trench area of missing dimers.

However, the surface structures are different even though the depths are similar in both samples. High resolution STM images suggest that suppression of segregation resulted in the $\beta(2 \times 4)$ -like structure, indicated by circles in Fig. 4.3(c), as in $\text{GaAs}(001)\text{-}2 \times 4$ reconstruction,¹¹ while mixed $\beta(2 \times 4)$ of three dimers and $\alpha(2 \times 4)$ structures for the segregated one, circles in Fig. 4.3(d), as in epitaxial growth of InAs on $\text{InAs}(001)$ surfaces.¹⁸ The patterns in Fig. 4.1 are consistent with assigning the segregated sample surface to have $\beta(2 \times 4) / \alpha(2 \times 4)$ structures,^{5, 21} as we follow Farrell and Palmstrom's assignments for surface reconstructions from RHEED patterns. These assignments are consistent with the STM images while the almost non-existent $3/4^{\text{th}}$ spot in the RHEED pattern is not consistent with any structures suggested. This suggests the surface structure may be different than those sub-phases of either $\text{GaAs}(001)\text{-}2 \times 4$ or $\text{InAs}(001)\text{-}2 \times 4$ reconstruction.^{11, 18} The appearance of mixed surface structures in the more segregated surface might be due to higher strain caused by more segregation.

The STM image (d) for the segregated surface also shows zig-zag arrangements along the

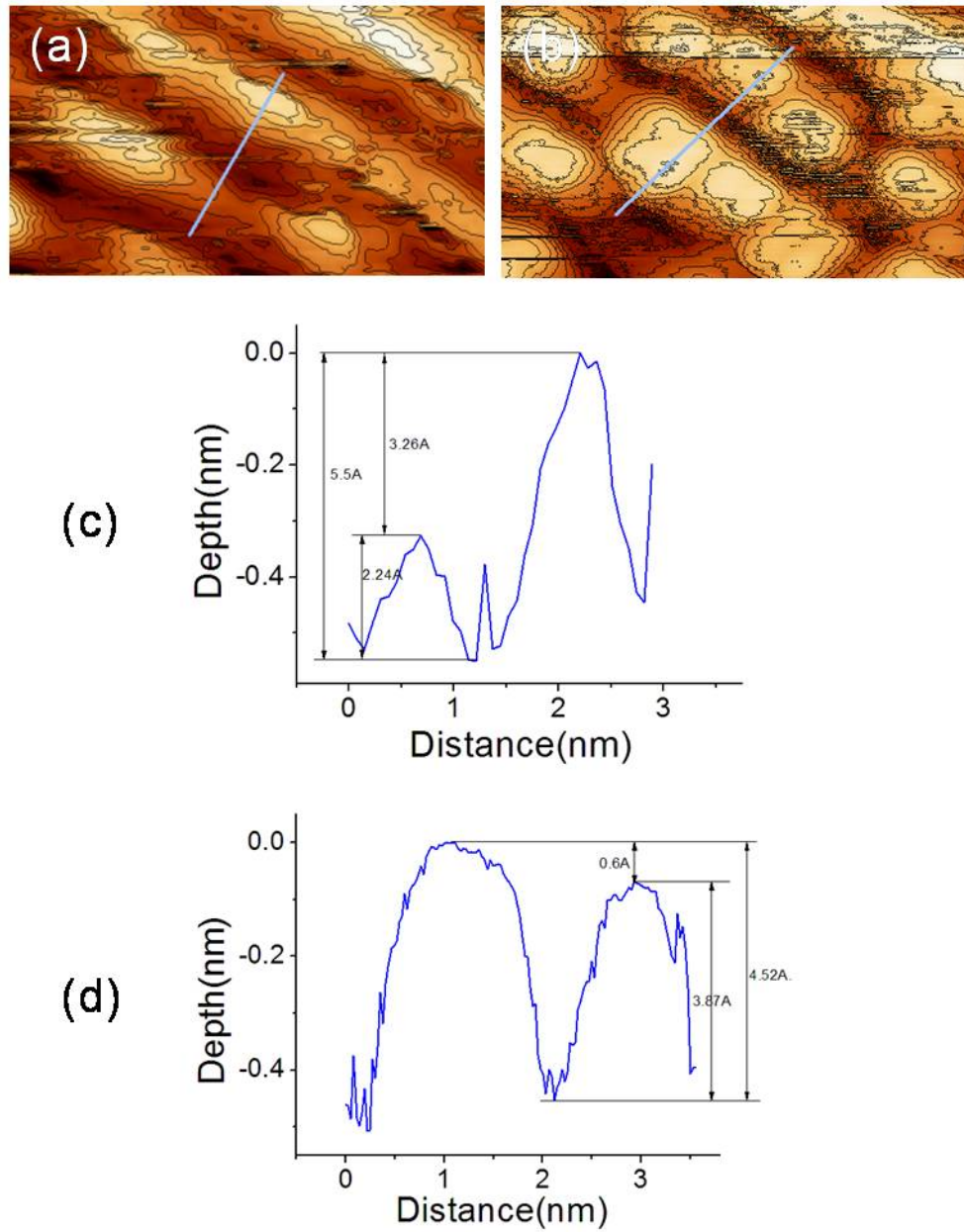


FIG. 4.4. Filled state STM images of the pseudomorphic $\text{In}_{0.4}\text{Ga}_{0.6}\text{As}$ epilayers at different resolutions. The flux ratio of 35 was used during the growth of samples in the left column and 25 for the right one. The size of contour plots (a) and (b) is $7\text{ nm} \times 4\text{ nm}$, which are cropped out of the lower half of Fig. 4.3(c) and Fig. 4.4(d), respectively. The contour plot (b) indicates that the dark circles in Fig. 4.3(d) are on the same height plane, which is $\sim 0.06\text{ nm}$ higher than the plane with blue circles. All the circles in Fig. 4.3(c) are on the same height plane as confirmed by the contour plot (a). The depth profiles along the blue lines in the contour plots are shown

dimer row, [1-10] direction, which is quite similar to those recently reported by Bickel *et al.*⁹ on an $\text{In}_{0.27}\text{Ga}_{0.73}\text{As}$ surface. However neither diffraction patterns nor the STM images studied in this letter showed the reported 4×3 by Bickel *et al.*⁹ or 1×3 for arsenic-stabilized surfaces.²⁰ This difference is possibly due to the fact that the V/III flux ratio employed was 3 about 10 times smaller than this study and smaller strain with a lower indium composition of 27%.^{9, 20}

4.5 Summary

In summary, arsenic overpressure was found to be useful in controlling the indium segregation in pseudomorphic InGaAs epilayers on GaAs(001) surfaces. The STM image analysis on the segregated surface suggests that the indium segregation resulted in several different reconstructions at different heights, which would significantly influence the kinetics of adatoms on the surface, subsequent growth and self-assembly. The growth at a higher arsenic flux resulted in less segregation and the surfaces were dominated by a single sub-phase of a 2×4 reconstruction. The depth profiling on the atomic scale suggests that the growth favors the reconstructed area over the trench area of missing dimer rows in a 2×4 reconstruction.

References

- [1] Z. Zhang, F. Wu, and M. G. Lagally, *Annu. Rev. Mater. Sci.* **27**, 525 (1997).
- [2] E. Penev, S. Stojkovi, P. Kratzer, and M. Scheffler, *Phys. Rev. B*, **69**, 115335 (2004).
- [3] H. Yang, V. P. LaBella, D. W. Bullock, Z. Ding, J. B. Smathers, and P. M. Thibado, *J. Cryst. Growth* **201/202**, 88 (1999).
- [4] V. A. Shchukin, N. N. Ledentsov, and D. Bimberg, *Epitaxy of Nanostructures* (Springer, New York, 2004).
- [5] H. H. Farrell and C. J. Palmstrøm, *J. Vac. Sci. Technol. B* **8**, 903 (1990).
- [6] A. Y. Cho, *J. Cryst. Growth* **201/202**, 1 (1999).
- [7] G. Ariyawansa, V. Apalkov, A. G. U. Perera, S. G. Matsik, G. Huang, and P.

- Bhattacharya, App. Phys. Lett. **92**, 111104 (2007).
- [8] D. J. Kim, D. A. Everett, and H. Yang, J. Appl. Phys. **101**, 106106 (2007).
- [9] J. E. Bickel, N. A. Modine, A. V. D. Ven, and J. M. Millunchick, App. Phys. Lett. **92**, 062104 (2008).
- [10] D. J. Kim, D. Cha, G. J. Salamo, and H. Yang, J. Vac. Sci. Technol. B **24**, 2776 (2006).
- [11] V. P. LaBella, H. Yang, D. W. Bullock, P. M. Thibado, and P. K. Scheffler, Phys. Rev. Lett. **83**, 2989 (1999).
- [12] S. Martini, A. A. Quivy, E. C. F. d. Silva, and J. R. Leite, App. Phys. Lett. **81**, 2863 (2002).
- [13] K. Muraki, S. Fukatsu, Y. Shiraki, and R. Ito, App. Phys. Lett. **61**, 557 (1992).
- [14] J. M. Moison, C. Guille, F. Houzay, F. Barthe, and M. V. Rompay, Phys. Rev. B **40**, 6149 (1989).
- [15] C. W. Snyder, B. G. Orr, D. Kessler, and L. M. Sander, Phys. Rev. Lett. **66**, 3032 (1991).
- [16] C. W. Snyder, B. G. Orr, and H. Munekata, App. Phys. Lett. **62**, 46 (1993).
- [17] T. R. Ramachandran, R. Heitz, P. Chen, and A. Madhukar, Appl. Phys. Lett. **70**, 640 (1997).
- [18] F. Grosse, W. Barvosa-Carter, J. Zinck, M. Wheeler, and M. F. Gyure, Phys. Rev. Lett. **89**, 116102 (2002).
- [19] H. Yang, V. P. LaBella, D. W. Bullock, and P. M. Thibado, J. Vac. Sci. Technol. B **17**, 1778 (1999).
- [20] P. A. Bone, J. M. Ripalda, G. R. Bell, and T. S. Jones, Surf. Sci. **600**, 973 (2006).
- [21] V. P. LaBella, D. W. Bullock, C. Emery, Z. Ding, and P. M. Thibado, Appl. Phys. Lett. **79**, 3065 (2001).

CHAPTER 5

SHAPE CONTROL OF INGAAS NANOSTRUCTURES ON NOMINAL GAAS(001):

DASHES AND DOTS*

Abstract

A way to fabricate self-assembled InGaAs quantum dashes on a nominal GaAs(001) substrate is presented. InGaAs layers were grown on nominal GaAs(001) substrates at a low temperature to suppress the Stranski-Krastanov transition, then annealed at elevated temperatures to induce self-assembly. This approach enabled us to control the shape of self-assembled nanostructures from quantum dashes to quantum dots and eventually quantum dot-chains while typical direct growths at the annealing temperature have yielded only quantum dot shapes. The thickness of the pseudomorphic $\text{In}_{0.4}\text{Ga}_{0.6}\text{As}$ layer was found to be the major factor for the shape control.

5.1 Introduction

Shape control in self-assembly for nanostructures has been vigorously pursued because it enables us to control their electronic and optical properties to develop novel optoelectronic devices. Other than quantum dots (QDs), different shapes such as quantum dashes (QDhs) and quantum wires (QWr) have been realized using the Stranski-Krastanov (S-K) growth mode. For example, InAs QDhs were reported from high index¹ GaAs(211) substrates as well as metamorphic² layers grown on nominal GaAs(001) substrates and self-assembled InAs QWr and QDhs were reported on nominal InP(001) substrates.

So far, there has been no report of direct growth of InGaAs QWr or QDhs on nominally (001) oriented GaAs substrates.³ This is in stark contrast to InP(001) substrates that allow us to control the shape of either dots or wires. For example, InAs QWr form on InP(001) substrates by either direct deposition⁴ or exchange processes⁵ between As and P. These QWr later transform

*Dong Jun Kim and Haeyeon Yang, Nanotechnology **19**, 475601 (2008)

into dots when they are annealed at the growth temperature. Different strain relaxation mechanisms have been reported, including anisotropic relaxation^{3,6} for InAs/InP systems and isotropic relaxation⁷ for InGaAs on GaAs(001) substrates, as possible reasons for QWrS and QDs respectively. In addition, InAs QWrS⁸⁻¹⁰ and QDhs¹¹ were observed on InGaAs, InAlAs and InAlGaAs alloys that are grown, lattice matched, on InP(001) substrates.

In this letter we report *in-situ* scanning tunneling microscopy (STM) studies on shape control of InGaAs nanostructures, either QDhs or QDs. The self-assembled In_{0.4}Ga_{0.6}As nanostructures were grown on nominal GaAs(001) substrates by molecular beam epitaxy (MBE) using a two-step process. The experimental approach employed here is different from the conventional S-K growth mode. Instead, the pseudomorphic epilayers were grown at low enough temperatures and subsequently annealed at higher temperatures so that the S-K transformation from 2D layers into 3D islands was suppressed during the deposition period.¹² The low temperature growth has several advantages over the conventional S-K growth such as suppression of indium segregation¹³ and desorption,¹⁴ composition modulation due to segregation,¹⁰ and intermixing.¹⁵ Especially, it has been reported¹⁶ that indium segregates over a wide temperature range from 370 to 520°C, which overlaps with the S-K growth window because the conventional S-K mode typically requires the GaAs substrate to be above 400°C for the adatoms to diffuse into lower energy sites to form islands. This overlap makes segregation unavoidable during S-K growth. The segregation is problematic because it makes strain distribution non-uniform due to its random nature during the S-K transformation period even under very high arsenic overpressure.^{13,17,18} The redistribution of strain greatly influences the shape of SAQDs because strain relaxation, the main driving force for the S-K mode, depends on indium composition on the growth front, which depends on segregation and intermixing. The benefits due to the low temperature deposition have enabled us to focus the strain effect more accurately since the composition of the pseudomorphic InGaAs layers can be regarded as being much closer to the

nominal deposition amount of indium. A similar approach was employed to fabricate high quality InAs SAQDs¹⁹ for better performing optoelectronic devices. Unlike direct deposition process at a high growth temperature, the annealing process discourages intermixing and segregation at the same temperature because the already deposited pseudomorphic layer acts as a barrier for intermixing and segregation when it is thicker than the effective surface layers (~ 4 layers) for intermixing, according to Tu and Tersoff.¹⁵ Of course, there will be interlayer diffusion at the later stage of annealing due to thinning of the pseudomorphic layer caused by the 3D transition but it will be much weaker on those nanostructures that were already formed during the initial stage of annealing. The employed approach enabled us to fabricate InGaAs quantum dashes on nominal GaAs(001) substrates. Furthermore, we were able to control the shape of self-assembled nanostructures by the simple control of growth parameters.

5.2 Experimental Procedure

The growth studies were carried out using an MBE machine equipped with a computer controlled, valved arsenic cracker cell and an ultra high vacuum STM for *as-grown* surface images.²⁰ An *n*-type GaAs substrate with a nominal (001) orientation was loaded into the load-lock chamber and degassed in the preparation chamber of mid 10^{-10} torr of vacuum. After removal of the oxide layer at 580°C under arsenic overpressure in the growth chamber, a one micrometer thick GaAs buffer was grown on the substrate at 580°C. To calibrate the substrate temperature, the *oxide-off* temperature was used in conjunction with the substrate temperature monitored by reflection high energy electron diffraction (RHEED) pattern changes at a constant arsenic flux.²¹ Our previous MBE-STM study²⁰ from this system suggests that the buffer surface was smooth and well ordered with 2×4 surface reconstructions. After buffer growth, the samples were cooled down to 360°C for $\text{In}_{0.4}\text{Ga}_{0.6}\text{As}$ deposition that was done in a layer-by-layer fashion at a deposition rate of 0.17 ML/sec and confirmed by RHEED oscillations. The pseudomorphic InGaAs epilayers were grown using the same growth parameters that have

resulted in smooth and flat surfaces, as confirmed by RHEED and STM.¹² The indium composition of 40% was estimated by subtracting the GaAs growth rate from that of the InGaAs, both grown at the same low temperature. Upon finishing the InGaAs growth, the substrate was rapidly cooled down below 200°C.¹² The substrate was then moved to the STM chamber for imaging the as grown surfaces. Samples were brought back to the growth chamber after imaging and heated to the annealing temperature at a ramp rate of 20°C/min. The arsenic valve was opened at 300°C to have an arsenic overpressure of 5×10^{-6} torr on the sample surface. The annealing was carried out at 460°C for 120 seconds under the same arsenic pressure. Upon finishing annealing, the substrate was rapidly cooled down while closing the arsenic valve within 10 seconds from the end of the annealing process. The sample was moved back to the STM chamber for surface imaging at a constant current mode of 0.1nA with the surface bias at -3V for filled surface states. For comparison, samples were grown by the conventional S-K growth mode at the annealing temperature without growth interruption, and imaged in a similar way.¹²

5.3 Quantum Dash Formation

The epilayer thicknesses of all samples were set to be larger than the critical thickness of 6.0ML of the conventional S-K growth mode. The S-K transition was confirmed by separate MBE-STM experiments, where RHEED patterns and STM surface images showed chevrons and SAQDs, respectively. However, no chevrons were observed from the RHEED patterns after annealing the sample with a thickness of 6.6ML, where faint fractional order peaks, a strong specular peak and the integer order peaks with their positions unchanged were observed. These observations alone seemed to suggest that there was no 3D transformation from the 2D epilayers²² through the annealing process. Nevertheless, in-situ STM images from this surface showed quantum dashes as shown in Fig. 5.1(a). The RHEED observations of no chevrons may be due to a smaller facet area brought about by low QDhs density and the small height as well as

the flat top surface as seen in the lower half of Fig. 5.1(a), which would effectively reduce the number of coherent electrons reflected from the facets.

The STM observation of quantum dashes is surprising because only InGaAs dots have been observed on GaAs(001) by using the conventional S-K growth method.³ A kinetically limited condition along with anisotropic strain was suggested to explain^{3, 23} the observation of nanowires, but anisotropic strain relaxation was suggested⁶ as a reason for formation of InAs QWrs on InP(001) substrates. However, anisotropic strain relaxation can be ruled out as a possible explanation of the observed QDhs since the InAs epilayers relax isotropically¹³ on GaAs(001) substrates. Hence, the formation of InGaAs QDhs can be explained by the kinetically limited condition during the annealing process, which requires that the height grows much more slowly than the length and width²³ so that dots begin to elongate when the base area becomes larger than a certain critical size.

5.4 Indium Segregation Effect

On the other hand, SAQDs with a much smaller width of 16.2nm were observed when a similar amount, 6.7ML of In_{0.4}Ga_{0.6}As, was deposited on nominal GaAs(001) by using the conventional S-K technique with the substrate held at the same annealing temperature at a growth rate of 0.16ML/sec, as shown in Fig. 5.1(b). The observation of QDs instead of QDhs can be explained by the indium segregation effect happening actively¹⁶ at the growth temperature of 460°C. It has been reported that indium segregation induces higher strain on the growth front, more so than the nominal deposition value due to the almost 100% indium composition,^{16, 17} well before the onset of the S-K transition. This higher than nominal indium composition on the growth front induces a higher strain field on the surface, which results in smaller dots by the conventional S-K growth because relaxation of larger strain energy favors small islands with steep facets during conventional S-K growth.^{24, 25} The low deposition temperature along with high arsenic flux employed in this approach effectively suppresses the floating indium effect¹³

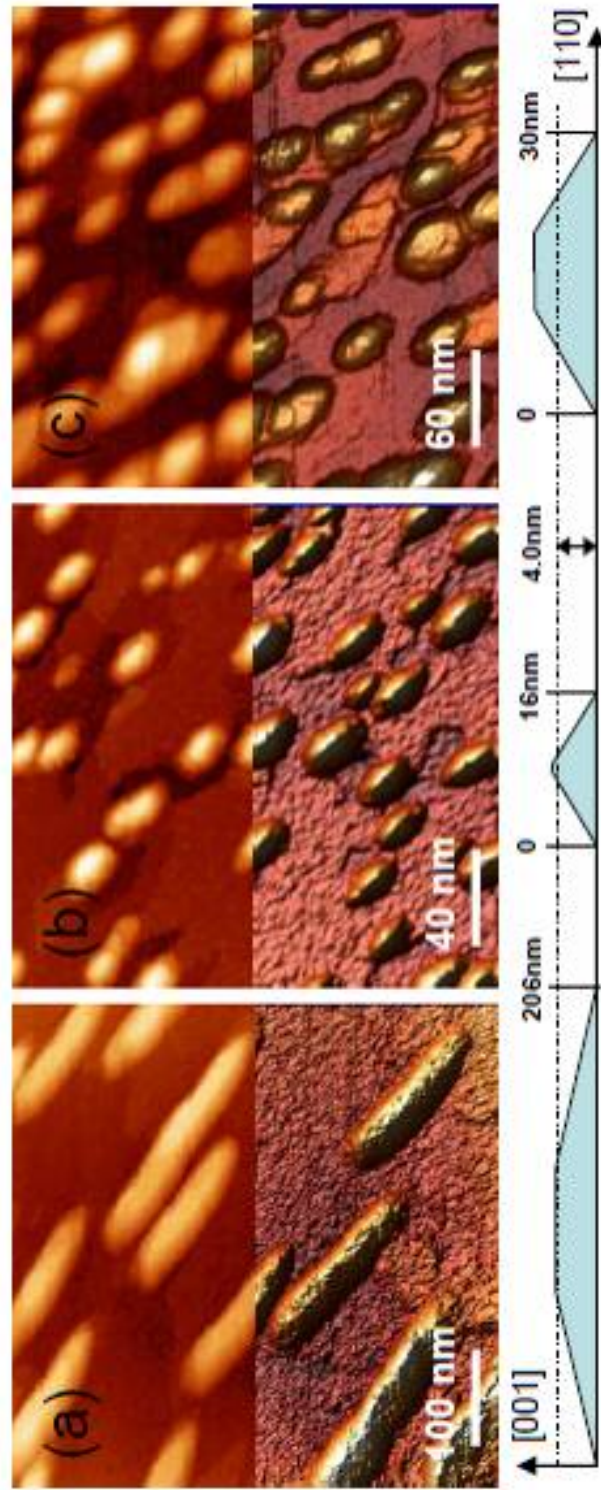


FIG. 5.1. STM images; from the surface prepared by annealing the pseudomorphic $\text{In}_{0.4}\text{Ga}_{0.6}\text{As}$ layers with thicknesses of 6.56 ML (a); 8.85 ML (b); and by continuous growth of 6.7 ML (c). Note the sizes are (a) $500 \text{ nm} \times 300 \text{ nm}$; and (c) $200 \text{ nm} \times 200 \text{ nm}$. Corresponding cross sectional areas of average values of width, height, and facet angles are shown to scale, below each image.

that is due to the segregation. The suppression of segregation during the low temperature deposition is further supported by the STM observations from annealed samples with a larger thickness, which resulted in taller and wider dots as shown in (c) than that of dots in (b), although their top surfaces are still truncated. The STM image shows QDs as well as a few very short dashes formed by annealing 8.9ML of $\text{In}_{0.4}\text{Ga}_{0.6}\text{As}$ deposited at the same low temperature. The annealing of the thicker strained layer would provide larger amounts of adatoms from the strained layer due to the thickness and a higher accumulated strain, effectively breaking the kinetically limited condition,²³ resulting in taller dots with smaller width. This is supported by our report of dot-chains¹² that were formed when an even thicker pseudomorphic layer of 10.2ML was annealed at the same temperature.

5.5 STM Study of Quantum Dashes

The dashes are fairly straight and wide, aligned along the dimer row direction with truncated top surfaces as shown in the 3D image (upper half of Fig. 5.1(a)). The length ranges from 140nm to 250nm while the width ranges from 30 to 55nm, the truncated top width ranging from 8 to 30nm and the height ranging from 3 to 7nm. The measured average height from the STM images with standard deviation is 4.3 ± 0.9 nm while the average length, top width, and base width are 205.9 ± 50.3 nm, 12.3 ± 6.6 nm, and 50.0 ± 10.2 nm, respectively. The aspect ratio of the dashes, length over width, is 4.1 and its facet angle was measured as $14.4 \pm 2.5^\circ$, which is similar to that of the arsenic-rich InAs/InP system²⁶ but smaller than that of encapsulated²⁷ InAs/InP. Meanwhile the facet angles for dots are even larger; they are $29.2 \pm 3.4^\circ$ for (b) and $30.5 \pm 4.9^\circ$ for (c). The average dot sizes for dots in (b) are 27.0 ± 5.4 nm long, 16.2 ± 3.0 wide, and 4.7 ± 1.1 nm tall, while the top width is a small but non-trivial 0.7 ± 0.6 nm; average sizes for dots in (c) are 42.0 ± 10.0 nm long, 29.5 ± 4.6 nm wide, and 6.5 ± 2.0 nm tall while the top width is 7.9 ± 4.0 nm. The growth of wires or the elongation of dots into huts requires a certain base area while the height is somehow kept small either kinetically²³ or energetically.²⁸ The smallest width of the

QDhs is 30nm, which is larger than that of dots produced either by continuous growth or by annealing pseudomorphic 2D layers. The observed minimum width suggests that the critical size is less than 30nm for this system to grow into wires. The aspect ratios, length over width, of SAQDs and dots formed by annealing are similar: 1.7 and 1.4 for (b) and (c) of Fig. 5.1, respectively. The slightly larger aspect ratio for dots prepared by the S-K mode seems to be due to higher anisotropic diffusion, according to the theoretical study by Penev et al.,²⁹ which is caused by the larger strain induced by indium segregation. The average aspect ratio measured from samples with a larger deposition amount approaches unity either by the approach described here (10.2ML deposition)¹² or by the conventional S-K growth method, 9.1ML (STM image not shown here), which seems to be due to a higher strain amount per unit area caused by the smaller dot-to-dot distance.

The truncated top surface was observed in InAs QWr^s⁵ and QDhs²⁷ on InP(001) systems, but pointed tops were observed from InAs huts¹ on GaAs(211)B and InAs QDhs¹¹ on an InGaAlAs buffer layer lattice-matched to InP(001). The observation of the truncated top surface and large base width from the annealed samples as shown in the lower panel of Fig. 5.1 is consistent with the reported AFM observations⁸ of InGaAs QWr^s and QDs grown on InGaAs buffer layers that are lattice matched to InP(001) substrates, as well as the growth model by Tersoff and Tromp,²³ which employed a truncated cross section for nanowires as an energetically stable shape. The truncated top surface as well as large base area and larger volume from the annealed sample with 8.9ML, shown in (c), suggests that the segregation was not active during the annealing period since the segregation would have resulted in smaller dots as in (b). The shape evolution over the strain amount shown in the lower part of Fig. 5.1 can be explained by the theoretical model by Daruka et al.²⁵ The truncated tops observed from the annealed sample happen when the “additional” surface energy due to facet formation is larger with the steeper facet than that of the shallow facet, while the pointed tops are due to negative (decrease in surface

energy for the “new” facet of a dot) surface energy for the facets.²⁵ Comparison with the model suggests that the relative surface energy is a delicate function of growth parameters.

5.6 Summary

In summary, the approach of low temperature growth and annealing at high temperature was found useful in controlling the shape of self-assembled nanostructures, ranging from quantum dashes to dots and then dot chains. The strain amount corresponding to the thickness of the pseudomorphic layer was found to determine the shape of the nanostructures. The shape control studied in this letter suggests that kinetics plays a significant role in determining the shape of nanostructures at low strain energies to yield anisotropic shapes (dashes), and the energetics of surface energy and strain relaxation dominates to produce isotropic shapes (dots) when the accumulated strain energy dominates over diffusion kinetics.

References

- [1] S. P. Guo, H. Ohno, A. Shen, F. Matsukura, and Y. Ohno, *App. Phys. Lett.* **70**, 2738 (1997).
- [2] G. Balakrishnan, S. Huang, T. J. Rotter, A. Stintz, L. R. Dawson, K. J. Malloy, H. Xu, and D. L. Huffaker, *App. Phys. Lett.* **84**, 2058 (2004).
- [3] M. U. González, L. González, J. M. García, Y. González, J. P. Silveira, and F. Briones, *Microelectron. J.* **35**, 13 (2004).
- [4] X. Mu, Y. J. Ding, H. Yang, and G. J. Salamo, *App. Phys. Lett.* **81**, 1107 (2002).
- [5] H. Yang, P. Ballet, and G. J. Salamo, *J. Appl. Phys.* **89**, 7871 (2001).
- [6] J. M. García, L. González, M. U. González, J. P. Silveira, Y. González, and F. Briones, *J. Cryst. Growth* **227-228**, 975 (2001).
- [7] M. U. González, Y. González, and L. González, *Appl. Phys. Lett.* **81**, 4162 (2002).
- [8] J. Brault, M. Gendry, G. Grenet, G. Hollinger, Y. Desières, and T. Benyattou, *Appl.*

Phys. Lett. **73**, 2932 (1998).

[9] H. Li, T. Daniels-Race, and M.-A. Hasan, Appl. Phys. Lett. **80**, 1367 (2002).

[10] L. Nieto, J. R. R. Bortoleto, M. A. Cotta, R. Magalhães-Paniago, and H. R. Gutiérrez, Appl. Phys. Lett. **91**, 063122 (2007).

[11] A. Sauerwald, T. Kümmell, G. Bacher, A. Somers, R. Schwertberger, J. P. Reithmaier, and A. Forchel, Appl. Phys. Lett. **86**, 253112 (2005).

[12] D. J. Kim, D. A. Everett, and H. Yang, J. Appl. Phys. **101**, 106106 (2007).

[13] J. M. García, J. P. Silveira, and F. Briones, Appl. Phys. Lett. **77**, 409 (2000).

[14] A. Ohtake and M. Ozeki, App. Phys. Lett. **78**, 431 (2001).

[15] Y. Tu and J. Tersoff, Phys. Rev. Lett. **93**, 216101 (2004).

[16] K. Muraki, S. Fukatsu, Y. Shiraki, and R. Ito, App. Phys. Lett. **61**, 557 (1992).

[17] J. M. Moison, C. Guille, F. Houzay, F. Barthe, and M. V. Rompay, Phys. Rev. B **40**, 6149 (1989).

[18] S. Martini, A. A. Quivy, E. C. F. d. Silva, and J. R. Leite, App. Phys. Lett. **81**, 2863 (2002).

[19] H. H. Zhan, R. Nötzel, G. J. Hamhuis, T. J. Eijkemans, and J. H. Wolter, J. Appl. Phys. **93**, 5953 (2003).

[20] D. J. Kim, D. Cha, G. J. Salamo, and H. Yang, J. Vac. Sci. Technol. B **24**, 2776 (2006).

[21] V. P. LaBella, H. Yang, D. W. Bullock, P. M. Thibado, and P. K. Scheffler, Phys. Rev. Lett. **83**, 2989 (1999).

[22] K. Kanisawa, H. Yamaguchi, and Y. Horikoshi, Phys. Rev. B **54**, 4428 (1996).

[23] J. Tersoff and R. M. Tromp, Phys. Rev. Lett. **70**, 2782 (1993).

[24] D. Bimberg, M. Grundmann, and N. N. Ledentsov, Quantum Dot Heterostructures (John Wiley & Sons, New York, 1999).

- [25] I. Daruka, J. Tersoff, and A.-L. Barabási, Phys. Rev. Lett. **82**, 2753 (1999).
- [26] H. Yang, J. B. Smathers, P. Ballet, C. L. Workman, and G. J. Salamo, in 2000 MRS Spring Meeting, edited by J. M. Millunchick, A.-L. Barabasi, E. D. Jones and N. Modine (MRS, San Francisco, 2000), Vol. 618, p. 141.
- [27] P. Miska, J. Even, C. Platz, B. Salem, T. Benyattou, C. Bru-Chevalier, G. Guillot, G. Bremond, K. Moumanis, and F. H. Julien, J. Appl. Phys. **95**, 1074 (2004).
- [28] I. Goldfarb, L. Banks-Sills, and R. Eliasi1, Phys. Rev. Lett. **97**, 206101 (2006).
- [29] E. Penev, S. Stojkovi, P. Kratzer, and M. Scheffler, Phys. Rev. B. **69**, 115335 (2004).

CHAPTER 6

SUPPRESSED SEGREGATION AND INTERMIXING OF INGAAS/GAAS QUANTUM DOTS BY A NOVEL GROWTH METHOD*

Abstract

Using nearly equivalent growth thicknesses, we obtained significantly different quantum dots (QDs) in shape, density, and volume by two different growth procedures. Two QD samples were fabricated by different growth methods, a conventional direct epilayer growth and a novel growth. The novel growth employs a two step-growth process: a pseudomorphic layer growth and then an annealing process. STM morphological measurements from two QD samples suggest isotropic diffusion from QD shape changes in the novel growth while anisotropic diffusion in the conventional epilayer growth. Total QD volume measurements suggest a significant difference in surface segregation and intermixing during dot formation due to the two different growth mechanisms.

7.1 Introduction

Strain and strain relaxation in the wetting layer play a critical role in determining the properties of quantum dots.¹ In particular, a few top layers of the wetting layer play an important role in quantum dot formation, because strain relaxation from the top few layers and subsequent surface segregation are the main factors that determine a QD formation and shape changes.^{2,3} In addition, deformation of island shape can occur as a result of the strain reduction of the wetting layer due to compositional drop through intermixing.⁴ To suppress intermixing during growth, least growth conditions, especially growth temperature, can be employed. Because behavior of intermixing is temperature dependent and it can be intensified with a higher temperature in the Stranski-Krastanov (S-K) growth.⁵ Mass transport due to surface diffusion can also be reduced by those least growth conditions preserving the shape of the 3D islands.⁶ Comparison of this least

*Dong Jun Kim, Haeyeon Yang (to be published).

condition growth with conventional S-K growth indicates that the transformation from 2D to 3D generates QDs with different features due to the different strain relaxation mechanisms, suppressed surface segregation and intermixing.

In this chapter, we present evidence of suppressed mass transport and intermixing during molecular beam epitaxy (MBE) growth of InGaAs QDs on GaAs(001) substrates. Suppressed mass transport and intermixing reduces compositional changes in the wetting layer, and preserves the initial shapes of QDs as well as the wetting layer thickness.⁷ This analysis is based on experimental results of InGaAs QD surfaces and is obtained by *in situ* scanning tunneling microscope (STM) measurements, which leads to an estimation of QD size and wetting layer thickness. *In situ* STM imaging and an improved volume calculation method developed by our group have enabled us to determine the volume of InGaAs QDs more accurately.

7.2 Experimental Details

To obtain different features of QD due to the modified growth mechanism, we adopted different growth processes but approximately the same coverage as shown in Fig. 6.1. We fabricated two samples with different mechanisms, a conventional direct epilayer growth (sample A) and a novel growth (sample B). The novel growth is employed by a two step-growth, a pseudomorphic layer growth, and a subsequent temperature-increasing process. For the first sample (sample A in Fig. 6.1), we deposited 10.2 ML InGaAs on top of GaAs with a constant growth temperature of 460°C. It is similar in nature to the conventional S-K growth method, which is influenced by enough indium segregation and intermixing. Initially, the GaAs substrate temperature was set to a growth condition of 460°C, and then InGaAs wetting layer deposition was begun. Transformation to three dimensions from two dimensions, or the critical point of coverage in the wetting layer, was around 6 ML during the 10.2 ML InGaAs growth. For the second sample (sample B in Fig. 6.1), we deposited 9.8 ML of an InGaAs wetting layer at a lower temperature, 380°C. This temperature is slightly lower than that required to get to get QDs.

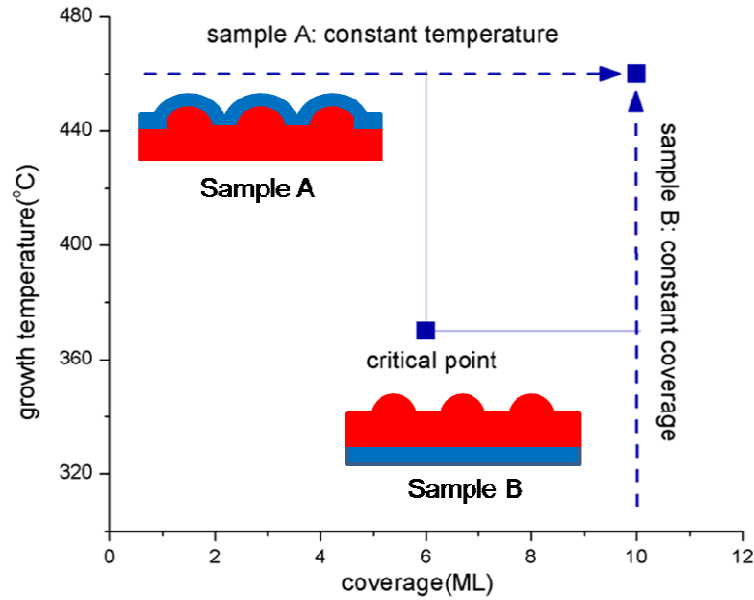


FIG. 6.1. Schematic diagram of two different growth methods: modified growth with a constant coverage (sample A) and conventional growth mode with a constant temperature (sample B) during the InGaAs growth. Dashed lines represent the coverage increasing with a constant temperature (a), and growth temperature increasing with a constant coverage (b). Critical point indicates the minimum condition of growth temperature and coverage for the QD formation.

After deposition, we increased the temperature with a heating rate $20^{\circ}\text{C}/\text{min}$ until the temperature reached 460°C . QDs started to form by strain relaxation at certain temperatures during the temperature increasing. This growth method allowed formation of 3D islands and rare shape changes with small segregation process and intermixing. The critical point in Fig. 6.1 is a minimum condition for a growth temperature and coverage under a certain amount of arsenic flux. Even if the finite thickness of a strained wetting layer doesn't define well due to the compositional gradient, the lower part of the wetting layer (see sample B in Fig. 6.1) works as a buffer to reduce the intermixing effect to the top layers of wetting layer, resulting in a high strained wetting layer from the upper most layers.

InGaAs QD samples were grown on a GaAs(001) surface with a combined STM-MBE system. A (001) oriented *n*-type GaAs substrate was used to grow InGaAs QDs. A $1\text{-}\mu\text{m}$ thick GaAs buffer layer was grown first at 580°C for all samples. For the first sample, the temperature

was cooled down and kept at 460°C during InGaAs QD growth after the buffer layer growth. The 10.2 ML of InGaAs QD was deposited at a growth rate of 0.16 ML/sec. The transition from 2D to 3D growth was monitored by the changes of the reflection high electron energy diffraction (RHEED) pattern from streaks to chevron shapes. The arsenic flux was maintained at 6.0×10^{-6} torr during the InGaAs QD growth. After InGaAs growth, the sample was cooled down to room temperature by cutting off power to the growth stage heater. The sample was then transferred to the STM chamber via the preparation chamber to obtain *in situ* surface images.

For the second sample, the temperature was immediately cooled down to 380°C after the GaAs buffer layer growth. The InGaAs pseudomorphic epilayer was grown at 380°C under an arsenic flux of 1.3×10^{-6} torr, and then cooled down to room temperature. For the annealing process, the sample temperature was increased to 460°C for 10 sec under arsenic flux 6.0×10^{-6} torr. The heating power was then disconnected to cool down the sample temperature to room temperature. After the cool down, the sample was transferred under UHV to the STM chamber. The sample was analyzed for its morphological properties by constant current mode STM (omicon) with a tungsten wire tip. Detailed system information is described elsewhere. To obtain quantitative information of QD volume, a new calculation we developed was used to analyze the raw data directly obtained by the *in situ* STM.

7.3 Results and Discussion

Figure 6.2 shows STM images of QD surfaces grown by different growth processes. These STM images show a clear difference in the QD shape, size, and density between the two samples. QD shape in Fig. 6.2(a) is elongated in [1-10] direction while shapes in Fig. 6.2(b) are round and dome-shaped with the average diameter of 32 nm and height of 9 nm from the image. Scatter-plots in Fig. 6.3 show QD length in one direction and aspect ratio of dot length in two directions, [1-10] and [110] direction. For the conventional growth sample, sample A in Fig. 6.3, gives a mean value of the aspect ratio of dot length [1-10] to width [110] as 1.4, with lengths of

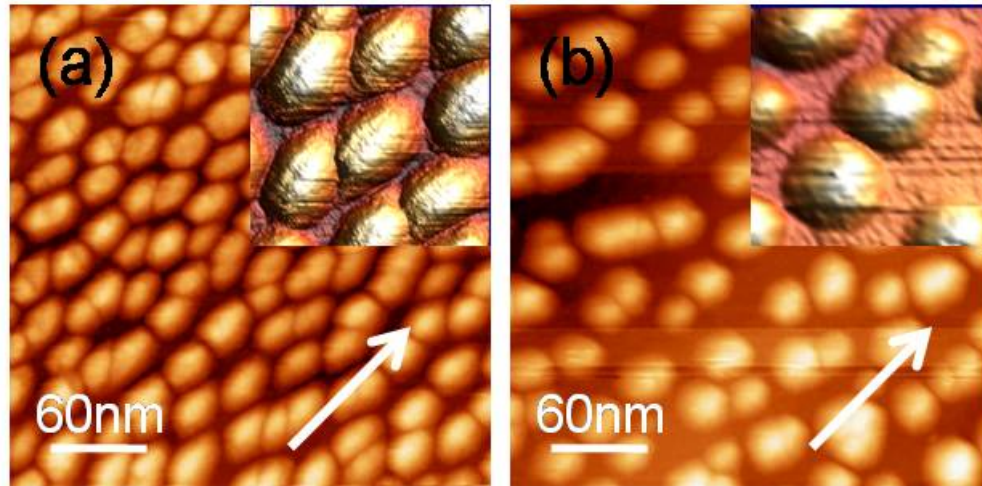


FIG. 6.2. STM images of InGaAs QDs formed after a 10.2 ML deposition(a) and 9.8 ML deposition (b). The equilibrium shape of InGaAs islands (a), and initial shape of InGaAs islands (b) on GaAs(001) were shown by different growth mechanism.

$34.02 \pm 6.57\text{nm}$ and width of $24.19 \pm 3.97\text{nm}$. QDs are elongated in the $[1-10]$ direction due to the diffusion by a high arsenic overpressure range of 5.9×10^{-6} torr. In Fig. 6.3(a), dot length in the $[1-10]$ direction is increased with aspect ratio increasing. But dot length in the $[110]$ direction has small variation by aspect ratio changes, shown in Fig. 6.3(b). This elongation to the $[1-10]$ direction gives expected results in conventional S-K growth mode due to the dimer row structure of the GaAs (001) reconstruction surface.^{8,9} For the novel growth sample, sample B in Fig. 6.3, the aspect ratio of dot length $[1-10]$ to width $[110]$ is 0.98, with lengths of $31.31 \pm 7.5\text{nm}$ and $32.3 \pm 5.4\text{nm}$, respectively. Irregular and dome-shaped dots are observed due to the isotropic diffusion. The aspect ratio in Fig. 6.3(c) and (d) doesn't increase as dot length increases. Those shapes are evidence of the suppressed surface segregation to dimer row direction. Figure 6.2(a) shows that the occupancy of the QD base area on the substrate is 76.4%, resulting from the 10.2 ML deposition. Dot density tends to saturate at 3.9×10^6 dots/cm², while the average neighbor-dot distance to the $[1-10]$ direction is $29.2 \pm 6.2\text{nm}$, and $25.3 \pm 4.4\text{nm}$ in the $[110]$ direction. From the STM image in Fig. 6.2(b), the occupancy of the QD base area on the substrate is 56.6%. The

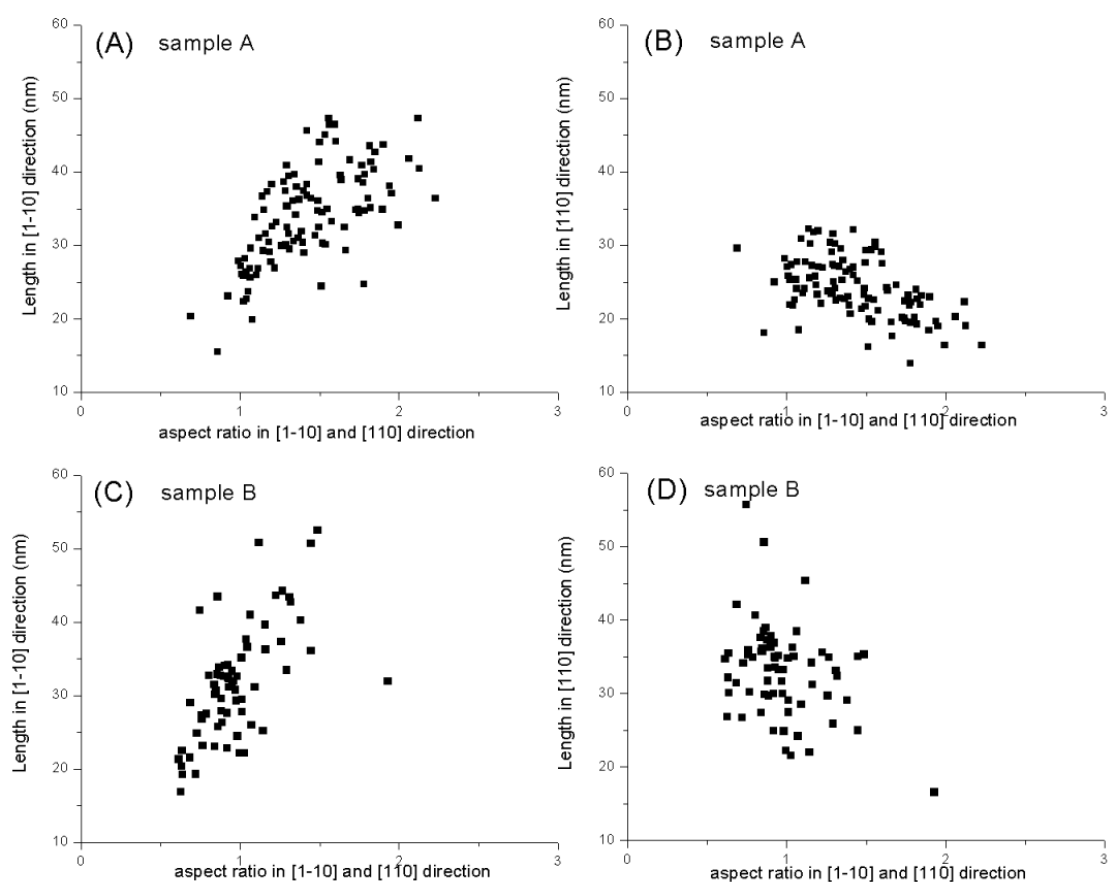


FIG. 6.3. Scattering plots of the aspect ratio and dot length in the [1-10] and [110] direction. Sample A represents the conventional S-K growth method and sample B represents the novel growth method.

dot density is 2.2×10^6 dots/cm², while the average neighbor dot distance in the [1-10] direction is 30.4 ± 10.3 nm and the average neighbor dot distance in the [110] direction is 43.3 ± 10.3 nm. Size uniformity in sample A is more increased than in the transform only sample (sample B). The growth and transform of the 10.2 ML InGaAs (sample A) improved QD size uniformity by possibly eliminating the formation of large-size dots, and the reason for this uniformity improvement is probably due to the isotropic diffusion on the surface and the even strain distributions in the wetting layer.

The histogram of the QD volume [Fig. 6.4(a)] clearly shows the broader Gaussian curve [Fig. 6.4(b)] than that of sample B [Fig. 6.4(b)] because of the decreased size uniformity measured by mean volume and the standard deviation of QDs. The average value of dot volume and standard deviation measured from high resolution STM images is 2037 ± 700 nm³ for sample A and 2945 ± 142 nm³ for sample B. Total QD thickness is 9.2 ML for sample A and 6.78 ML for sample B. Those results shows a significant difference with the result of Joyce's experiment.¹⁰

Figure 6.5 represents the thickness of the wetting layer in order to compare relative changes of the average QD volume and QD density. The wetting layer thickness was estimated by the subtraction of each QD volume from the quantitative measurements of total coverage. In case of growth under high arsenic overpressure, indium surface segregation can be suppressed due to the higher concentration of arsenic.¹¹ Negligible indium desorption probably occurred during QD formation on the WL surface at the low temperature growth. Significant changes in the QD volume and density with different wetting layer thicknesses are observed. The average volume of QDs was decreased with a thicker wetting layer by a dividing factor of 1.5 while density was increased by a factor of 1.5. A thick wetting layer probably has a more even compositional distribution as shown in Fig. 6.6.¹² A higher strain due to the higher indium composition probably reduces the critical thickness in the wetting layer to form QDs. The growth and transformation sample, sample A, may have more chance to have indium segregation due to the higher

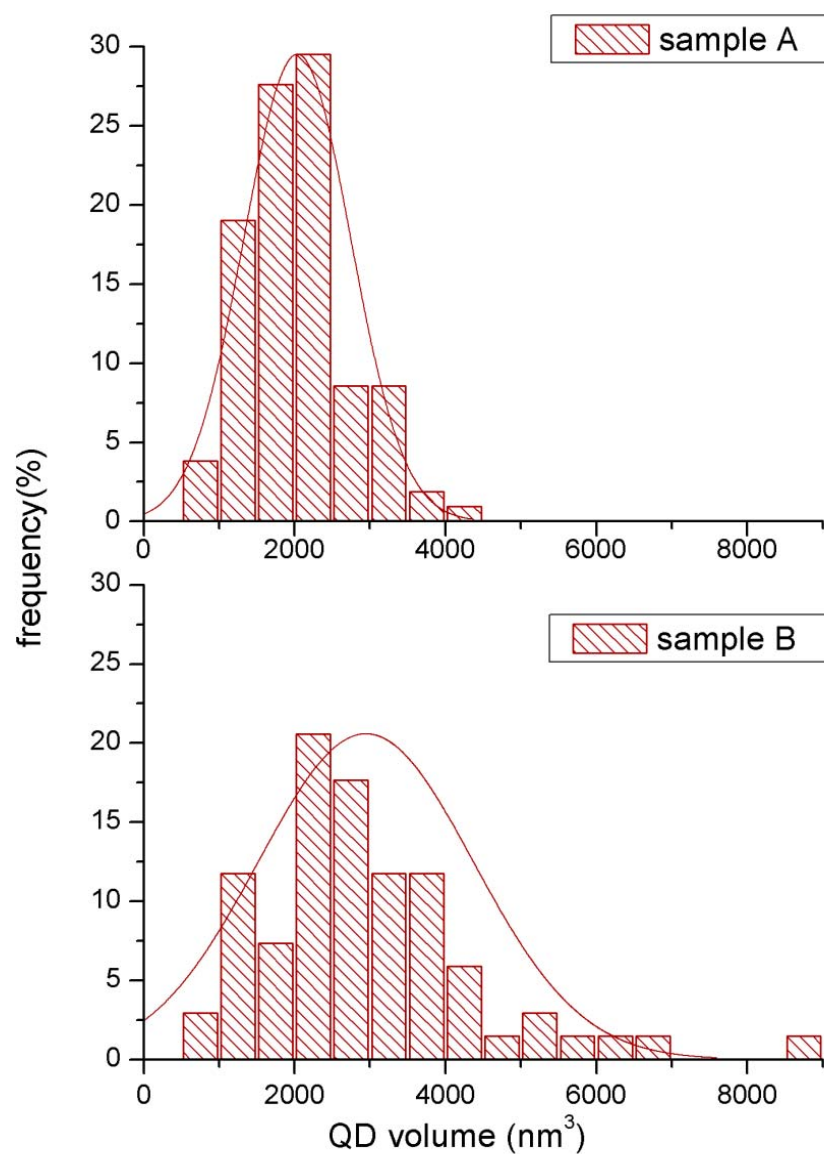


FIG. 6.4. Volume distributions of InGaAs QDs grown at 460 °C with InGaAs coverage of 10.2 ML (a) and 9.8 ML (b), respectively. The STM pictures of these two samples are shown in Fig. 7.2.

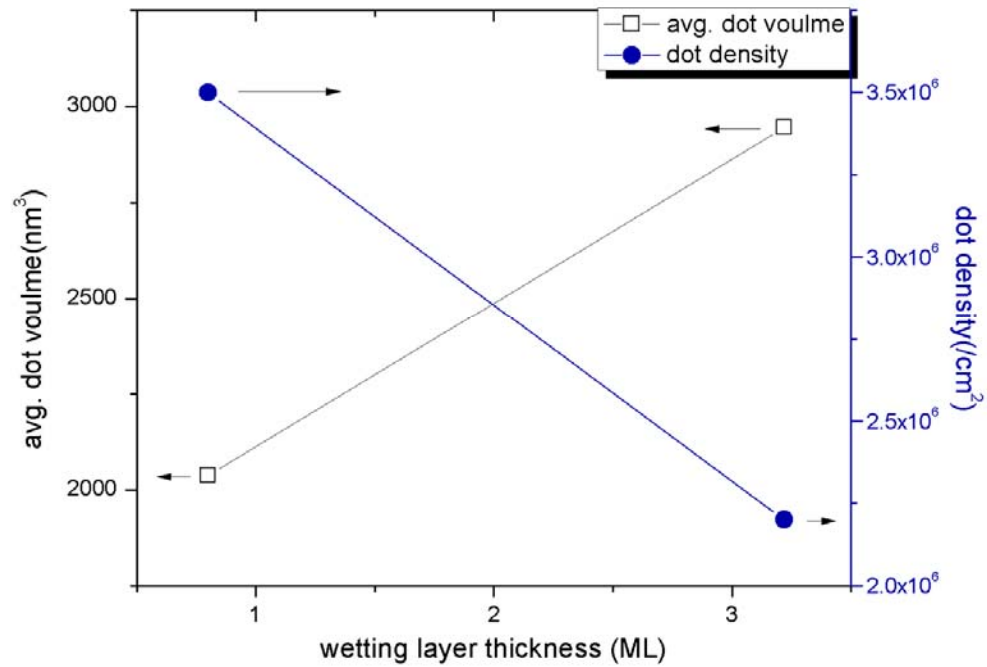


FIG. 6.5. Average dot volume (empty squares) and dot density (filled circles) as a function of nominal wetting layer thickness.

growth temperature and simultaneous status of deposition and desorption during the whole 10.2 ML InGaAs growth. From sample A, the complete strain relaxation is a reason to have thin wetting layer and bigger QDs. In the transform only sample, sample B, has partial strain relaxation at top few layers due to the least growth temperature. It can be a reason to have small volume of QDs and thick wetting layer.

7.4 Summary

In conclusion, we studied the effect of novel growth on the structure of InGaAs/GaAs QDs grown by solid source MBE and STM studies of QD surface morphology. This method strongly suggests a significant suppressed surface segregation and intermixing during dot formation and leads to a size increase of QDs with the substantial thickening of the wetting layer. This method also showed a different strain relaxation mechanism due to different growth methods that are related to strain distribution and the thickness of the wetting layer.

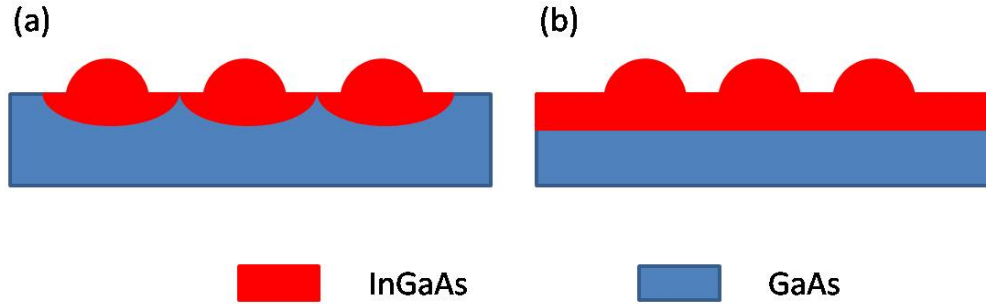


FIG. 6.6. Cross-sectional views of the strain distribution in the wetting layer for two different growth mechanisms: (a) represents sample A, and (b) represents sample B.

References

- [1] G.Biasiol *et al*, Phys. Rev. Lett. **87**, 223106 (2005).
- [2] A. G. Cullis, D. J. Norris, T. Walther, M. A. Migliorato, and M. Hopkinson¹, Phys. Rev. B **66**, 081305 (2002).
- [3] S. Hinooda *et al.*, Appl. Phys. Lett. **78**, 3052 (2001).
- [4] D. Bimberg, M. Grundmann, and N. N. Ledentsov, *Quantum dot heterostructures*, (John Wiley & Son, New York, 1988).
- [5] Y. Tu and J. Tersoff, Phys. Rev. Lett. **93**, 216101 (2004).
- [6] A. Rosenauer, D. Gerthsen, D. V. Dyck, M. Arzberger, G. Bohm, and G. Abstreiter, Phys. Rev. B **64**, 245334 (2001).
- [7] T. J. Krzyzewski and T. S. Jones, J. Appl. Phys. **96**, 668(2004).
- [8] Y. Hasegawa *et al.*, App. Phys. Lett., **72**, 2265 (1998).
- [9] V. P. LaBella, H. Yang, D. W. Bullock, P. M. Thibado, and P. K. Scheffler, Phys. Rev. Lett. **83**, 2989 (1999).
- [10] P. B. Joyce, T. J. Krzyzewski, G. R. Bell, B. A. Joyce, and T. S. Jones, Phys. Rev. B **58**, R15981 (1998).
- [11] K. Muraki, S. Fukatsu, Y. Shiraki and R. Ito, Appl. Phys. Lett. **61**, 557 (1992).
- [12] G. Biasiol *et al.*, Appl. Phys. Lett. **87**, 223106 (2005).

CHAPTER 7

CONCLUSION AND FUTURE WORK

7.1 Conclusion

The goal of this research was to provide a greater understanding of the growth mechanisms in self-assembled growths at the nanoscale. The MBE grown, compound semiconductor, $\text{In}_{0.4}\text{Ga}_{0.6}\text{As}$, was used to grow nanoscale quantum dots on GaAs(001) substrates. We employed a novel growth mode to better understand the growth mechanism. This growth mode consists of a two-step process which includes low temperature growth and annealing process at high temperature. Low temperature growth has several advantages than higher temperature growth in the conventional S-K growth, such as suppression of indium segregation and desorption, composition modulation due to segregation, and intermixing due to the small diffusion length at low temperature.

From the novel growth mode, suppressed surface segregation and intermixing during the growth was observed, resulting in quantum dot chains and quantum dashes by the formation of self-assembled QDs. Dot chains were formed during the 120-sec annealing of 2D 10ML pseudomorphic layers of $\text{In}_{0.4}\text{Ga}_{0.6}\text{As}$ /GaAs. The pseudomorphic layer was grown at the low temperature of 380 °C. This temperature is a slightly lower temperature to form a 3D island. QDhs formed during the annealing of 6ML pseudomorphic $\text{In}_{0.4}\text{Ga}_{0.6}\text{As}$ /GaAs layers. The observation of dot chains and QDhs can be explained by the suppressed indium segregation effect at the growth temperature of 460 °C. The smaller indium composition on the growth front due to the suppressed segregation induces a smaller strain field on the surface. And relaxation of lower strain energy favors bigger islands with small angle facets. The approach of low-temperature growth and annealing at a high temperature was useful in controlling the shape of self-assembled nanostructures. The shape control research suggests that kinetics plays a significant role in determining the shape of nanostructures at low-strain energies to yield anisotropic QDhs and the

energetics of surface energy and strain relaxation dominate to produce isotropic dots shapes when the accumulated strain energy dominates over diffusion kinetics.

Arsenic overpressure was also useful to control the indium segregation in pseudomorphic InGaAs epilayers. STM image analysis suggests that the growth at a higher arsenic flux resulted in less segregation and the surfaces were dominated by a single sub-phase of 2×4 reconstruction. Depth profiling on the atomic scale suggests that the growth favors reconstructed areas over trench areas of missing dimer rows in a 2×4 reconstruction.

Finally, we studied the effect of the wetting layer on the structure of InGaAs/GaAs QDs grown by solid source MBE. We also presented STM studies of QD surface morphology. These studies strongly suggest a size increase of QDs with a substantial thickening of the wetting layer. We also proposed a different strain relaxation mechanism by utilizing different growth methods, which are related to strain distribution and thickness of the wetting layer.

7.2 Future Work

This thesis presented some significant observations concerning self-assembled growth with low surface diffusion and limited intermixing. Among the most important results, the morphological analysis of QD chains formed by our new growth method provides more opportunities to understand the growth mechanisms of dot alignment. The morphological analysis can be performed by measuring the size and the shape of each dot. In addition, a clearer understanding of the compositional properties of the wetting layer for QD alignments from the different growth methods is needed, which is not well documented in the literature. A more detailed study is necessary in order to clarify the precise reasons for this QD alignment, which could include:

- (i) The growth and imaging of InGaAs surfaces with other compositional ratio and growth thickness, to identify the changes of QD alignments over a larger range.

- (ii) The growth and imaging of InGaAs surfaces with various annealing times from a few seconds to a few minutes, to obtain different shapes of QD alignment, because longer annealing times lead to more diffusion between dots and between dots and the wetting layer.
- (iii) Compositional analysis of QD alignment which includes dot chains and QDhs, to identify electrical properties of the nanostructures.
- (iv) The imaging of pseudomorphic surfaces with various growth conditions, to identify the relation between the terraces and QD alignment. This will allow the estimation of diffusion lengths and their relationship with surface reconstructions.

APPENDICES

APPENDIX A

GROWTH OF NANODOTS ON A STRAINED GAAS EPILAYER USING SCANNING
TUNNELING MICROSCOPE*

Abstract

We report growth of nanodots on strained GaAs surfaces using a scanning tunneling microscope at room temperature. The 5-nm-thick GaAs strained layer was epitaxially deposited over InGaAs quantum dots by molecular beam epitaxy. Nanodots of various shapes were observed on the surface when high-bias voltages at various feedback currents were pulsed at a few hundred milliseconds at room temperature. The resultant dots were elongated along the (1-1 0) direction and had dimer rows of a 2×4 reconstruction. The analysis of the resultant morphologies suggested that the diffusion on the tensile strained GaAs surface is anisotropic, faster along the dimer row direction.

A.1 Introduction

In nanoscale materials research, scanning tunneling microscopy (STM) has unique advantages. It provides valuable information on surface atomic arrangement, chemical analysis, and morphologies of three-dimensional (3D) nanostructures. It also allows us to construct artificial nanoscale features on the surface by manipulating surface atoms as well as etching the surface. The manipulation of surface atoms enables us to test new aspects of physics such as diffusion under an electric field on the nanoscale.¹ Diffusion is a critical component in understanding a self assembly process such as the Stranski–Krastanov (S–K) growth mode in the fabrication of self-assembled quantum dots and chains.² Better understanding of diffusion on strained layers is necessary for the growth of stacked quantum dots (QDs), as well as the initial transition of flat strained layers into 3D islands. In this report, we study nanodots fabricated on strained surfaces by an STM that were epitaxially grown by molecular beam epitaxy (MBE). The

* Coauthored by J. Abel, D. J. Kim, E. A. Everett, and H. Yang, J. Crystal Growth **310**, 2244(2008).

morphological analysis of the nanodots suggests that diffusion of adatoms on the tensile-strained surface of GaAs is anisotropic at room temperature.

A.2 Experimental Procedure

The strained epitaxial layers were prepared by a commercial MBE machine, SVTA model BLT-35N. An *n*-type (Si-doped) GaAs substrate (carrier concentration of 2×10^{18}) with a nominal (0 0 1) orientation was loaded into the load-lock chamber, then into the preparation chamber of mid 10^{-10} torr of vacuum. The wafer was outgassed in the preparation chamber at 300 °C for 30 min before it was loaded into the growth chamber. After the oxide layer was removed at 580 °C under arsenic pressure in the growth chamber, confirmed by reflection high-energy electron diffraction (RHEED), a 1 μ m-thick GaAs buffer was grown on the substrate at 580 °C at a growth rate of 0.5 mm/h. The substrate was then cooled down below 360 °C, where about ten monolayers (ML) of InGaAs were deposited at 0.20 ML/s on the buffer layer with an indium composition of about 40%. The temperature of the substrate was then raised to 460 °C and annealed for 2 min to induce formation of the QD chains as previously reported by Kim et al.,³ where STM images of the flat-but-strained layer were also reported. Details of the STM images for the morphology of strained-but-flat InGaAs layers and transformed InGaAs QD chains via annealing can be found in the previous report.³ After confirming the formation of QDs by RHEED chevron patterns, GaAs layers of about 5 nm thickness were deposited at 0.16 ML/sec over the InGaAs QD chains immediately after annealing at the same temperature. During the capping period, the chevrons and spots for 3D islands gradually disappeared and the integer order peaks and the specular peaks reappeared. After the GaAs capping, the substrate was rapidly cooled by turning the power off to the substrate heater. The GaAs cap layer is believed to be tensile-strained due to InGaAs dot chains underneath.

The grown sample was then moved to an ultra high vacuum (UHV) STM (Omicron room temperature STM) attached to the MBE machine through an UHV port to obtain the *as-*

grown surface images.⁴ The STM tips were prepared by electro-chemically etching polycrystalline tungsten wires.⁵ The tips were cleaned *in situ* by electron bombardment heating (600V at 2.5mA of electron current for 60 s) under low (10^{-10} torr) vacuum. Four separately prepared tips were used for imaging and nanostructuring. The nanodots were created using the Nanostructuring program of the Omicron SPM software (version 2.1) that came with the Omicron STM, provided by the Omicron. STM imaging before and after nanostructuring used a constant current mode at 0.1 nA, and a bias voltage between -2.5 and -3 V (filled state). High resolution images of the surface were studied for the detailed morphologies of the nanodots formed on the surface.

A.3 Nanostructuring on the GaAs Cap Layer

The 400×400 nm STM image, Fig. 1(a), from a strained GaAs surface shows strips that are typically ~ 4 nm high and ~ 100 nm wide. The elongation direction of the strips is the (1 1-0) direction. The strip formation can be attributed to the underlying dot chains formed during the annealing process. (See STM pictures of dot chains in the previous publication).³ It is interesting to note that the strips are all elongated along the elongation direction of dots instead of along the dotchain directions, which are mostly off the (1 1-0) direction.³ The high-resolution image of the starting GaAs-strained surface around a nanodot shows dimer rows as in Fig. 1(c), which is consistent with the reappearance of integer order peaks in the RHEED patterns after the GaAs capping.

After the STM imaging, using the Omicron software, the surface such as in Fig. 1(a) was selected and the STM was programmed to create a 5×5 grid of structuring events, covering the areal size of 280×280 nm² within the image size of 500×500 nm². After the structuring, the STM was set back to the “normal” scanning mode of -3 V at 0.1 nA feedback current to image the structuring event as shown in Fig. 1(b). The events were programmed with three parameters. The first two parameters were the bias voltage and tunneling current. Both were changed while

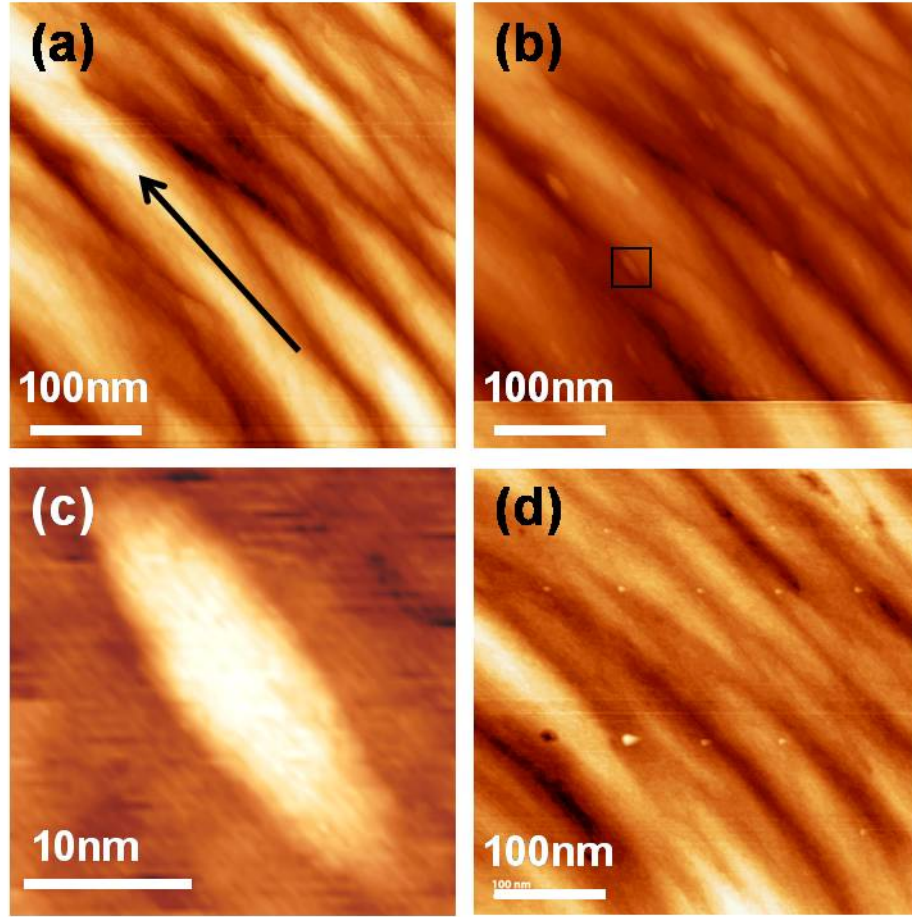


FIG. 1 All STM images were obtained using 3V (filled state) with a constant current mode at 0.1nA; (a) is a $400 \times 400\text{nm}^2$ STM image of the 5-nm thick GaAs epilayer grown at 460 °C. The same surface after nanostructuring is shown in (b) with the same STM parameters as in (a). Oval-shaped nanodots are visible in (b). A zoomed-in STM image of a nanodot, marked by a square in (b), is shown in (c). Circular cones were observed on a smoother surface as in (d). Arrows indicate the (1-1 0) direction in (a) and (c), and the orientation of the image (d) is the same as that of (a).

the feedback loop was still active. The third parameter was the amount of time each event was active for. That is, the amount of time the bias voltage and tunneling current were changed from the values used for imaging to the values used for creating nanostructures. We will refer to this as the structuring time. In this experiment, values varied from 6 to 10V for bias voltage; 5 to 12 nA for tunneling current; and 100, 200, and 300 ms for structuring time.

A.4 Nanodots Formed by STM Structuring

The STM image was taken after the set of whole nanostructuring events were completed, which is shown in Fig. 1(b). Comparison of the images before and after the nanostructuring indicates that the selected surface was traced back exactly after the nanostructuring events finished. For the nanostructuring, the STM tip was set for 100 ms at each point for three times, for a total structuring time of 300 ms, with a 10ms interval between each structuring time. Size variations of nanodots are visible in the image, which seems to be due to the variation of the local strain field. This can be attributed to the fact that diffusion and diffusion anisotropy of available adatoms on the surface depend on strain as reported by Penev et al.⁶ The zoomed-in image of the dot in the square of Fig. 1(b) shows that the top surface of the ovaldome-shaped nanodot has dimer rows, which is similar to those in the surrounding background GaAs epilayers in Fig. 1(c). Although the dimer rows are not as continuous as in a smooth GaAs(0 0 1)- $\beta(2 \times 4)$ surface, dimer rows of a typical 2×4 surface reconstruction are clearly visible, which suggests the crystalline quality of the nanodots formed by STM.

The nanostructures that were created took on three distinct shapes, irrespective of the bias voltage, tunneling current, and structuring time. The shapes formed were cones, shown in Fig. 1(d), oval domes, and holes. Holes were observed to form with cones and oval domes, but oval domes and cones were never observed to form in the same area. Formation of almost symmetric, circular nanocones seems to be due to local variation of the strain field also as the two STM images of (a) and (d) in Fig. 1 are compared. The oval domes were found in surface areas with

high corrugation such as (a), which seems to have bigger variation in strain field; meanwhile, circular domes were fabricated on smoother surfaces as in (d), which was confirmed by the actual STM line profiles on these surfaces. This is supported by the report of circular cones⁷ produced on flat, smooth GaAs(0 0 1) surfaces by an STM tip.

A.5 Size Dependence by Structuring Parameters

The analysis of dot size indicates that the size of nanodots increases as the bias voltage increases, as shown in Fig. 2, and that the aspect ratio (length over width) stayed more or less the same over the bias voltage increase at 7 nA of tunneling current. However, the increase in tunneling current showed mixed results, as shown in Fig. 3. Although the nanodot size increases with bias voltage over the whole tunneling current range measured, the increase is somewhat suppressed at the higher tunneling current. An increase in the tunneling current usually brings the STM tip closer to the sample surface. The increased local electric field is not effective for growing dots due to the small area affected by the increased field. Rather, the results suggest that the diffusion induced by local electric fields requires a certain distance from the surface to cover enough area to influence adatoms on the area. This result contrasts with a recent report on growth of gold nanofingers on Au(1 1 1) surfaces,⁸ where the atom extraction required a very high current of 30 nA at a low bias voltage of 1.5 V, which brings the STM tip very close to the surface for the growth. The difference can be attributed to different mechanisms of extraction for gold surfaces and electric field-induced diffusion for strained GaAs surfaces. Regular continuous STM scans on the strained GaAs surfaces, however, did not yield any morphological changes as in the Au (1 1 1) surface. It is reasonable to expect nanodots to grow larger when the electric field stays on longer due to the continued growth from the diffusing adatoms under the localized electric field as suggested by Whitman et al.¹ Growth of nanodots can be visualized as their size depends on structuring time, which is shown in Fig. 4. The fitting shows that the growth exponents for length and height over time are similar, $0.0031x$ and $0.0032x$, respectively, where x is the time.

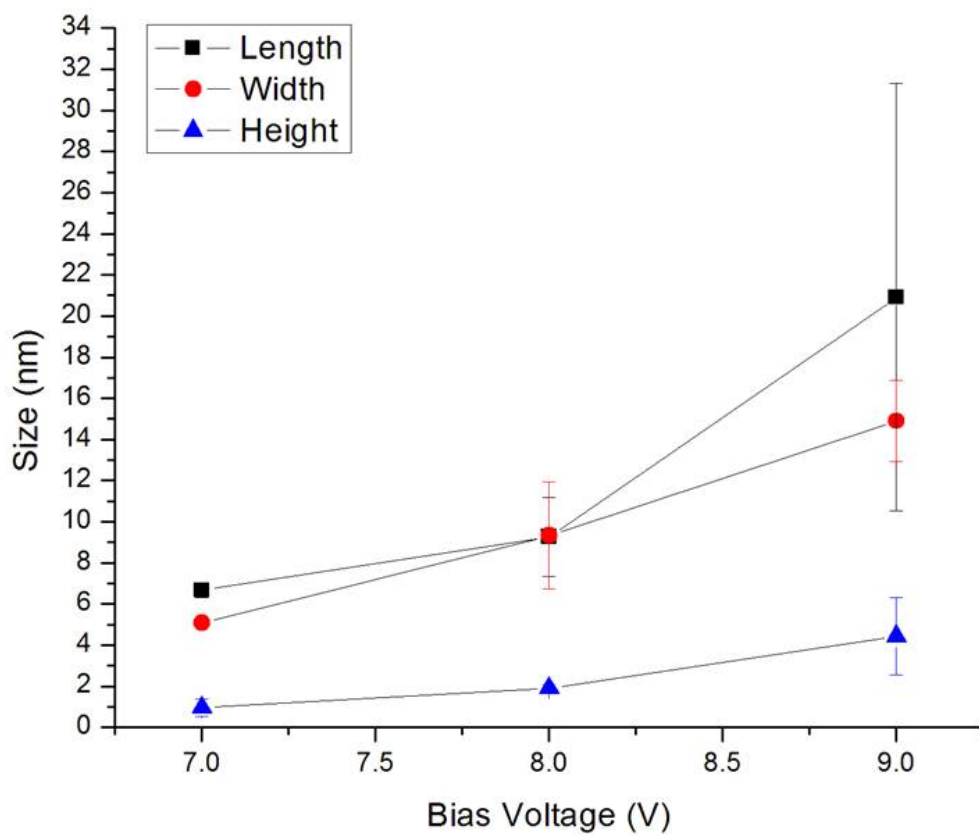


FIG. 2. Size dependence on applied bias voltage. The STM tips stayed on each spot for 100 ms at 7 nA of the tunneling current. This graph is a subset of Fig. 6.3. The height, width and length increased with bias voltage at almost the same rate.

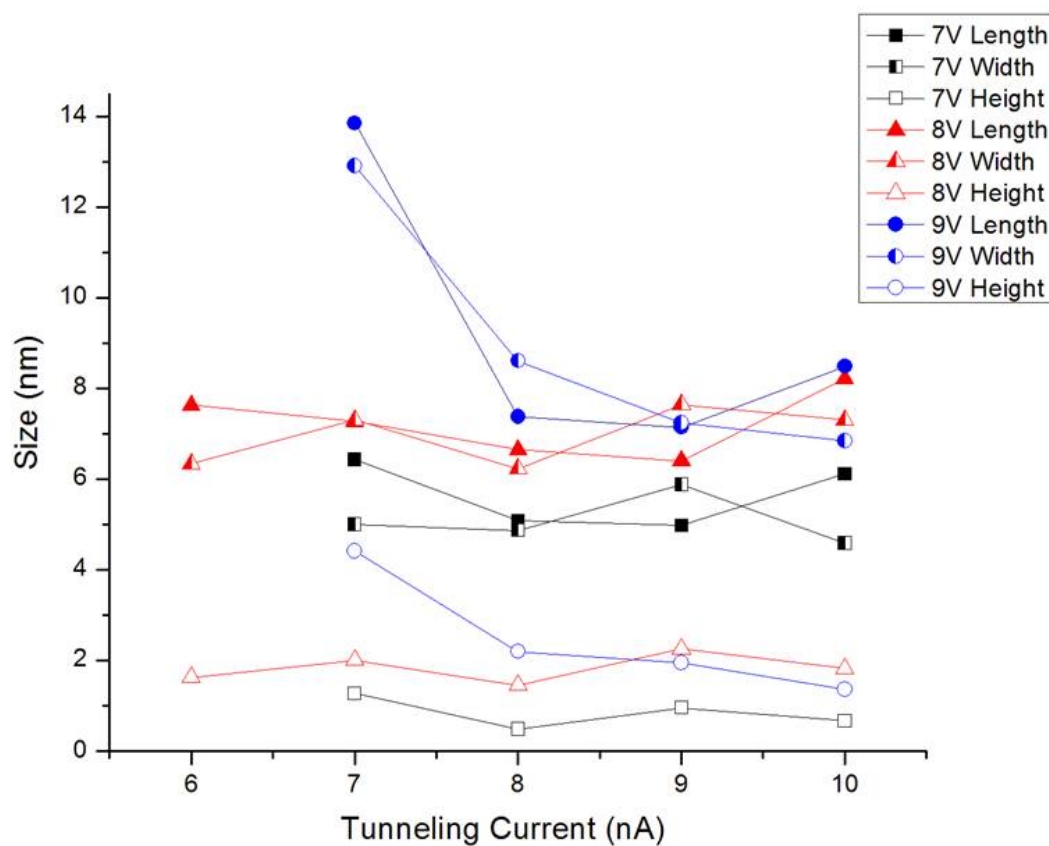


FIG. 3. Size dependence on tunneling current and bias voltage. The structuring time is 100 ms for all nanodots. For all bias voltages, the nanodot size decreases with the tunneling current, which is indicative of the tip to surface distance at the same bias voltage.

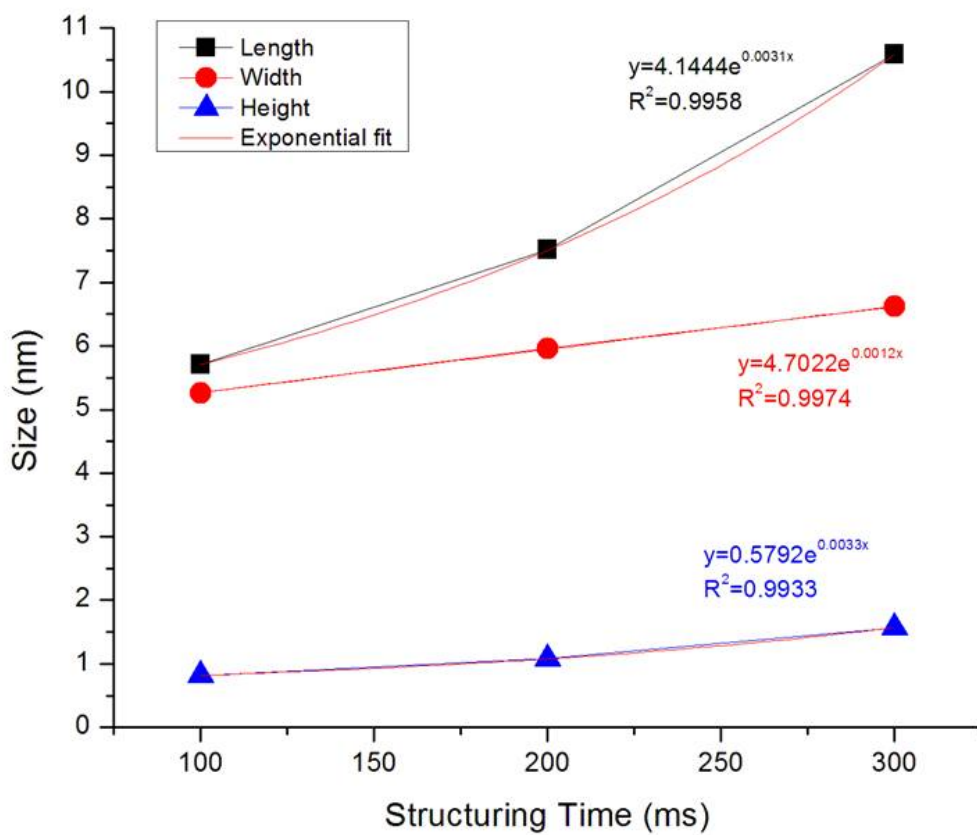


FIG. 4. Growth of oval-shaped nanodots over structuring time. The growth is anisotropic as the aspect ratio, length over width, increases over time.

The width exponent, however, is $0.0012x$, which is about two-and-a-half times smaller than those of length and height, which suggests that the growth is faster along the length direction, the dimer row direction. The zoomed-in STM image, Fig. 1(c), shows that the nanodots are elongated along the dimer row direction, which is a faster diffusion track for surface adatoms on GaAs(0 0 1)- 2×4 surfaces.⁶ Not surprisingly, the dots elongate more as the time increases and as the exponents are growth parameters. This is consistent with lower diffusion barriers along the dimer row direction for Ga and As surface atoms at elevated temperature around 300 °C or higher, so that two-dimensional islands of GaAs on GaAs(0 0 1) by homoepitaxy result in elongated islands along the (1 1-0) direction.⁹ Our results suggest that diffusion anisotropy is still valid at room temperature for strained GaAs epilayers with dimer rows present.

A.6 Summary

In summary, it has been shown that the STM can create various nanodots on a GaAs tensile strained surface. The shapes of the dots were circular cones, oval domes, and holes. The oval dots were found to be elongated along the (1 1-0) direction and the top surface had reconstruction with dimer rows. The width, length, and height of the oval dots grow exponentially over the bias application period. However, the growth exponents for the length and height were found to be two-and-a-half times larger than that of the width. The analysis of the growth exponents suggests that the localized diffusion on the tensile strained GaAs surface is anisotropic at room temperature, faster along the dimer row direction.

References

- [1] L. J. Whitman, J. A. Stroscio, R.A. Dragoset, and R. J. Celota, *Science* **251**, 1206 (1991).
- [2] V. A. Shchukin, N. N. Ledentsov, and D. Bimberg, *Epitaxy of Nanostructures*, (Springer, New York, 2004).
- [3] D. J. Kim, E. A. Everett, and H. Yang, *J. Appl. Phys.* **101**, 106106 (2007).

- [4] D. J. Kim, D. Cha, G. J. Salamo, and H. Yang, *J. Vac. Sci. Technol. B* **24**, 2776 (2006).
- [5] A. J. Melmed, *J. Vac. Sci. Technol. B* **9**, 601 (1991).
- [6] E. Penev, S. Stojkovi, P. Kratzer, and M. Scheffler, *Phys. Rev. B* **69**, 115335 (2004).
- [7] S. Kohmoto, H. Nakamura, T. Ishikawa, and K. Asakawa, *Appl. Phys. Lett.* **75**, 3488 (1999).
- [8] Q. Guo, F. Yin, and R. E. Palmer, *Small* **1**, 76 (2005).
- [9] H. Yang, V. P. LaBella, D. W. Bullock, Z. Ding, J. B. Smathers, and P. M. Thibado, *J. Crystal Growth* **201/202**, 88 (1999).

Appendix B

RIGHTS <Rights@aip.org> Mon, Nov 3, 2008 at 7:53 AM

To: Dong Kim dong.kim@aggiemail.usu.edu

Dear Dr. Kim:

Thank you for requesting permission to reproduce material from American Institute of Physics publications.

Permission is granted – subject to the conditions outlined below – for the following:

Annealing induced transition of flat strained InGaAs epilayers into three-dimensional islands,
JOURNAL OF APPLIED PHYSICS *101*, 106106 (2007),

To be used in the following manner:

Reproduced in your dissertation for submission to Utah State University, which will send the dissertation to Bell & Howell Dissertation Services to be made available for reproduction.

1. The American Institute of Physics grants you the right to reproduce the material indicated above on a one-time, non-exclusive basis, solely for the purpose described. Permission must be requested separately for any future or additional use.

2. This permission pertains only to print use and its electronic equivalent, including CD-ROM or DVD.

3. The following copyright notice must appear with the material (please fill in the information indicated by capital letters): "Reprinted with permission from [FULL CITATION]. Copyright [PUBLICATION YEAR], American Institute of Physics."

Full citation format is as follows: Author names, journal title, Vol. #, Issue #, Page #, Year of publication. For an article, the copyright notice must be printed on the first page of the article or book chapter. For figures, photographs, covers, or tables, the notice may appear with the material, in a footnote, or in the reference list.

4. This permission does not apply to any materials credited to sources other than the copyright holder.

5. If you have not already done so, please attempt to obtain permission from at least one of the authors. The author's address can be obtained from the article.

Please let us know if you have any questions.

Sincerely,
Susann Brailey

~~~~~  
Office of the Publisher, Journals and Technical Publications  
Rights & Permissions

American Institute of Physics

Suite 1NO1

2 Huntington Quadrangle

Melville, NY 11747-4502

516-576-2268 TEL

516-576-2450 FAX

[rights@aip.org](mailto:rights@aip.org)

**RIGHTS <Rights@aip.org> Mon, Nov 3, 2008 at 7:48 AM**

To: Dong Kim [dong.kim@aggiemail.usu.edu](mailto:dong.kim@aggiemail.usu.edu)

Dear Dr. Kim:

Thank you for requesting permission to reproduce material from American Vacuum Society publications.

Permission is granted – subject to the conditions outlined below – for the following:

**Enabling in situ atomic scale surface imaging for vertical molecular beam epitaxy machines, J. Vac. Sci. Technol. B 24\*(6), 2776, Nov/Dec 2006,**

To be used in the following manner:

Reproduced in your dissertation for submission to Utah State University, which the University will send to Bell & Howell Dissertation Services to be made available for reproduction.

1. The American Vacuum Society grants you the right to reproduce the material indicated above on a one-time, non-exclusive basis, solely for the purpose described. Permission must be requested separately for any future or additional use.
2. This permission pertains only to print use and its electronic equivalent, including CD-ROM or DVD.
3. The following copyright notice must appear with the material (please fill in the information indicated by capital letters): "Reprinted with permission from [FULL CITATION]. Copyright [PUBLICATION YEAR], American Vacuum Society." Full citation format is as follows: Author names, journal title, Vol. #, Issue #, Page #, Year of publication. For an article, the copyright notice must be printed on the first page of the article or book chapter. For figures, photographs, covers, or tables, the notice may appear with the material, in a footnote, or in the reference list.
4. This permission does not apply to any materials credited to sources other than the copyright holder.
5. If you have not already done so, please attempt to obtain permission from at least one of the authors. The author's address can be obtained from the article.

Please let us know if you have any questions.

Sincerely,

Susann Brailey

~~~~~

Office of the Publisher, Journals and Technical Publications

Rights & Permissions

American Institute of Physics

Suite 1NO1

2 Huntington Quadrangle

Melville, NY 11747-4502

516-576-2268 TEL

516-576-2450 FAX

rights@aip.org



"Kim, Dong Jun"
<DongJun.Kim@pnl.gov>
17/12/2008 22:47

To <permissions@iop.org>
cc
bcc
Subject permission to reprint as a chapter in my dissertation

December 17, 2008

2100 Bellerive Dr. #51

Richland, WA 99352

To Permissions Editor:

I am preparing my dissertation in the physics department at Utah State University. I hope to complete me degree in the Fall of 2008. An article, Shape control of InGaAs nanostructures on nominal GaAs(001): dashed and dots, of which I am first author, and which appeared in your journal **Nanotechnology 19** (2008) 475601, reports an essential part of my dissertation research. I would like permission to reprint it as a chapter in my dissertation.

Please note that USU sends dissertation to Bell & Howell Dissertation Services to be made available for

reproduction. I will include an acknowledgment to the article on the first page of the chapter, as shown below. Copyright and permission information will be included in a special appendix. If you would like a

different acknowledgment, please so indicate.

Please indicate your approval of this request by signing in the space provided, and attach any other form necessary to confirm permission. If you charge a reprint fee for use of an article by the author, please indicate that as well.

If you have any questions, please call me at the number above or send me an e-mail message at the above address. Thank you for your assistance.

Dong Jun Kim

I hereby give permission to Dong Jun Kim to reprint the requested article in his dissertation, with the following acknowledgment:

(Acknowledgment, including full bibliographical information, including title, journal, volume,

date, and page numbers)

Signed _____

Date _____

Fee _____

Dong Jun Kim

Fundamental & Computational Sciences Directorate

Pacific Northwest National Laboratory

902 Battelle Boulevard

P.O. Box 999, MSIN K8-87

Richland, WA 99352 USA


Tel: 509-371-6313

Fax: 509-371-6242

DongJun.Kim@pnl.gov


www.pnl.gov

PERMISSION TO REPRODUCE AS REQUESTED
IS GIVEN PROVIDED THAT:

- ~~(a) the consent of the author(s) is obtained~~
- (b) the source of the material including author/editor, title, date and publisher is acknowledged. 

IOP Publishing Ltd
Dirac House
Temple Back
BRISTOL
BS1 6BE

19/12/08 
Date Rights & Permissions

 Please include the IOP Copyright line, mention the journal's homepage at: www.iop.org/journals/nano

and provide a link back to the article's abstract on our website from the electronic version of your thesis.

Thank you!

CIRICULUM VITAE

Dong Jun Kim

Fundamental & Computational Sciences Directorate, Pacific Northwest National Laboratory
902 Battelle Boulevard , P.O. Box 999, MSIN K8-87, Richland, WA 99352 USA
Tel: 509-371-6313, Fax: 509-371-6242
DongJun.Kim@pnl.gov

Education

- Ph.D., Physics, Utah State University, Logan, Utah, May 2004~Dec. 2008
- M.S., Physics, University of Utah, Salt Lake City, Utah, Aug. 2000~May 2004

Research Experience

- Molecular beam epitaxy: growth of self-assembled quantum dots and wires
- Surface analysis with *in-situ* and *ex-situ* scanning probe microscopy: atomic force microscopy, scanning tunneling microscopy, scanning capacitance microscopy and electrostatic force microscopy
- Surface analysis with *in-situ* scanning electron microscopy and electron diffraction: reflection high energy electron diffraction and low energy electron diffraction, auger electron spectroscopy, ultraviolet photoelectron spectroscopy
- Ultra high vacuum: experiment, practices, and maintenance
- Semiconductor device fabrication/characterization: thin film deposition by sputtering and thermal evaporation, metal deposition and ion diffusion
- High-sensitivity measurement: of forces, voltage, current, and capacitance, especially with scanning probe microscopy at the nanometer scale
- Computer skills: Proficiency in MS Office, LabView, Origin, Sigma Plot, Mathematica, Maple, and HTML; familiarity with Linux, Unix, Windows, and Mac OS X

Publications

- “Shape control of InGaAs nanostructures on nominal GaAs(001): dashes and dots,” Dong Jun Kim and Haeyeon Yang, *Nanotechnology*, **19**, 475601 (2008).
- “Growth of Nanodots on a Strained GaAs Epilayer Using Scanning Tunneling

Microscope,” Joseph Abel, Dong Jun Kim, E. Addison Everett, and Haeyeon Yang, *Journal of Crystal Growth*, **310**, 2244 (2008).

- “Annealing Induced Transition of Flat Strained InGaAs Epilayers into Three-dimensional Islands,” Dong Jun Kim, E. Addison Everett, and Haeyeon Yang, *Journal of Applied Physics* **101** (10), 106106 (2007).
- “Enabling In-situ Atomic Scale Surface Imaging for Vertical Molecular Beam Epitaxy Machines,” Dong Jun Kim, Deokjoon Cha, Gregory J. Salamo, and Haeyeon Yang, *Journal of Vacuum Science and Technology B*, **24(6)**, 2776 (2006).
- “Single-electron Tunneling to Insulator Surfaces Measured by Frequency Detection Electrostatic Force Microscopy,” Ezra. Bussmann, Dong Jun Kim and Clayton. C. Williams, *Applied Physics Letters* **85**, 2538 (2004).